Bed-load transport over inlet sills of longitudinal training walls

Experimental study

W.J. van Os

TU Delft

Bed-load transport over inlet sills of longitudinal training walls

Experimental study

by

W.J. van Os

to obtain the degree of Master of Science
at Delft University of Technology,
to be defended publicly on Wednesday June 24, 2020 at 4:00 PM.

Student number:	4500628	
Project duration:	May 1, 2019 – June 24, 2020	
Thesis committee:	Prof. dr. ir. W.S.J. Uijttewaal,	TU Delft, chair
	Dr. ir. E. Mosselman,	TU Delft, supervisor
	Dr. ir. R.J. Labeur,	TU Delft
	Ir. L.R. Lokin,	HKV

TU Delft

Preface

The master thesis presented here is part of my Hydraulic Engineering master program at the faculty of Civil Engineering and Geosciences at Delft University of Technology.

Firstly, I would like to thank my supervisors and the graduation committee: Wim Uijttewaal, Erik Mosselman, Robert Jan Labeur and Lieke Lokin for their excellent guidance and support during this process. All the discussions and comments during and beyond the committee meetings really helped to structure my research and resulted in many new insights. Thanks to Ana Luisa Osorio for the collaboration. The day trip, our discussions and your feedback were great. Matthew Czapiga and Merel Verbeek, thanks for our conversations. Thanks to the lab staff: Sander, Arno, Pieter, Jaap and Frank for all the help and the many cups of tea. Your practical solutions and help made it possible to perform the experiments.

Also, I would like to thank HKV Consultants and its employees for the last year. I have enjoyed the time at HKV very much. Lieke, your support and comments helped me greatly throughout my research.

This thesis would not have been possible without the love and support of my parents and Mariëlle, Robert, Gert-Jan, Jorina and Margreet. Your advise and our discussions have been very helpful for my work.

I hope you enjoy reading this thesis.

W.J. van Os
Delft, June 2020

Summary

Groynes have been replaced by longitudinal training walls in an 11-km long pilot project to optimize training of the river Waal in the Netherlands. Longitudinal training walls are trapezoid-shaped structures of stones oriented aligned with the river banks which divide the river into a main and sheltered channel. These training walls improve navigability, reduce flood levels, create a sheltered second channel with more favourable ecological conditions, and decrease the erosive action on the river bed that is responsible for large-scale bed degradation. River managers wish to assess whether longitudinal training walls could have similar advantages along other parts of the Dutch Rhine branches (without excessive increase of maintenance costs). The required maintenance dredging depends on the amount of sediment entering the sheltered channel over an entrance sill situated at the upstream edge of the longitudinal training wall. Currently operational morphodynamic models cannot reliably compute this sediment flux.

The aim of this study was to develop a formulation on transport of sediments over the inlet sill of a longitudinal training wall, from the main channel towards the sheltered channel, for implementation in two-dimensional depth-averaged river models. To this end, laboratory experiments have been performed to study the passage of bed sediment at different discharge distributions between the main and sheltered channel, and different degrees of submergence. During and after these experiments the effect of these parameters on the sediment transport was deduced from the measured flow velocities.

The geometry of the experiment was schematized to a main channel with next to it upstream a no-discharge zone, then an inlet area and downstream the sheltered channel separated from the main channel with a vertical plate. The sill at the inlet, aligned with the walls of the flume, was extended over the length of the flume to reduce secondary flow effects. The discharge distribution between the main and sheltered channel and the degree of submergence were varied within three experimental conditions with the same total discharge. In addition, three types of measurements were performed per experimental condition: 1) flow field measurements at the surface with particle image velocimetry, 2) point measurements at mid-depth with acoustic Doppler velocimetry and 3) particle trajectory measurements at the bottom with particle tracking velocimetry. The measurements in different layers provide knowledge about the variation of the flow patterns over the depth, where the measurements at the water surface and near the bottom show the horizontal patterns. Hence, three-dimensional flow structures can be identified from the measurements.

In general, the results of this experiment show an increase of the flow angle and the lateral velocity magnitude towards the sheltered channel in longitudinal and lateral direction. The flow angle is generally smaller for lower depths at the upstream side of the inlet and larger at the downstream side of the inlet. The results show an area with strong divergence above the sill.
For a larger discharge distribution towards the sheltered channel, both the lateral and longitudinal component increase and the flow angle increases too. Since two-dimensional effects are included in depth-averaged models, this is not further considered. Besides, for a larger discharge distribution towards the sheltered channel, the flow angle near the bed over the flow angle at mid-depth decreases. This effect reduces the sediment transport over the inlet sill compared to a theoretical sediment transport based on the near-bottom flow velocity magnitude and the depth-averaged flow angles.
For the experiment with a smaller sill height to water depth ratio, the velocity magnitudes are also smaller due to the chosen experimental condition. In addition, the streamlines at the water surface are more gradual and the velocity measurements near the bottom give a considerably different flow pattern compared to other conditions. These effects can be explained respectively by effects of a smaller flow velocity on the tracer particles and sill effect, in accordance to Van Rijn [1993] and Wols et al. [2006] respectively. So, the effect of the sill height to water depth ratio on the sediment transport could not be deduced from the experimental results, because side effects of the experimental condition dominate.

It is recommended to use local flow parameters as input parameters for the parameterisation. For further research on the development of a parameterisation of sediment transport over the inlet sill of longitudinal

training walls. As a next step in the development, the blocking effect needs to be investigated in more detail by an experimental study. The velocity averaged over the cross-sectional area in the sheltered channel has to be kept constant for experimental conditions with variation of other parameters.

Contents

List of Figures

List of Tables

List of Symbols

General constants		
g	gravitational acceleration	m/s^2
κ	Von Karman constant	0.4
Coordinates		
x	longitudinal coordinate	m
y	lateral coordinate	m
z	vertical coordinate	m
r	radial coordinate	m
Fluid mechanisms		
u	velocity in longitudinal direction	m/s
v	velocity in lateral direction	m/s
w	velocity in vertical direction	m/s
U	velocity magnitude	m/s
α	flow angle (tan u/-v)	-
ρ	density of water	kg/m^3
River engineering		
C	Chézy coefficient	$m^{1/2}/s$
c_f	roughness coefficient	-
d	water depth	m
d_e	equilibrium water depth	m
F_1	empirical constant for vertical position	-
F_2	empirical constant for vertical position	-
H	energy head	m
i_b	bed slope	-
q	specific discharge	m^2/s
η	vertical position z/d	-
Weir structures		
a	sill height (same as w)	m
B_w	width of the sill	m
w	sill height (same as a)	m
W_{inlet}	dimensionless crest height (w/H)	-
α	transverse slope angle	^{0}
β	deviation of the flow direction from the perpendicular direction to the sill crest	^{0}
β_a	coefficient for the oblique effects	-
ϕ	angle between weir crest and channel axis	^{0}
Sediment transport		
A	surface particle	m^2
C_D	drag force coefficient	-
C_L	lift force coefficient	-
F_D	drag force	N
F_G	gravitational force component	N

F_L	lift force	N
F_R	friction force	N
u_r	relative velocity	m/s
ρ_s	density of sediment	kg/m^3

Subscripts

0	upstream of the weir
$\perp$	representative for plain weir
inlet	at the inlet
main	in the main channel
side	in the side channel (same as sheltered channel)
sheltered	in the sheltered channel (same as side channel)
up	upstream of the inlet

Abbreviations

ADV	acoustic Doppler velocimetry
PIV	particle image velocimetry
PTV	particle tracking velocimetry

1 Introduction

1.1. Context

Longitudinal training walls are an alternative for groynes which prevent bank erosion due to meandering processes and maintain the channel depth with additional advantages compared to groynes. To gain understanding of the processes and access the effects of these structures on morphology and ecology, the Dutch water authority Rijkswaterstaat initiated a pilot project with longitudinal training walls in the river Waal between Wamel and Ophemert. The construction started in 2015 and was completed in 2017. The effects of the longitudinal training walls have been monitored and studied partly in projects of the research programme RiverCare [NCR, 2019].

A longitudinal training wall (LTW) is a structure parallel to the river channel that divides the river into a fairway for navigation and a sheltered channel, see Figure 1.1. Research studies about LTWs show several positive effects. The mild flow conditions in the sheltered channel are favourable for ecology compared to the (dynamic) flow in groyne fields [Collas et al., 2016]. Groynes reduce the conveyance width of the river, resulting in a larger water depth and flow resistance and the latter contributes to the on-going bed degradation. Since longitudinal training walls are aligned with the flow, they cause less flow blockage and resistance than groynes oriented perpendicularly to the flow. Therefore, longitudinal training walls may generate less bed degradation compared to groynes. In addition, the reduction of blockage for the sheltered channel contributes to the discharge capacity for large discharge conditions and the water level is higher at low water levels.

Figure 1.1: The longitudinal training walls in the Waal near Wamel. The longitudinal training walls are located in the inner bend and groynes in the outer bend. [Your Captain Luchtfotografie]

Because of these positive effects following from the pilot project, the river authority Rijkswaterstaat would like to extend these longitudinal training walls towards other river sections. Knowledge on the sediment transport towards the sheltered channel is the missing link for the feasibility of new construction projects with longitudinal training walls, because this knowledge is essential to prevent high sedimentation rates and hence excessive dredging costs. A sill at the inlet of the sheltered channel is used to regulate the distribution of discharge and sediment transport. To evaluate the morphological stability of the main and sheltered channel, a numerical model is needed that is able to predict the morphological effect of the design of longitudinal training walls with an inlet sill. However, existing models were not effective in predicting the sediment distribution over the sill.

1.2. Problem statement

Longitudinal training walls are a new type of river training structures. Designing longitudinal training walls for other locations requires an accurate and efficient model to evaluate the effects of conceptual designs on morphology. Previous research concerns a hydraulic evaluation of the flow around longitudinal training walls [Van Linge 2017] and a theoretical description of the sediment particle trajectories over the inlet sill [Jammers 2017]. Van Linge proposed a formula for the discharge over the weir with discharge and submergence coefficients based on comparison with results of detailed two-dimensional models. Since this promises a good approach for modelling two-dimensional flow, the coefficients should be validated with measurement data of flow above the weir. However, these data are not available from field measurements or the experimental study of De Ruijsscher et al. [2019]. The particle model of Jammers with input of near-bed flow field calculated with the depth-averaged model of Van Linge gives no sediment transport over the sill for conditions in the river Waal. However, bed measurements show sedimentation in the sheltered channel [De Ruijsscher 2018]. Therefore, the sediment transport over the inlet sill is not understood. In conclusion, the following knowledge is lacking:

- The mechanisms of sediment transport over the inlet sill of longitudinal training walls are not known.
- Validation data to test model concepts about the flow and sediment transport above the inlet sill are not available from previous studies or field measurements.

In depth-averaged river models a logarithmic profile has been assumed. However, the geometry is expected to induce three-dimensional flow patterns, based on knowledge on similar structures (see section 2.2.1 and 2.2.3) and velocity measurements in front of the sill (see section 2.2.2). The three-dimensional flow patterns that are expected are: deformation of the logarithmic velocity profile due to accelerations and decelerations, helical flow due to curvature and blocking and deflection of the flow due to obstacles. The software has options to correct for the following three-dimensional effects: energy losses over weirs and the effect of helical flow on the bed shear stress (see section 2.2.4). Descriptions of the effect of 1) the deformation of the logarithmic velocity profile and 2) the effect of blocking and deflection due to obstacles on flow structures are lacking. Therefore, knowledge on three-dimensional flow structures and the resulting relation between depth-averaged and near-bed flow is a missing link.
In addition, the simple sediment transport formulas are not valid for the sediment transport over the inlet sills of longitudinal training walls. Firstly, the flow does not have a logarithmic or another unambiguous relation between the mid-depth flow and the flow at the water surface. Secondly, the inlet sill has slopes. Thirdly, the bottom is non-alluvial, since the sill consist of rocks. Finally, the bed surface is irregularly due to the rocks.
This research focuses on knowledge about the three-dimensional flow structures around the inlet sill: the identification of the flow structures, understanding of the processes and the effect of these flow structures for sediment transport over the inlet sill. The scope of this study is limited to bed-load conditions and a non-alluvial smooth bed has been assumed.
To gain insight in the mechanisms behind the three-dimensional structures, experimental data of the flow around the sill are needed for different experiments in which parameters that affect these three-dimensional flows are varied. The geometrical dimensions of the inlet and flow conditions affect these flow patterns. The total discharge is expected to have hardly any effect on the flow patterns. The discharge distribution will affect the horizontal flow patterns. Besides, a strong flow towards the sheltered channel can result in a strong accelerating flow with enhanced three-dimensional flow structures. The water depth is expected to affect mainly the flow acceleration. Therefore, the discharge distribution and the water depth should be varied in the experiments.

In conclusion, knowledge of the effect on the discharge distribution and water depth above the sill on three-dimensional flow structures around the inlet sill is needed to identify the sediment transport mechanisms and patterns a basis for a semi-empirical parameterisation of the sediment transport towards the side channel.

1.3. Objective and research questions

The objective is to develop a formulation on transport of sediment over the inlet sill of a longitudinal training wall, from the main channel towards the sheltered side channel, for implementation in two-dimensional depth-averaged river models.

The research question is therefore: How does the flow affect bed-load transport over an inlet sill of longitudinal training walls and how can this be described for implementation in two-dimensional depth-averaged models?
To answer the main question, four sub-questions are formulated:

1. How can an experiment be designed to make relevant observations on bed-load transport over an inlet sill of longitudinal training walls?
2. How does the discharge distribution affect the bed-load transport distribution at an inlet sill of longitudinal training walls?
3. How does the sill height to water depth ratio affect the bed-load transport distribution at an inlet sill of longitudinal training walls?
4. What recommendations can be made to develop a parameterisation of bed-load transport over an inlet sill of longitudinal training walls for two-dimensional river models based on the findings of this research?

1.4. Approach

The research consists of a literature study, an experimental study and a contribution to theory development. The literature study focuses on processes that affect the flow and sediment transport at the inlet of the LTWs. It is concluded with the construction of a theoretical framework summarizing the findings and identifying the lack of knowledge. The experimental study was performed at the Environmental Fluid Mechanics Laboratory at Delft University of Technology. There, the flow has been studied under predefined and constant conditions. A simplified physical model of the area around the inlet of the LTW was constructed. The following techniques were used: Acoustic Doppler Velocimetry (ADV), Particle Image Velocimetry (PIV) and Particle Tracking Velocimetry (PTV) to determine the velocities at different levels in the water column. The experimental setup and method are described in Chapter 3. The experiments offer the opportunity to investigate three-dimensional flow at the inlet of longitudinal training walls and validate flow models. Due to the limited possibilities for variation in the geometry, further research is needed to eventually develop the parameterisation.

1.5. Thesis outline

The literature review in Chapter 2 is introduced with a description of the research case and definitions. The literature review concerns a discussion of knowledge on flow and sediment transport processes and patterns around the inlet of longitudinal training walls. The theoretical concepts about relevant flow and sediment mechanisms for the inlet of longitudinal training walls are summarized in the theoretical framework. The research methods to answer the research questions are described in the methodology, Chapter 3. The results of the experiments are presented in Chapter 4. These results have been analysed in Chapter 5 and 6. Chapter 7 contains the discussion of the experimental design and the effect on sediment transport. The last chapter, Chapter 8, contains answers on the research questions and recommendations for further research.

2

Literature review

2.1. Introduction

The sediment transport over the sill of longitudinal training walls is important for the effect of these walls on the morphology. The flow steers the sediment and therefore knowledge of the flow is important for understanding the sediment transport. This chapter provides knowledge about longitudinal training walls and insight in the flow and sediment transport in general and comparable geometrical configurations.

Longitudinal training walls are built in the river Waal between Wamel and Ophemert over a length of 10 km. They divide the river cross section in a main channel for navigation and a sheltered channel behind the longitudinal training wall. The channels are connected by an inlet, two openings and an outlet. The openings balance the water levels in the channels. At the inlet, sills are built that affect the discharge and sediment distribution. They reduce the discharge and sediment towards the sheltered channel. The effect on the distribution of bed-load sediments is larger than the effect of the discharge, resulting in a larger decrease of the sediment supply relative to the sediment transport capacity and therefore less sedimentation, compared to the situation without a sill. The challenge is to reach morphological stability for the bifurcation for which the dimensions of the sill can be used as variables. The height of these sills can be adapted by adding or removing rocks to control morphological changes to reduce dredging costs for this pilot project and to study the effects of the sill geometry on flow and morphology for future designs (see the morphological study of De Ruijsscher et al. [2019]).

Moreover, this research study aims to gain understanding of the processes behind the sediment supply of the sheltered channel. Because the flow drives the sediment transport, the sediment transport towards the sheltered channel is studied based on knowledge of the flow. The study area is the inlet area of the longitudinal training dams and therefore it does not include the openings and outlet. At low water levels, the openings and possibly the inlet become emerged. At high discharges, the entire longitudinal training wall construction is submerged. Moderate conditions where the inlet sill is submerged and the longitudinal training wall is emerged are investigated in this study. The river section near Wamel (river kilometre 911.5 - 918.2) has been used a case for this research in connection with the studies of Jammers [2017] and Van Linge [2017], see Figure 2.1a and 2.1b for a map and sketch of the longitudinal training walls near Wamel.

(a) Map with the longitudinal training walls in the river Waal near Wamel [EduGIS]

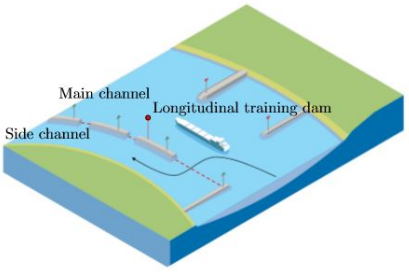

(b) Schematisation of the longitudinal training walls in the river Waal near Wamel [Jammers 2017]

Figure 2.1: Case study of this research and schematisation of the area of interest

Longitudinal training walls divide the river cross section in a main channel and side channel. Flow characteristics in the Waal can be used to determine representative design conditions (see Subsection 3.1.3). The discharge in the river Waal is approximately 2/3 of the discharge in the Bovenrijn near Lobith. The average discharge is 2200 m^3/s in the Bovenrijn at Lobith and 1500 m^3/s in the Waal. This is a moderate condition where the inlet sill is submerged and the longitudinal training walls are emerged. The discharge towards the sheltered channel is ca. 20-30% of the total river discharge for moderate conditions according to Czapiga [personal communication, 2020].

2.2. Flow over the inlet sill

The morphological response in the side channel depends on the discharge and sediment transport over the inlet sill. The discharge determines the sediment transport capacity, during which the sediment availability, i.e. sediment transport over the sill, can be a limiting factor for the actual sediment transport. To optimize the design of longitudinal training walls for a morphological equilibrium, insight into sediment transport over the inlet sill is needed, see Figure 2.2. The flow is the driving force of sediment transport and therefore knowledge of the flow is the starting point for understanding the sediment transport towards the side channel. Hence, first, the flow is discussed in this chapter in this study.

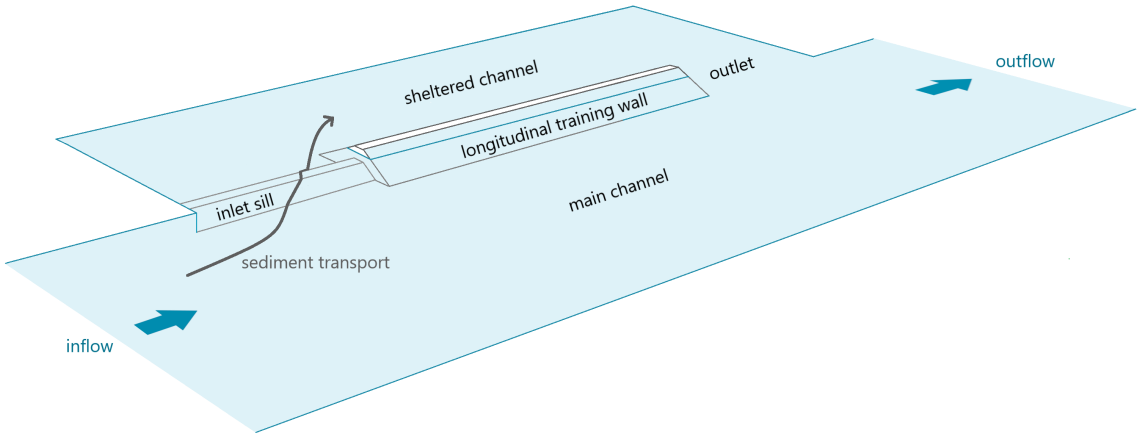

Figure 2.2: Sketch of the channel system around a longitudinal training wall without openings with bed-material transport towards the sheltered channel

The processes and flow structures around individual geometrical features are also present in the complex combined geometry. The inlet area of the longitudinal training walls can be regarded as a bifurcation with a sill. The sill is the entrance to the side channel where the flow approaches the sill nearly perpendicularly. Therefore, the inlet sill is comparable to side weirs. Firstly, literature about similar channel systems without sill is studied. Secondly, the flow processes around the sill are discussed. Finally, knowledge on the flow around the inlet of longitudinal training walls is shown.

2.2.1. Channel system

The channel system of the longitudinal training walls can be considered as a side channel system. The flow bifurcates at the inlet of the side channel and confluences at the outlet of the side channel. The study area is the inlet area of the longitudinal training walls near Wamel with a bifurcating channel system, shown in Figure 2.3. The physical processes in bifurcating and side channel systems without the effect of inlet sill are discussed in this section. Processes related to the inlet sill are discussed in the next section.

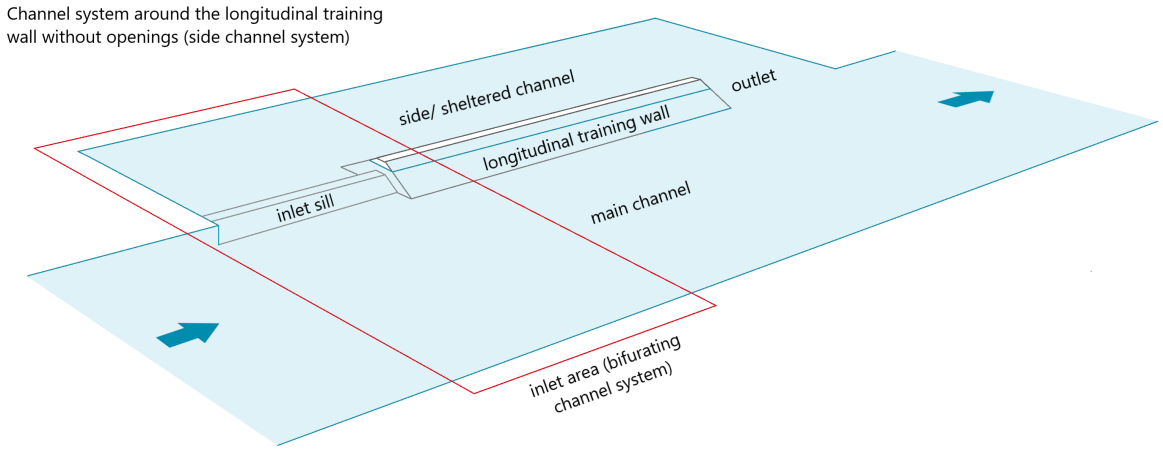

Figure 2.3: Sketch of the channel system around a longitudinal training wall with inlet sill and without openings where the studied inlet area is indicated

Firstly, longitudinal **water level gradients** are the main driving factor for flow in rivers. Lateral water level gradients at the inlet drive lateral transport at the inlet and, hence, affect the discharge distribution between the channels. A difference in the longitudinal water level gradients of the channels and lateral water level gradients in the channels results in lateral water level gradients at the inlet [Van Linge 2017], see Figure 2.4. The equilibrium water depth equation, Equation 2.1, gives insight in factors of the flow mechanism driven by a longitudinal water level difference:

$$d_e = \left(\frac{c_f}{i_b} \frac{q^2}{g} \right)^{1/3} \tag{2.1}$$

where d_e is the equilibrium water depth, c_f is the roughness coefficient, i_b is the bed slope, q is the specific discharge and g is the gravitational acceleration. The longitudinal water level difference is the water level difference between the bifurcated channels caused by differences in the flow driven by longitudinal water level gradients. The water depth depends on the water level. Therefore, the bed roughness, bed slope and specific discharge affect the difference between the equilibrium water levels in the channels for the flow in longitudinal direction. The geometry of the sill affects the discharge towards the sheltered channel [Van Linge 2017]. The relatively larger bed slope due to the river bend is negligible in comparison to the bed interventions in the sheltered channel in the design. Bending flow induce in secondary flow. The resulting water level gradients at the inlet, openings and outlet cause lateral water level differences driving a gross lateral flow from the sheltered channel towards the main channel, see Figure 2.4 [Van Linge 2017].

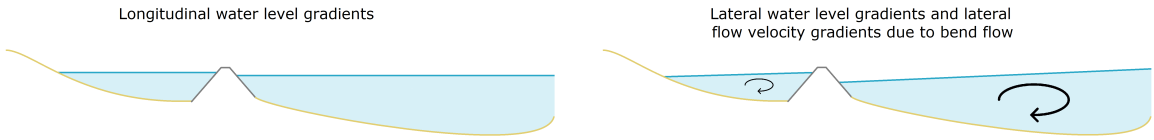

Figure 2.4: Sketch of the channels with different longitudinal water level gradients in the channels (left) and different lateral water level gradients in the channels and lateral velocity differences due to helical flow in river bends (right) based on Van Linge [2017]

Another flow mechanism is driven by **flow velocity gradients**. Velocity differences in longitudinal direction result in lateral transport creating turbulent mixing layers (separation layers) at the inlet. The 2D depth-

averaged model results of Van Linge [2017] show a recirculation zone at the upstream side of the sheltered channel and stagnation just downstream the inlet along the longitudinal training wall in the sheltered channel, see Figure 2.10. Transport due to velocities in lateral direction can also occur, for example due to secondary flow in bends. The order of magnitude of the radial velocity component in bends (v) can be estimated with the equation of Rozovskii [1957], Equation 2.2:

$$v = \frac{ud}{r}\frac{1}{\kappa}\left(F_1(\eta) + \frac{\sqrt{(}g)}{\kappa^2 C}F_2(\eta)\right)\left(1 - exp(-\frac{2\kappa C}{\sqrt{(}g)\frac{z}{d}})\right) \tag{2.2}$$

where d is the water depth, r is the radius, C is the Chézy coefficient, κ is the Von Karman constant (κ = 0.4) and F_1 and F_2 are empirical correction coefficients for the vertical position $\eta = z/d$ [Rozovskii 1957].

Side channels start at a bifurcation and end at a confluence. In side-channel systems, the water levels should be equal for both channels at the bifurcation and confluence. The flow processes due to water level and velocity differences are also present at the confluence. The flow through the openings is mainly driven by the water level differences, based on a 1D-analysis of Van Linge [2017]. Since the study area is limited to the inlet area, it should be noticed that the downstream water levels in the bifurcated channels are interrelated due to the openings and confluence downstream of the study area.

2.2.2. Sill

An inlet sill of longitudinal training walls, which is aligned with the river axis, is similar to side weirs. The flow is aligned with the sill or weir and the flow bifurcates at the sill or weir. A classification of weirs is based on differences in the alignment with the flow. The flow is perpendicular for a plain weir, the flow is at an angle between 0 and 90 degrees for an oblique weir and the flow is aligned for a side weir. The processes of the flow around plain weirs and oblique weirs can also be present in the flow around inlet sills due to similar geometrical properties. Moreover, the inlet sill may function as an obstacle in the flow. The blocking effect of obstacles on the flow has been studied extensively for bottom vanes. The flow processes around plain weirs, oblique weirs and bottom vanes are discussed in this section.

Plain weir

A weir in a uniform channel oriented perpendicularly to the channel axis with a uniform geometry over its width is called a plain weir. The flow accelerates or decelerates when it passes a slope that is oriented perpendicularly to the flow. The acceleration or deceleration causes deformation of the vertical profile. Besides, vertical velocity components can arise at the transition of the slope and the crest resulting in curved flow lines in the vertical plan. A categorization based on this type of curvature is developed by Bos [1976]. Flow lines are more curved atop the weir for larger values of $(H - w)/B_w$ where H is the energy level, w is the sill height and B_w is the width of the sill. Secondary flows in longitudinal direction result in deformation of the vertical velocity profile. Examples of deformed velocity profiles above an upwards slope are shown in Figure 2.5, where Figure 2.5a shows flow measurements above the upstream part of a sill from Blom [1993], Figure 2.5b show flow measurements above a plain weir in the baseline experiments from M.C. Verbeek [van Os 2019] and Figure 2.5c the results of Ali [2013] obtained with the artificial intelligence technique LDA, see the third and fourth profile in Figure 2.5a the second profile in both in Figure 2.5b and 2.5c. For curved streamlines, secondary flow in transverse direction results in helical flow which mainly affects the direction of the bottom shear stress. Besides, vortices are formed behind a plain weir for vertical walls and steep slopes, i.e. abrupt widening in vertical direction, due to flow separation resulting in energy losses [Mosselman, 1998]. This introduction shows the processes around plain weirs: acceleration and deceleration, possible curvature of the flow atop the weir, non-logarithmic or three-dimensional velocity profiles for strongly accelerating flow and helical flow for curved streamlines, vortices behind the weir.

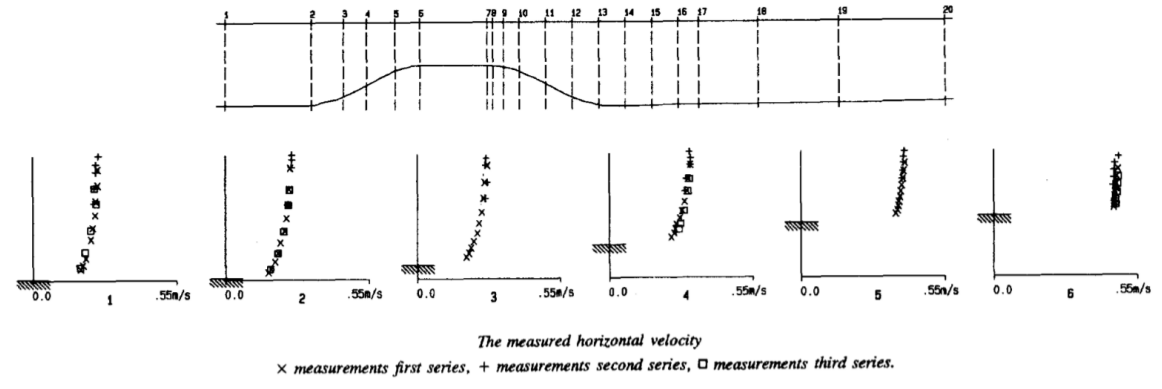

(a)

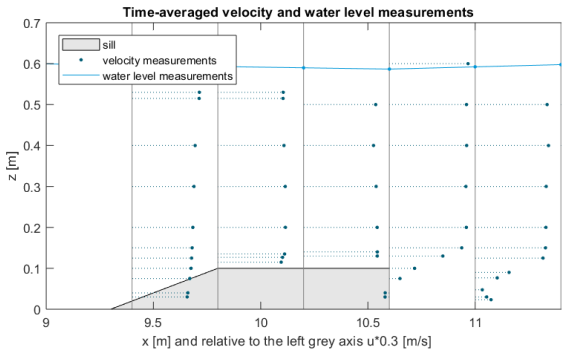

(b)

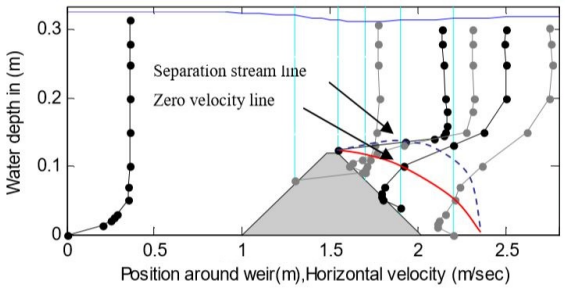

(c)

Figure 2.5: Experimental and modelling results of the flow over sills based on (a) experiments from Blom [1993] (b) experiments from M.C. Verbeek van Os [2019] and (c) LDA results from Ali [2013]

Oblique weir

The flow at the inlet sill approaches the inlet sill under an angle. This phenomenon can be studied considering a straight channel with an obliquely placed weir, see Figure 2.6. Flow over an oblique weir has a perpendicular and parallel component relative to the weir crest. The perpendicular component experiences an acceleration or deceleration on the upward and downward slope, respectively. The pressure differences affect the angle of the perpendicular component. On the downward side of the sill, flow separation due to a steep slope or a large oblique angle with respect to the channel axis results in local energy losses. The component parallel to the upward slope of the sill exchanges lateral momentum with the sill (wall friction) resulting in a slower flow behind the weir. This exchange affects the flow at both sides. Besides, the velocity gradients perpendicular to the flow create helical flow [Mosselman 1998].

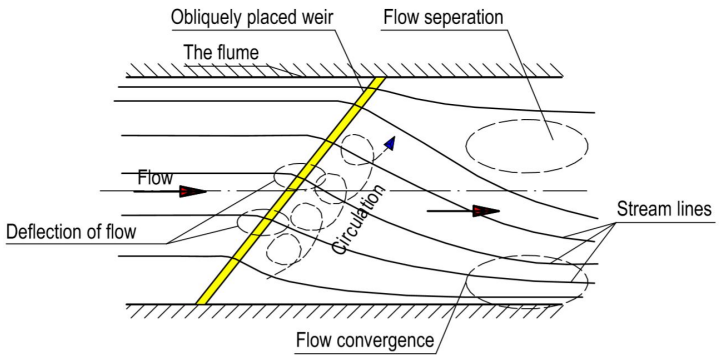

Figure 2.6: Flow patterns around an oblique weir [Nguyen 2006]

Aichel [1953] developed an empirical relation for the specific discharge for an oblique weir dependent on the

specific discharge of a plain weir, Equation 2.3.

$$\frac{q}{q_\perp} = 1 - \beta_a \frac{h_0 - a}{a} \tag{2.3}$$

where q is the specific discharge of the oblique weir, $q_\perp$ is the specific discharge of a plain weir, β_a is the coefficient for the oblique effects, a is the sill height and h_0 is the upstream water level.

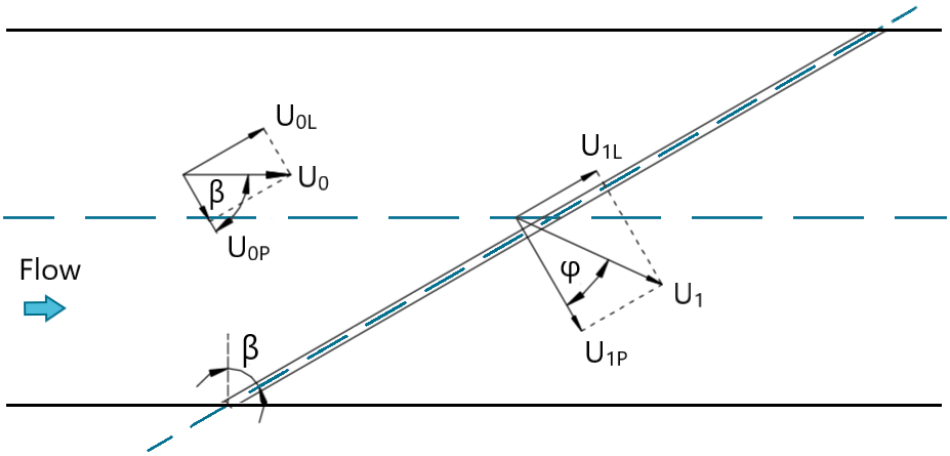

Figure 2.7: Oblique weir with decomposed vectors of the flow velocity [based on Nguyen [2006]]

Since available discharge formulas for oblique weirs are highly empirical, Wols et al. [2006] did a thought experiment to improve understanding of the processes. The flow component parallel to the weir is assumed not to be affected by the weir, since pressure gradients are not significant in this direction. The bed friction is neglected, but not the energy losses downstream of the weir. Therefore, the energy balance can be applied to the perpendicular flow velocity component for the upstream part of the weir. In addition, the momentum balance is applied for the downstream part, because of the energy losses.

This provides the following insights. At the upstream slope, the flow direction changes towards the crest-normal direction due to the increase in velocity. For larger water levels, the relative increase of the velocity above the weir is smaller resulting in a larger angle with respect to the weir crest. For very high water levels, the effect of the weir is not significant anymore. Then, the deviation of the flow direction from the perpendicular direction to the sill crest is approximately equal to the angel between the weir crest and channel axis, $\beta \approx \phi$, see Figure 2.7. This is in accordance with the empirical formula of Aichel [1953]. For an increasingly wide weir, the flow would downstream keep its direction. Energy losses due to vertical widening and bed friction reduce the velocity magnitude. In the middle of the flume just behind the sill, the flow direction is expected to be in accordance with the momentum conservation for the perpendicular flow component. Far upstream, the flow angle is parallel to the channel. Tuyen [2005] shows that the analytical computation based on velocity decomposition for oblique weirs fits quite well with experimental results for two angles of obliqueness (45 and 60°).

Bottom vanes

The inlet sill may function as an obstacle by blocking the flow towards the sheltered channel in the lower layers. The blocking effect can be understood from processes around submerged bottom vanes.

Bottom vanes can be placed under an angle of attack. For small angles of attack, the bottom vanes induces helical flow structures [Odgaard and Wang 1991]. Blockage and turbulence principles come into play for large angles of attack [Marelius and Sinha 1998]. The blocking effect is especially relevant for inlet sills. Marelius and Sinha [1998] investigated bottom vanes with larger angles of attack and found that the vortex and thus the transverse flow velocities reaches its maximum strength for an angle of 40 degrees. The dominant flow structures were two suction side vortices and a horseshoe vortex, see their experimental results in Figure 2.8.

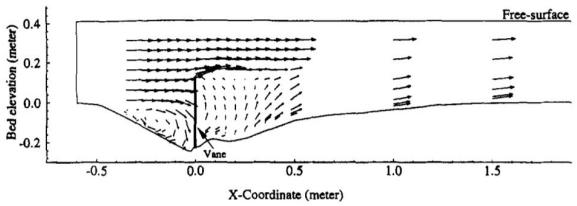

(a) Longitudinal cross sectional view (at y = 0.0m) of velocity vectors at optimal angle of attack (40°) [Marelius and Sinha 1998]

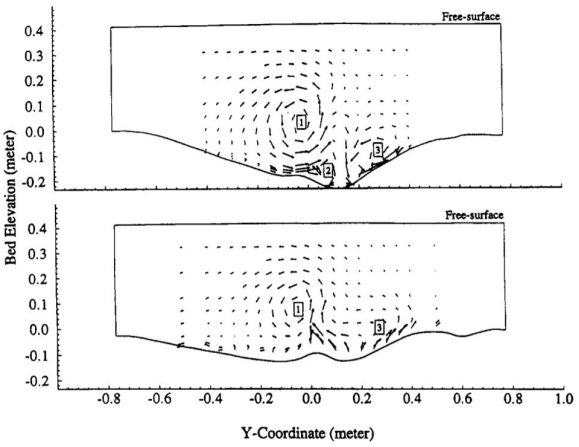

(b) Velocity vectors at two cross sections at optimal angle of attack (40°): (a) X = 0.15 m; (b) X = 0.48 m; Indicated vortices are identified as (1) counterclockwise suction side vortex, (2) clockwise suction side vortex and (3) horseshoe vortex [Marelius and Sinha 1998]

Figure 2.8: Flow structures around submerged bottom vanes

The mechanism of these flow structures are explained in this paragraph. A bottom vane is oriented perpendicular to the flow and has a hydrostatic pressure distribution at both sides. Upstream flow forces work according to the momentum balance which (initially) can be coupled to a logarithmic velocity profile. This distribution can be added to the hydrostatic pressure distribution. The result is a steeper pressure distribution on the bottom vane. This implies overpressure at the top and under pressure at the bottom. Due to this overpressure at the top, the flow dives to the bottom, resulting in a vortex in the vertical plane. At the upper side, a pressure difference is present between the upstream and downstream side of the vane. Therefore, the flow does not dive downward close to the upper side, but this pressure difference pulls the flow upward over the vane, see Figure 2.9a. Another bottom vane is oriented obliquely in the flow. The flow near the bottom is directed along the vane, see Figure 2.9b. In combination with the vortex due to the diving flow, this results in a helical flow whose direction of rotation is opposite to that of the helical current due to curved streamlines atop the vane, see Figure 2.9c.

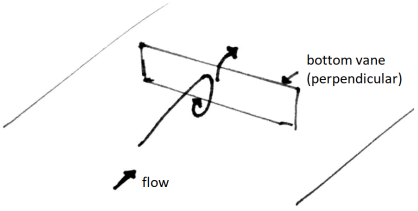

(a) Flow patterns in front of a perpendicular bottom vane

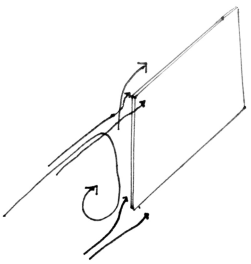

(b) Separate flow patterns in front and along an oblique bottom vane

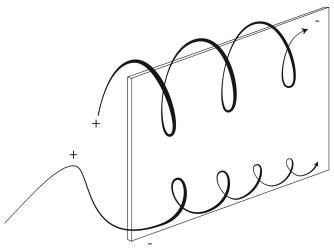

(c) Combined flow patterns in front and along an oblique bottom vane

Figure 2.9: Flow structures around submerged bottom vanes

2.2.3. Inlet of longitudinal training walls

The effect of the sill height on the morphology around longitudinal training walls has been studied by De Ruijsscher et al. [2019]. The angles with respect to the main flow direction at the upstream toe of the sill show differences over the sill length and water depth for variation in discharge and sill height, see the results in Appendix A.1.2. The variation of the flow angle over depth indicates the presence of three-dimensional flow structures.

Van Linge [2017] has evaluated the flow using depth-averaged models. He defines a dimensionless crest height W_{inlet} as the crest height to energy level ratio $W_{inlet} = w/H$. Besides, he refers to the sheltered channel as side channel. A top view with velocity vectors and flow magnitudes is shown in Figure 2.10. A secondary circulation cell is formed in the sheltered channel at the location of the inlet which has approximately the same length as the inlet and the flow returns at the bank of the sheltered channel. Just downstream of the inlet against the longitudinal training wall a stagnant zone is located where the velocity is nearly zero at the longitudinal training wall.

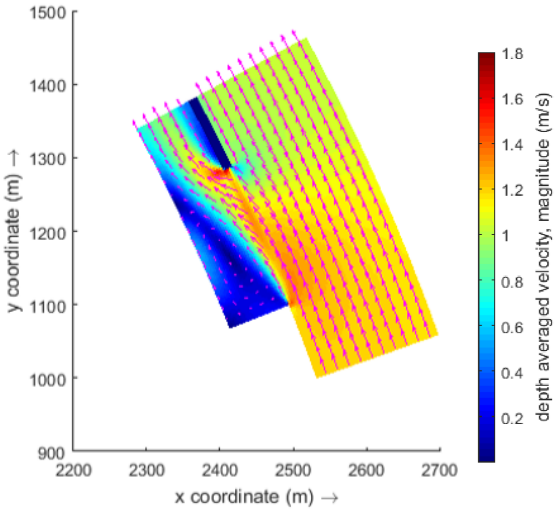

Figure 2.10: Velocity magnitudes and flow angles around the inlet from the Delft3D-Flow model runs with W_{inlet} = 0.46 [Van Linge 2017]

Figure 2.11 shows the variation of the specific discharge in longitudinal direction to the cross-sectional averaged discharge for various dimensionless crest heights. This shows at which location most discharge enters the sheltered channel. The specific discharge increases in downstream direction. This increase is stronger for smaller crest heights. The curves with nearly constant discharge correspond to critical flow above the crest (W > 0.9).

Flow angles atop the inlet increase for larger dimensionless crest heights (W = w/H), see Figure 2.12. The increase in flow angle in longitudinal direction is biggest at the downstream side. The flow angle is maximum at the downstream end, where it has a value of about 85 degrees, independent on the crest height.

The largest velocities are noticed above the inlet crest. Figure 2.13 shows the transverse, lateral and total velocity magnitudes above the inlet crest in longitudinal direction for a dimensionless crest height of W = 0.46. The total velocity has a peak at the downstream end. Van Linge expects this effect to be "partly numerical due to the sharp step-wise increase in bathymetry at the transition of the inlet and longitudinal training dam" [Van Linge 2017]. The quick acceleration in longitudinal direction at the upstream side can be explained by the abrupt widening. The longitudinal velocity magnitude has a small negative tangent at the middle of the crest and, at the downstream end, it decreases quickly. In lateral direction, velocity magnitude increases relatively linear in downstream direction and it is maximum at the downstream end.

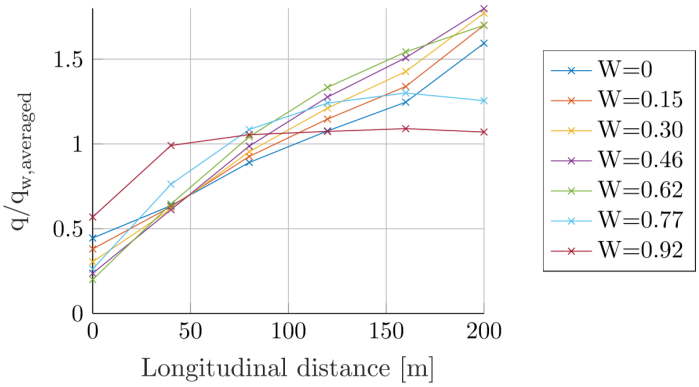

Figure 2.11: Longitudinal variation of specific discharge over the inlet for various dimensionless crest heights (W = w/H) [Van Linge 2017]

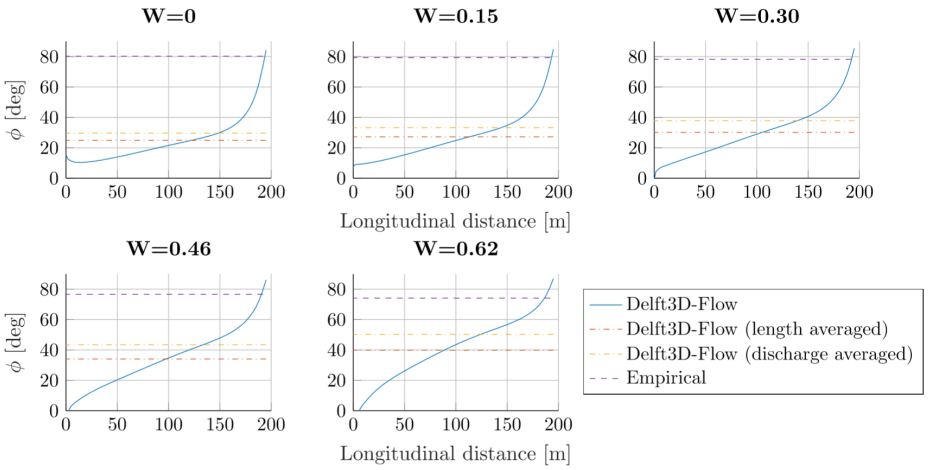

Figure 2.12: Flow angles atop the inlet increase for various dimensionless crest heights (W = w/H) [Van Linge 2017]

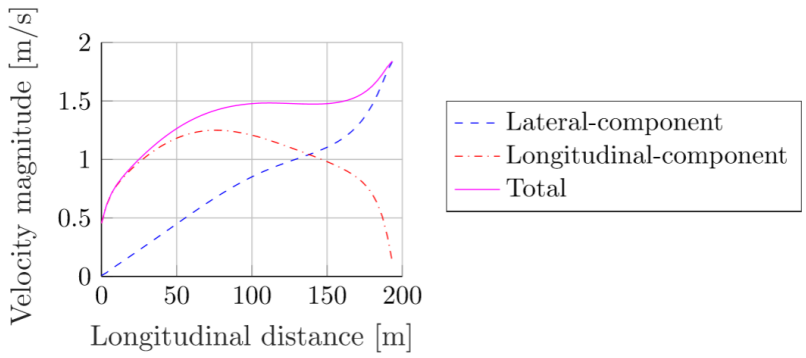

Figure 2.13: Velocities magnitude atop the inlet for specific dimensionless crest heights (W_{inlet} = 0.46) [Van Linge 2017]

Figure 2.14 shows the dependence of the discharge ratio on dimensionless design parameters: the dimensionless crest height and channel ratio. The discharge ratio towards the side channel decreases for larger relative sill heights with a relatively stronger decrease from W > 0.7. The discharge ratio towards the side channel decreases with a smaller relative side channel width. This knowledge has been used to discuss the experimental design, Chapter 7.

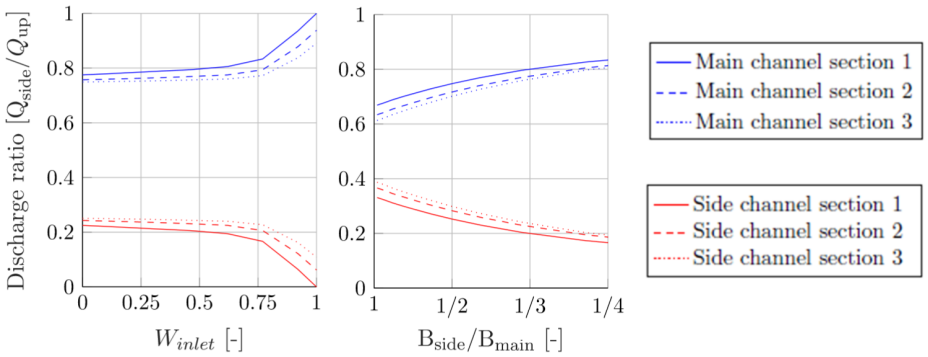

Figure 2.14: Influence of the dimensionless inlet crest height and channel width ratio on the discharge distribution towards the main (blue lines) and sheltered side channel (red lines)

2.2.4. Depth-averaged modelling of the flow at inlet of longitudinal training walls

This study aims to obtain knowledge about the three-dimensional flow structures for the development of a parameterisation of sediment transport over inlet sills of longitudinal training walls. To this end, it is important to know the assumptions for 2D flow and already available corrections for 3D flow effects. River modelling software Delft3D is used in the Netherlands to assess the hydrodynamic and dynamic-morphological effects of river interventions [Doornekamp et al. 2019]. In a depth-averaged model, an unambiguous relation has to be assumed for the vertical velocity profile. A logarithmic velocity profile is valid for developed turbulent flows in rivers. A logarithmic vertical velocity profile implies a no-slip condition at the closed boundary, in other words the bed, and a slip condition at the open boundary, in other words the water surface. The no-slip condition is valid when the velocity at the bed is nearly zero and thus negligible due to the bed shear stress. The slip condition is valid when the shear stress between the air and the water surface is negligible [Deltares 2020].

Correction for secondary flow

Delft3D has an option to correct for the effect of secondary flow due to curved flow on the bed shear stress. This adds the influence of helical flow such as in river bends to the momentum transport. The secondary flow is defined as the velocity component $v(\sigma)$ normal to the depth-averaged main flow. The magnitude of this velocity component along the vertical is expressed with the spiral motion intensity of the secondary flow I. The vertical distribution on the secondary flow is assumed to be a universal function of the vertical coordinate $f(\sigma)$). The local velocity distribution is implemented as a multiplication of this universal function with the spiral motion intensity. Then, the flow consists of the main flow with a logarithmic velocity profile and the secondary flow with a universal function directed perpendicularly to the main flow, see Figure 2.15.

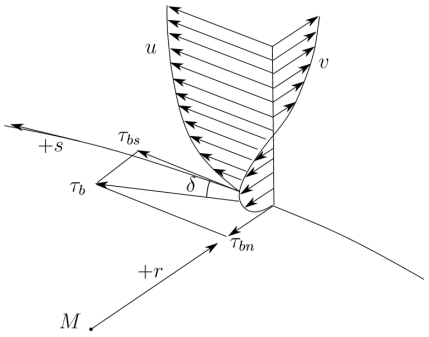

Figure 2.15: Vertical profile of secondary flow (v) in a river bend with radius r, along the streamline +s with primary flow (u) and the bed stress τ_b.

Correction for energy losses

The effect of energy losses due to 3D flow structures on the discharge can be calculated with discharge and

submergence coefficients. The discharge coefficient corrects of energy losses due to variation in weir types and flow conditions. The submergence coefficient makes the formula also applicable for transitional and submerged conditions. Van Linge [2017] found that the plain weir formula with discharge coefficient of Hager [1987] and the submergence coefficient of Ka-Leung Lee [2002] are most suitable, from the available formulas, for modelling the discharge over the inlet sill of longitudinal training walls in depth-averaged models. In addition, he suggested an improvement based on curve fitting for the case of inlet sills of longitudinal training walls. See Appendix A for details.

2.2.5. Overview flow processes and structures

Water level gradients and velocity gradients drive the flow. Bend flow affects these gradients. Possible flow patterns around the inlet are: secondary flow due to curvature, deformation of the velocity profile due to acceleration as shown for plain weirs, circulation behind the sill which occur for oblique weirs, blocking due to the sill similar to bottom vanes, flow separation with recirculation at the upstream part of the sheltered channel and stagnation along the longitudinal training wall in the sheltered channel. Flow mechanisms around longitudinal training walls are flow due to differences in longitudinal water level gradients, lateral water level gradients, flow velocity gradients. Possible three-dimensional flow processes around the inlet sill are curved flow inducing helical flow, deformation of the logarithmic velocity profile due to acceleration and deceleration of the flow and blocking and deflection of the flow due to obstacles. The flow has three-dimensional structures due to i) deformation of the logarithmic velocity profile due to acceleration and deceleration of the flow and ii) blocking and deflection of the flow due to obstacles. However, software for river models only includes the following three-dimensional effects: energy losses above weirs and the effect of helical flow on bed shear stresses.

2.3. Sediment transport over the inlet sill

To gain insight in sediment transport processes which contribute to understanding and description of sediment transport over inlet sills, the following topics has been discussed in the section below: sediment transport mode, sediment transport formulas, sediment transport on transverse slopes, and sediment transport over inlet sills of longitudinal training walls.

2.3.1. Sediment transport mode

Sediment transport can be distinguished according to origin by wash load and bed material load and in transport mechanism according to suspended load and bed load. See Figure 2.16a for an overview. Wash load is suspended load that originates only from the water column. The wash load does not affect the channel slope and sediment composition, since there is no interaction with the bed. Suspended bed-material load is suspended load that interacts with the bed sediment and thus affects the channel slope and bed surface texture. Bed load is the remaining part of the bed material load. Bed load responds faster to variations in flow conditions than suspended load. Bed load has small lag effects in time and space [Phillips and Shutherland 1989, 1990], but these are usually neglected in practice. In other words, immediate adaptation is assumed [Mosselman 2005]. Bed load is transported by rolling, sliding and saltation.

Only mobile sediment stays in contact with the bed and is transported by rolling and sliding [Bagnold 1977]. When the mobility is higher, the particles hop over the bed, periodically losing their contact with the bed. This transport mode is called saltation [Bridge and Bennett 1992]. Particles with a higher mobility lose their contact with the bed and are kept into suspension [Van Rijn, 1984]. The mobility and therefore transport mode are dependent on the flow velocity, grain size and density. It is possible that saltating particles move uphill in suspension and downhill in contact with the bed, because particles are not constantly affected by the gravitational pull due to their periodical contact with the bed [Sekine and Parker, 1992; Baar, 2019] So, the sediment trajectory on a transverse slope is affected by the transport mode. In this study, bed-material load in the main channel is considered. Thereby, the sediment in the studied area is expected to be bed-load based on two assumptions: 1) the bed-material load stays on the bed at least until the downstream edge of the sill and 2) sediment on the downstream slope is not transported back to the top of the sill.

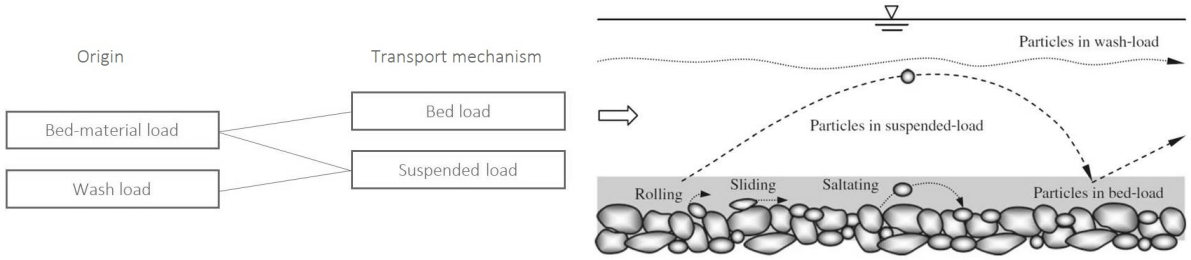

Figure 2.16: Classification of sediment transport: (a) based on origin and transport mechanisms [based on Jansen et al., 2010] and (b) drawing of transport mechanisms [Dey, 2014]

2.3.2. Sediment transport formulas

Formulas that describe sediment transport of bed-load are developed for horizontal alluvial beds. The sill has slopes and, since the sill consists of rocks, the bed is non-alluvial bed with an irregular surface. So existing total transport formulas are not valid for the sediment transport over the inlet sill. To gain insight in the bed-load transport, the behaviour of sediment particles on transverse slopes is discussed in the following subsection.

2.3.3. Transverse slopes

The bed-load transport on transverse slopes is discussed in this section. First, the force balance for particles on a transverse slope that stay in contact with the bed. Rolling and sliding particles are in constant contact with the slope. Secondly, the initiation of motion of sediment particles on slopes is discussed. Then, a thought experiment about particle trajectories of saltating particles which jump over the bed is described. This explains physical mechanisms that play a role for saltation.

Force balance for bed load

The forces acting on a particle on a transverse slope are described by Van Rijn [1993]. The forces are presented in Figure 2.17. The lift force F_L and the gravitational force component $F_G cos(\alpha)$ are perpendicular to the slope. The gravity force component $F_G sin(\alpha)$ is directed downwards on the slope. The drag force F_D is in flow direction and the friction force F_R against flow direction. Flow contraction at the top of the sediment particles cause an upwards lift force F_L, see equation 2.5. Energy loss behind the particle creates a drag force F_D in flow direction, see equation 2.4. There is no transverse force when the flow angle γ=0. The transverse drag force is uphill for a positive flow angle and downhill for a negative flow angle.

$$F_D = \frac{1}{2} C_D \rho u_r^2 A \tag{2.4}$$

$$F_L = \frac{1}{2} C_L \rho u_r^2 A \tag{2.5}$$

with the drag force coefficient C_D and lift force coefficient C_L, the density of water ρ, the surface particle A (for spheres: $A = (\frac{1}{4}\pi D^2)$. The ratio between the longitudinal and transverse drag force is equal to the flow angle. The relative velocity u_r is the difference between the flow and particle velocity.

The gravitational force acts in a downward direction on particles. The magnitude of the gravitational force F_G is the submerged weight of the sediment multiplied by the gravitational acceleration:

$$F_G = (\rho_s - \rho) g V \tag{2.6}$$

Friction depends on the angle of repose ϕ of the sediment and is the resulting force directed opposite to the motion:

$$F_R = tan(\phi)(F_L - F_G) \tag{2.7}$$

The lift and drag force are both affected by the flow and are both dependent on the relative velocity squared u_r^2. Neglecting friction, the particle velocity increases linearly with flow velocity for equal particle properties, geometry and coefficients. Because the lift force reduces the friction force, the lift force has an (indirect)

enhancing effect on the particle velocity for an increase in flow velocity. (Note that the lift force can affect the transport mode.) Furthermore, the lift and drag forces are dependent on the particle surface, whereas the gravitational force is dependent on the particle volume. Thus, the grain size is important in this balance.

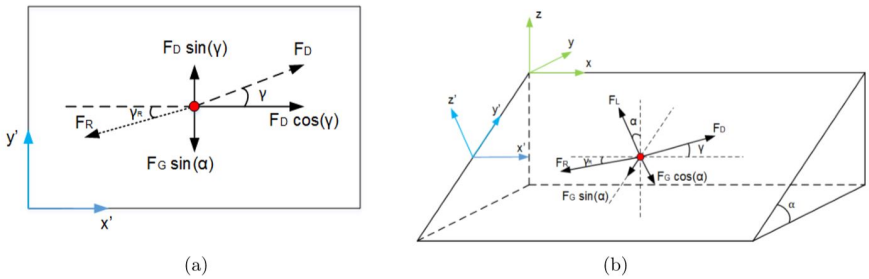

Figure 2.17: Force balance of particles: (a) schematisation of the forces in the x'y' plane and (b) schematisation of the forces in three directions, where the x'y' plain represents the slope [Jammers, 2017]

Particle trajectory

The force balance and initiation of motion are discussed for particles in contact with the bed. Saltation is a common transport mode during which a particle jumps over the bed. In this paragraph, the behaviour of a saltating particle is explained. Sekine and Parker [1992] did a thought experiment about the effect of gravity on saltating particles on a transverse slope. They considered a sequence of ballistic trajectories on a smooth surface on a slope that is only tilted in transverse direction y' in a vacuum space with a fully elastic collision with the bed. The initial particle velocity has no component in the y'-direction. At the end of a ballistic trajectory the velocity decreases to zero and the particle touches the bottom and rebounds elastically. The resulting velocity direction after the rebound has a component in the y'-direction. The gravity adds transverse momentum to the particle with every rebound. Therefore, the length of the trajectories increases and the velocity is more directed in the y'-direction with every bounce. In conclusion, due to this physical mechanism, saltating particles tend to move downward on transverse slopes.

The difference in the force balance between particles that stay in contact with the bed and particles that do not stay in contact with it, is the water pressure on the particle surface that can stay in contact with the bed. This additional water pressure on the particle depends on the shape and size of the particle, the bed roughness and the water depth. The effect of the described mechanism mainly depends on the relative velocity and the additional water pressure. In general, this effect is expected to be small.

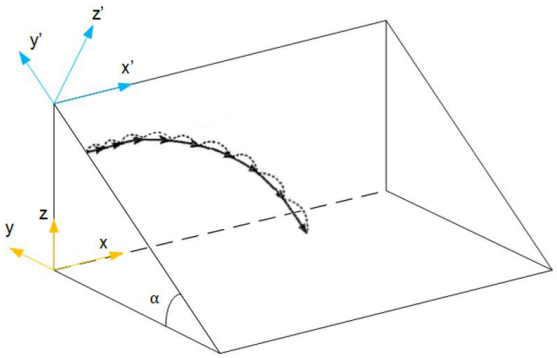

Figure 2.18: Sequence of ballistic trajectories over a transverse slope based on Sekine and Parker [1992] and Jammers [2017]

2.3.4. Inlet of longitudinal training walls

Jammers [2017] developed a particle model to calculate particle trajectories of bed-load sediments over the inlet sill of longitudinal training walls. This model is based on the force balance of Van Rijn [1993]. The published results with non-uniform flow, depth-averaged flow results have been used as input for this thesis. The flow angle and flow velocity magnitude of the input data are shown in Figure 2.19.

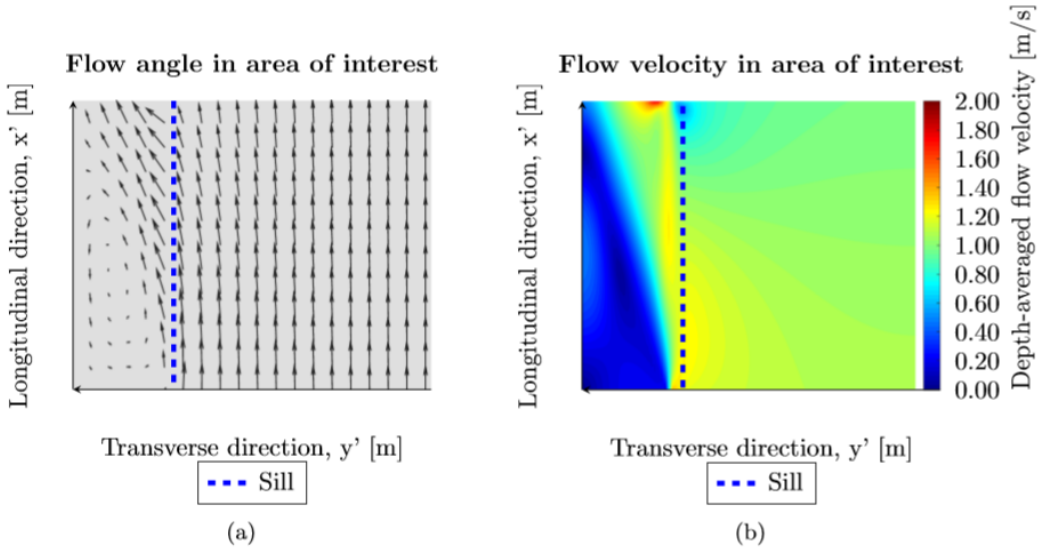

Figure 2.19: Flow angle and flow velocity magnitude of the data used as input for the particle model by Jammers [2017]

Figure 2.20 shows the result of the particle model for slope angles of 15°and 20°. The steeper the slope, the less sediment is transported over the sill. The slope of the inlet sill is 1:2.5, thus the angle is atan(1/2.5) = 21.80°. Since this is close to 20°, the model results for 20°can give insight in the sediment trajectories above the inlet sill. No particles entered the sill in the simulation, but field measurements show sedimentation in the sheltered channel. Hence, the results for a smaller slope angle are also shown, which give insight in possible paths of particles that enter the sill.

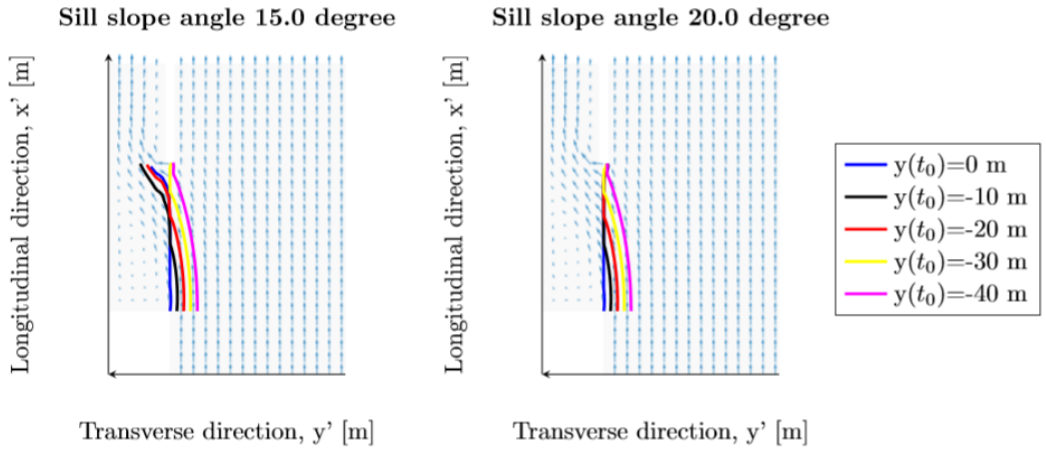

Figure 2.20: Particle trajectories for transverse slopes α=15°and α=20°.

2.4. Conclusion

Longitudinal training walls divide the flow in a main and sheltered channel. A sill at the inlet affects the discharge and sediment distribution to get a more morphologically stable system. How the discharge distribution can be calculated in a depth-averaged model is investigated by Van Linge [2017]. Besides, Jammers [2017] developed a particle model based on the force balance of Van Rijn [1993]. The particle model with flow from the depth-averaged model as input gives no sediment transport over the inlet sill, while bed measurements in the pilot project show sedimentation. Therefore, the sediment transport towards the sheltered channel is not fully understood.

The flow has three-dimensional structures caused by deformation of the logarithmic velocity profile due to acceleration and deceleration of the flow and due to blocking and deflection of the flow due to obstacles.

Software for river models includes (only) the following three-dimensional effects: energy losses above weirs and the effect of helical flow on bed shear stresses. Besides, the simple total transport formula is not valid for the sediment transport over the inlet sill, because (1) the flow has no logarithmic velocity profile with an unambiguous relationship between depth-average flow velocities and bottom shear stresses, (2) the bed has slopes; (3) the bed is non-alluvial (from rock) and (4) the bed has an irregular surface (from rock).

3

Methodology

The flow around longitudinal training walls has been investigated in a series of flume experiments in the Environmental Fluid Mechanics Laboratory of Delft University of Technology. The experiments aimed to obtain more knowledge on the flow around the inlet sill of longitudinal training walls for a better understanding of sediment transport over the inlet sill towards the sheltered channel behind longitudinal training walls. Insight into this sediment transport is needed for the development of a suitable parameterisation to be implemented in depth-averaged morphological models.

3.1. Experimental setup

3.1.1. Geometry

The geometry is schematized to filter processes and effects that are less relevant by reducing the complexity of the geometry. In addition, the geometry is scaled to fit into the flume. The choices for the scaling and schematisation are discussed first, then the design is shown and explained.

Design

The aim of the experiments is to represent the main flow structures at the inlet of longitudinal training walls to identify the sediment transport mechanisms. Therefore, the condition for scaling and schematisation of the geometry is that the representation of the main flow structures in the experiments have to be remained. Knowledge on the longitudinal training walls in the river Waal near Wamel has been used to determine the schematized geometry (e.g. dimensions of the design, flow characteristics, importance of flow mechanisms).

The study area is the inlet area of the longitudinal training dams. The openings and outlet of the channel system of the longitudinal training dams are not taken into account in this research project. The geometry in the flume should induce the same flow structures as in the river. Therefore, the dimensions of the sill and the width of the sheltered channel are scaled equally in the experimental setup (with scale 1:75). An exception has been made for the width of the main channel. This scale (1:125) is smaller relative to the other dimensions (with scale 1:75), because that allows for a larger variation of the sill height to water depth ratio. A relative reduction of width of the main channel implies a larger scale of the sill and hence makes a larger variation of the sill height to water depth ratio possible. Besides, the requirement for the experiments is to represent the main flow patterns and show the effect of the chosen parameters, thus not to represent as accurately as possible the flow in the pilot project.
Besides, it is important to reduce additional secondary structures for a clear reproduction of the main flow structures. In the river, the bank of the upchannel is located at the upstream toe of the sill. To prevent secondary flow effects above the sill as a result of the sharp edge at the upstream side of the inlet, the location of the bank has been shifted to the crest of the sill. In addition, the geometry of the sill is extended over the entire length of the experimental setup to reduce secondary flow effects as result of a break in this geometry.

The complexity of the geometry is reduced to schematize the geometry with the following simplifications:

– The longitudinal training wall is represented by a vertical plate. The function of the longitudinal training wall is to separate the flow and this function has been maintained. In addition, since the scope is

limited for conditions without overflow, it was not necessary to keep the same shape for the representation of the flow over the longitudinal wall.

- The plate that represents the longitudinal training wall was not scaled with other parts of the geometry, but has the same height as the flume. This is a practical choice to prevent overflow.

- The bottom in the main and sheltered channel have the same level, while the difference between the bed levels in the Waal is 1 meter. This difference in bed level does not have to be included, since it is not expected to introduce additional flow patterns.

- The bottom has a constant level over the width over channels, thus it does not include bed forms, banks with a gradual slope and other roughness elements. Bed forms can affect the sediment transport significantly. See for example the study on morphology around the longitudinal training walls in the Waal [De Ruijsscher et al., 2019] or the study on morphology around longitudinal training walls without sill [Le, 2019]. Although the corresponding sediment transport processes are important, this topic is out of the scope of this research study. Moreover, remnants of the previous groynes increase the roughness in the sheltered channel relative to the main channel.

- There is no river bend. The effect of the bend has a 1%-effect on the discharge distribution according to the 1D analysis of Van Linge [2017]. The secondary flow in bends can affect the sediment transport. Since flow and sediment transport in river bends are already studied extensively (e.g. Rozovskii [1957] and Baar [2019]), the bend does not have to be included into these experiments. Besides, the secondary bend flow disturbs other flow patterns that are needed to identify the main sediment transport mechanisms over an inlet sill of longitudinal training dams. Therefore, the bend is not included, although it is important to be aware of bend effects.

Schematisation
The experimental setup is a simplified representation of the inlet design of the longitudinal training wall near Wamel in the river Waal. The experiments have been carried out in a horizontal shallow-water flume made of glass. The bottom has been plated with white PVC plates. The flume is 3 m wide, 20 m long and 0.2 m high. Only the downstream 10.6 m part has been used for this experiment. The experimental setup consists of a bifurcation with a sill at the entrance of the sheltered channel. A top view is shown in Figure 3.1. The main channel has a width of 1.87 m. The other remaining 1.13 m of the flume consists of three areas. Upstream, there is a zero-discharge zone separated by a wooden plate. Then, there is an inlet area with a length of 2.66 m. Downstream of the inlet, the third zone, is the sheltered channel separated from the main channel by a wooden plate that represents the training wall. The width of the sheltered channel is 1.13 m. The sill is located at the entrance of the sheltered channel and has a height of 51.5 mm, a slope of 1:2.33 and a 27-mm wide crest. It is constructed out of wood, painted white and attached with white glue to prevent leakage underneath. The geometry of the sill is extended over the entire length of the experimental setup to reduce secondary flow effects as a result of a break in this geometry. A side view is shown in Figure 3.2.

The inflow discharge can be regulated with a valve. At the downstream end, two replaceable weirs are present to regulate the discharge distribution and water depths in the main channel and the sheltered channel, respectively. So, the valve and weirs were used to set the flow conditions. Downstream of the flume, water flows back to the central basin of the laboratory. Therefore, the inflow discharge is independent on the outflow. Additional measures have been taken to smooth the flow. At the upstream side, an inlet structure of corrugated sheets forming a honeycomb pattern is placed to make the flow more uniform. Downstream of this inlet structure, floating Styrofoam plates are placed to damp waves and increase turbulence. Furthermore, a sieve is placed behind the flume to catch tracer materials. This sieve does not affect the flow, because the water flows over a weir before it passes through the sieve.

The coordinate system is defined as follows: x is directed positive in streamwise direction and x = 0 is at the upstream end of the inlet, y is directed positive from the side channel towards the main channel and y = 0 is at the edge of the slope and the crest on the main channel side and z is directed positive downwards and z = 0 is at the bed level of the channels. The axes are indicated in the top view and side view, Figure 3.1 and 3.2.

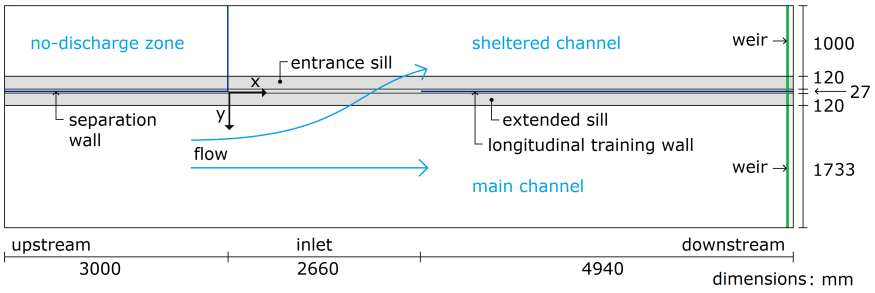

Figure 3.1: Top view of the experimental setup where the blue arrow indicates the flow direction, the grey area represents the sill, the blue lines are the wooden plates and the green lines represent the downstream weirs.

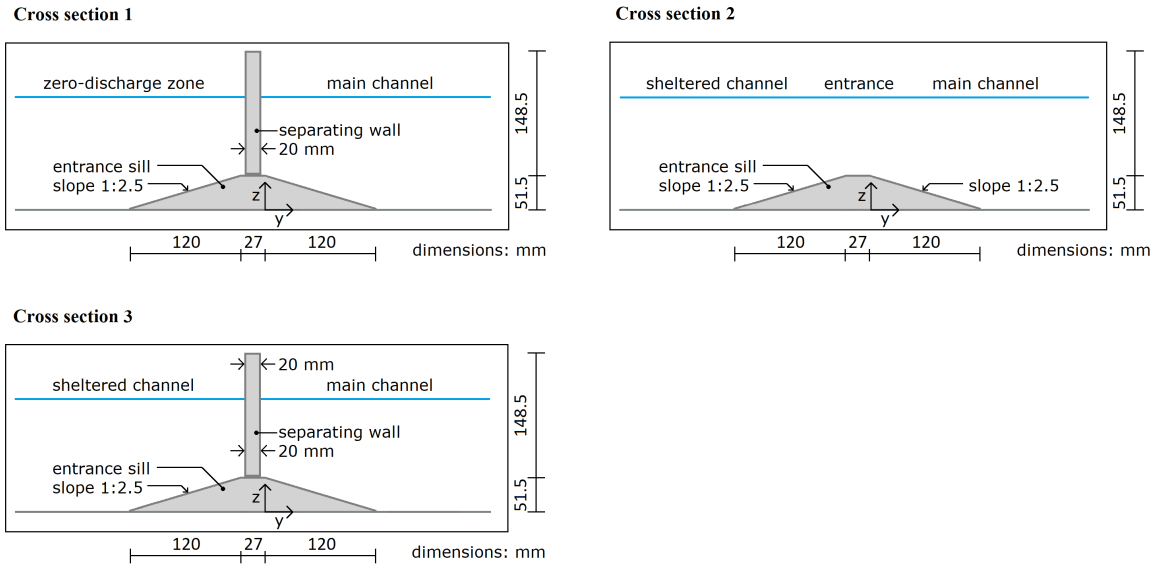

Figure 3.2: Side views of the experimental setup at cross section 1 located upstream of the entrance, cross section 2 at the entrance and cross section 3 downstream of the entrance.

3.1.2. Sediment

The bed in the flume consists of PVC plates connected with glue. Fine sediments are not allowed in the flume, because these cannot be caught to prevent entering of these particles in the central water system of the laboratory. Therefore, it is not possible to measure sediment transport in a direct way. Other material has been chosen to study the effects on the sediment distribution at the inlet. Solid plastic bullet balls for airsoft guns appear to be suitable for this purpose. The balls have a diameter of d_s = 5.9 mm and a density of ρ_s = 1050 kg/m^3. The balls have a slightly larger density than water and therefore sink to the bottom. The behaviour of these balls is mostly similar to water, although the transport is slightly different due to momentum and the submerged weight. The velocity of these balls can be determined with Particle Tracking Velocimetry (PTV), see Section 3.2.3 for more information about this technique. Therefore, the balls are visible on the image of the camera in the setup for PTV with multiple pixels per ball and enough contrast. These balls were available in a bright red color, which ensures a good contrast with the white bottom of the flume for the measurements. For more information about the measurements with these particles, see Section 3.2.3.

3.1.3. Experimental conditions

The effect of the following dimensionless parameters on the flow is studied in this research: 1) the sill height over water level above the sill crest and 2) the discharge through the side channel over the discharge through the main channel. Therefore, these parameters have been varied indirectly by adapting the downstream weir

heights, while keeping the total discharge of 35 l/s constant.

The experimental conditions were defined based on the downstream weir height combinations. Experimental setups defined with the letter A correspond to low downstream weir heights (less than 80 mm). The letter B setup, on the other hand has high weir heights (above 140 mm). The weir heights are approximately equal for cases 1, the weir height in the main channel is higher than in the sheltered channel in case 2. The experimental conditions are shown in Table 3.1. The difference in high and low downstream weir heights (indicated as A and B) results in a significant difference in the water depth above the sill crest. This can be coupled to the dimensionless ratio of sill height to water depth above the sill crest. Variation of the weir heights of the main and sheltered channel (indicated as 1 and 2) results in different discharge distributions towards the main and sheltered channel.

Table 3.1: Experimental conditions. The weirs are higher in cases A and lower in cases B. The weir heights are equal for cases 1 and the weir height in the main channel is higher than in the side channel for cases 2.

Name of experiment	Experimental conditions		Dimensionless parameters	
	Weir height sheltered channel [mm]	Weir height main channel [mm]	Discharge distribution $Q_{sheltered}/Q_{main}$ [-]	Sill height to water depth ratio [-]
A1	80	80	0.55	0.95
A2	60	80	0.75	1.10
B1	145	140	0.49	0.43

3.2. Measurements

The measurements consists of three parts: 1) point measurements with ADV in the middle of the water column, 2) flow field measurements at the water surface with PIV using floating tracer particles and 3) sediment transport or bed measurements with PTV, using the described red balls as tracer particles. The point measurements in the middle of the water column are done to obtain insight into the flow properties in the middle of the water column. These are meant to be representative for the depth-average flow. The PIV measurements give additional information about the flow patterns in the higher part of the water column. Together this will give a good overview of the flow conditions in the upper to middle part of the water column as depth-average flow models calculate. The measurements of particles rolling over the bed give as output particle trajectories, in which the behaviour of the traced particles is in between those of water and sediment. This combination of measurements is meant to give insight in the variation of the flow velocity over depth as well as over horizontally above the sill and therefore the three-dimensional flow structures. The choices for the techniques are discussed in more detail in Section 3.2.1-3.2.3. The techniques are also described in these sections.

The upstream discharge is measured with a discharge meter in the pipes between the valve and the flume. The type of discharge meter is PROline Prosonic Flow 93, which has an accuracy of circa 2 l/s. The effect of the discharge distribution and the sill height to water depth ratio on the flow is studied in the experiments. Therefore, these parameters need to be determined. The discharges in the main and side channel are determined by water level measurements and the theory of a Rehbock weir. Besides, the water level above the sill is determined using a point gauge. These measurements are described in Section 3.2.4. Finally, the specifications of the measurements are summarized in Section 3.2.5.

3.2.1. Acoustic Doppler velocimetry (ADV)

To improve understanding of the processes, data in which the (three-dimensional) flow structures can be identified are needed. These are data at locations spread in horizontal and vertical directions. It requires, in addition to data about flow near the bottom and at the water surface, data of flow in the water column. Assuming measurements at mid-depth are representative for depth-averaged model results, data at mid-depth might give better insight into the flow to make practical recommendations for the development of the parameterisation that solves the gap between mid-depth flow and bed-material transport originating from the

main channel. Field measurements cannot be used for measurements at mid-depth, because it is not possible to confine particles to a thin layer at mid-depth with variation in the distance from the bed. However, point measurements can be performed in the water column at mid-depth. The acoustic Doppler velocimetry (ADV) technique is preferred above electromagnetic techniques, because it is less sensitive to disturbances and it also provides vertical velocities that might contribute to the identification of flow patterns and hence understanding of processes.

The ADV measurement technique uses the principle of Doppler shift. The instrument transmits a beam of acoustic waves at a fixed frequency. These waves reflect by moving particles in the water and four probes receive the signal of the returning sound waves and determine the difference in frequency. This change in frequency is proportional to the flow velocity. Since the water depth is limited, a side looking ADV device was used. The used ADV device is a Nortec Vectrino 2D-3D Fixed Probe. The output consists of time series of the flow velocity in x, y and z direction. The device was placed downstream of the sampling volume. The sampling volume has a diameter 6 mm, and the distance between the centre of this volume and the sensor is 50 mm. The accuracy of the measurements is ±0.5% of the measured value ±1 mm/s. The point measurements are performed at a sampling rate of 25 Hz for 240 seconds.

However, the water in the laboratory does not contain enough matter that reflects sound waves. Therefore, gas bubbles were generated in front of the sampling volume with the technique developed by Clutter and Smith [1961]. By electrolysis of water, gas bubbles of oxygen and hydrogen are created. The hydrogen bubbles rise slower in water than oxygen bubbles and these can be used as reflection matter for the ADV measurements. The setup of the hydrogen bubble technique is as follows: a frame with platinum wires with a diameter of 0.01 mm is connected to a positive pole and placed in front of the sampling volume. An iron bar is connected to a negative pole and is also placed in the flume. The location of the frame has been checked with coloured fluid.

Sediment particles that pass the crest of the sill are not expected to return. Therefore, the locations of the point measurements are chosen upstream of the inlet sill, above the upward slope and the crest of the sill, and not downstream of the sill. Flow angles and transverse velocities are expected to increase along the slope in downstream direction, based on the results by Van Linge [2017] and De Ruijsscher et al. [2019]. To identify the flow patterns accurately and efficiently, the density of the measurement locations increases in the downstream direction, see Figure 3.3. The vectrino is placed on a holder that can be moved up and down. This holder is placed in a rail on the beam through which the vectrino can slide in y-direction. Furthermore, the beam can move in x-direction. A top view of the experimental setup is shown in Figure 3.4.

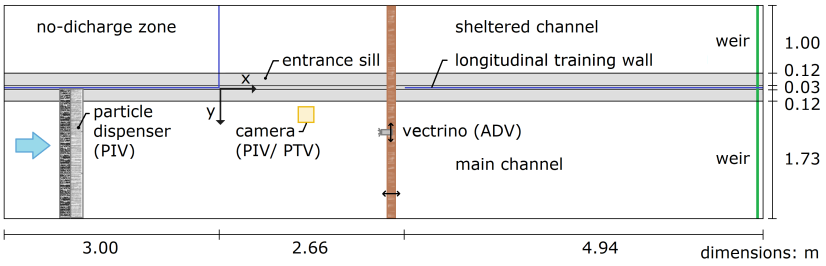

Figure 3.3: Schematic view of the experimental setup with the measurement devices for ADV, PIV and PTV measurements

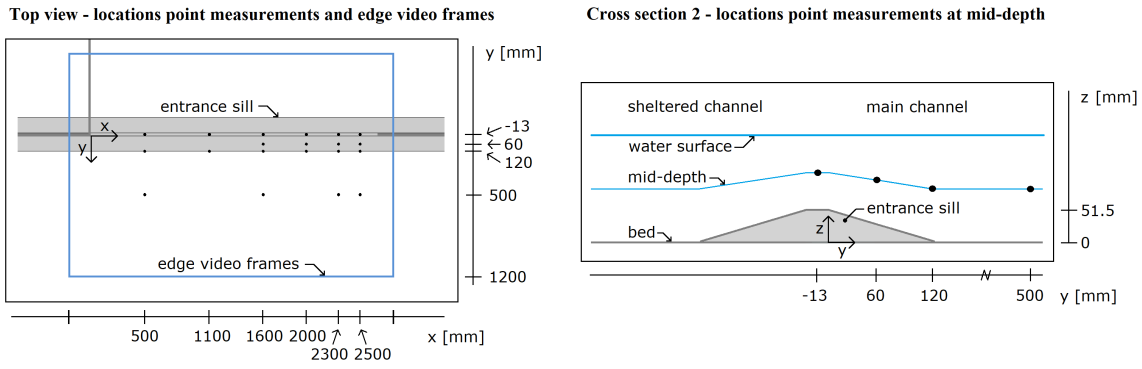

Figure 3.4: Schematic view of the experimental setup with the measurement locations

3.2.2. Particle Image Velocimetry (PIV)

The Particle Image Velocimetry (PIV) technique with floating particles is used, in addition to the point measurements at mid-depth, to obtain a more complete picture of the flow structures. The corresponding measurement data consist of flow fields at the water surface. Alternative types of measurements are additional point measurements with Acoustic Doppler Velocitymetry (ADV) or flow field measurements using the Particle Tracking Velocimetry (PTV) technique with floating particles. The latter technique is used for another purpose and described in the next section. PIV gives flow field data, whereas PTV gives particle trajectory data that can be used to calculate a flow field. The concentration of particles should be relatively low for PTV to track the individual particles. The PTV technique is more time consuming to obtain flow field measurements with the same resolution, since it requires a longer experiment and more frames to post-process. Small particles allow for a high concentration of particles that can be identified and hence a high resolution of the flow velocities of the field data. So, PIV is preferred above PTV to obtain insight in the flow structures for the top half of the water column. The time for measuring and processing the data to time-averaged velocities for flow field measurements with PIV is approximately the same as for 20 point measurements with ADV. A flow field contains more data compared to circa 20 point measurements in a certain layer, so PIV can capture the flow patterns in more detail than ADV within the same time. Besides, the variation in height is limited for point measurements with ADV up to ca. 25 mm below the water surface, whereas a PIV measurement with floating particles gives data over the surface layer. The surface layer has maximum distance to mid-depth and the bottom. Larger spreading of the measurements over depth can give additional insight in the three-dimensional flow structures. Therefore, the PIV technique with floating particles is chosen.

The used floating particles are black polypropylene particles with a density of 3 mm. For particle detection, the black colour has good contrast with the white bottom and the size of 3 mm is enough. Besides, the small size of the particles allows a high particle density and hence a high resolution of the flow field data. However, the particles tend to clump together which limits the maximum resolution, because 6-10 particles are needed per interrogation area.
Instantaneous velocity measurements have been obtained with the Particle Image Velocimetry technique. Black tracer particles with a lighter density than water are dispensed above the flow. A particle dispenser has been used to distribute the particles uniformly over the surface. A camera records from above. Velocities can be determined with software that detects the particles by size and compare couples of frames with correlation techniques. The PIV analysis consists of the following steps:

1. detect tracer particles
2. determine the interrogation area for the correlation technique
3. calculate the displacement of particles per interrogation area with autocorrelation
4. process the data: calibration, validation and creating plots

The MATlab toolbox PIVlab is used for the analysis [Thielicke 2020]. This package is developed by Thielicke and Stamhuis [2014] and can be used with MATlab 2014a. The images are prepared for particle detection by enhancing the contrast of the images by creating images with white particles on a black background using MATlab.

A Samsung NX1 camera with a 16-50mm f/2-2.8 S ED OIS Samsung lens is used to make videos. The videos are converted into images of the frames. The format for video recording was 4096 by 2176 pixels and the frame rate was 24 frames per second. To ensure enough contrast for analysis, the lens needs to catch enough light and the particles have to be sharp on the images. For cloudy days in winter, the used settings were: shutter speed is 1/250 s^{-1}, aperture is f/8 and ISO value is 12500. When more daylight was available, lower values for the aperture or ISO could be used. The conversion from video to images have been done by a self-written MATlab script. The PIV videos have a duration of at least 5 minutes.

For calibration of the images, black dots are painted on the bottom of the flume, see Figure 3.5. The dots are placed in three rows ($y = -0.50m$, $y = 0.50m$ and $y = 1.00m$) with distances of 0.50 m or 1.00 m from each other. The size of the view in reality is 3.55 m x 1.90 m. The coordinate system is the same as in the drawings.

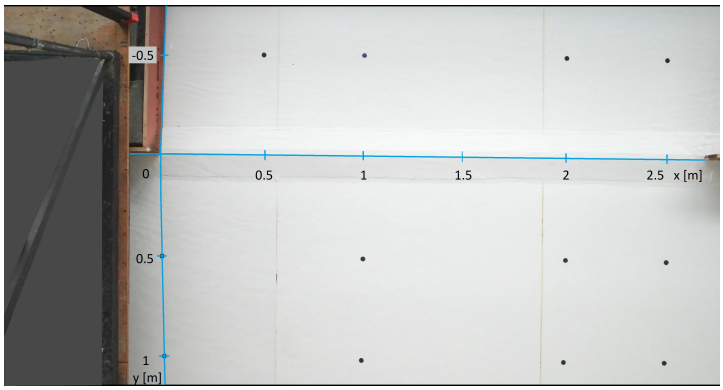

Figure 3.5: Top view of the experimental setup with calibration points

3.2.3. Particle Tracking Velocimetry (PTV)

Flow near the bottom is the driving force for bed-load transport. Data of the flow patterns near the bottom are needed to improve understanding of the bed-load transport. Besides, these data can also be used as validation data for future flow models to develop the sediment transport. The red particles described in section 3.1.2 can be used for this purpose. Particle Image velocimetry (PIV) is not suitable, because these particles require a large spreading to prevent frequent collision and PIV requires ca. 6-10 particles per interrogation area. The particle Tracking velocimetry (PTV) technique follows each particle and therefore the possible resolution depends on the frame frequency and the velocity of the particles. The maximum frame frequency for the camera is 24 frames per second. Assuming a maximum velocity of 0.2 m/s, the minimum possible accuracy is 0.2 ms^{-1} / 24 s^{-1} = 0.0083 m ≈ 10 mm. Therefore, PTV is suitable to obtain data near the bottom. Moreover, the trajectories can be transferred to a velocity field. The resolution for a flow field depends on the amount of particles that are tracked and other factors, such as the spreading of these particles.

The particles at the bottom are tracked individually with Particle Tracking Velocimetry, a Lagrangian technique. The camera records the flow from above. After which, the video is converged to frames that are processed into particle paths with PTVlab. In order to detect the individual particles, the particle density for PTV is smaller than for PIV where the interrogation area should contain 6-10 particles. The same camera, lens and settings are used for PTV. The recording time for PTV is ca. 4 minutes. The used software is the MATlab toolbox PTVlab version 1.0, developed by Antoine [2020].

3.2.4. Measurements of the experimental conditions

The experimental conditions are regulated by the total incoming discharge and the downstream weir heights. The studied parameters are the average water level on the sill and a discharge distribution. These parameters

have been varied indirectly in the experiments by adapting the weir heights and hence need to be determined by measurements.

The average water level on the sill is determined by measuring the water depth on 5 locations on the top of the sill and calculating the average of these measurements. The device measures the displacement of a point gauge that can be moved up and down. First, the point gauge is put on the top of the sill. There the device is calibrated to 0.00 mm. The point gauge is then moved just above the water level and slowly moved down until the point touches the water surface. Finally, the value for the water depth has been copied. This water depth measurement has been performed for the locations x = [50, 100, 150, 200, 250] cm with y = -1.3 cm. These locations are at the middle of the top of the sill. The point gauge is placed on a beam that can be moved in x-direction, see Figure 3.7.

The discharge distribution is determined with the theory of Rehbock about measuring discharges over a specific weir. The discharge for a perfect weir (sharp crested weir with critical flow above the crest and where the weir has the same width as the channel) is:

$$Q = \frac{2}{3} E_c \sqrt{\frac{2}{3} g B E_c} \tag{3.1}$$

where E_c is the energy head above the weir crest. This is the difference between the total energy head above the weir and the height of the weir $E_k = H - a$ [e.g. Battjes 1989], see Figure 3.6. g is the gravitational acceleration and B is the width of the weir. The discharge is calibrated for Rehbock weirs, for which Q is proportional $B \cdot E_c^{1.5}$. The shape of the weirs in the experimental setup is similar to the Rehbock weir. In addition, the difference in the velocity head between the channels is assumed to be negligible. Therefore, the discharge distribution can be determined based on the relation:

$$\frac{Q_m}{Q_s} = \frac{B_m}{B_s} \left(\frac{d_m}{d_s} \right)^{1.5} \tag{3.2}$$

where d is the water depth above the weir.

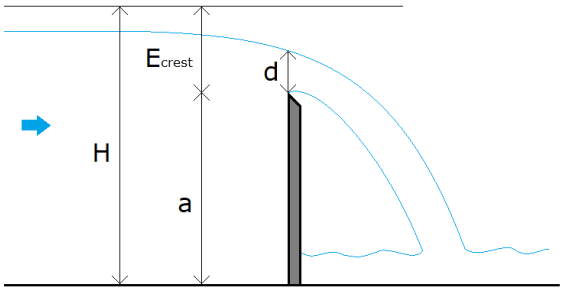

Figure 3.6: Side view of a sharp-crested weir

The water depth above the edge of the weir is determined with lasers, one in each channel, see Figure 3.7. The lasers are attached to the side walls of the flume and these are assumed not to move. The laser can measure distances when the light beam is reflected by the object. Therefore, a white sheet of paper (A4 format, 80 gr) was floated on the water surface below the laser. The thickness of the paper can be neglected and therefore, the laser measures the distance to the water level. The lasers are calibrated to measure the water depth above the top of the weir with zero for the top of the weir. Therefore, the water level measurements are water depths above the sill crest. The water levels are measured for at least 240 seconds.

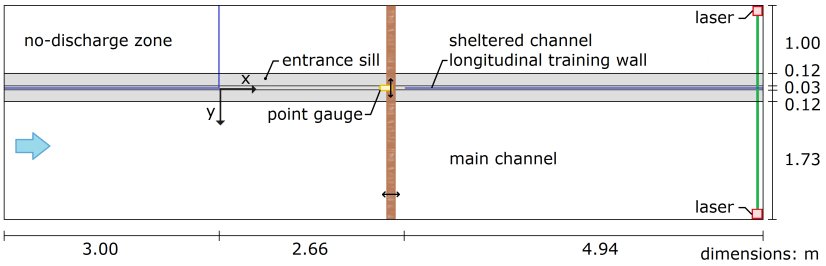

Figure 3.7: Schematic view of the experimental setup with the measurement devices for experimental-condition measurements

The nappe collapsed against the weir for the experimental condition A1 and A2. This means that downstream of the weir the area with air below the weir disappears and the water eventually flows against the weir downwards. Because the Rehbock formula is not validated for unaerated flow, the discharge distributions for these conditions are verified with additional depth measurements ca. 1 m upstream of the weirs, where the backwater caused by the weirs is negligible. As a solution the nappe is aerated with drainage pipes with a diameter of ca. 5 cm for the experiments with condition B1.

3.2.5. Overview measurements

The measurements have been summarized in the table below, Table 3.2. First the purpose is described for each type of measurement. Then, the type of data, the technique and the location are given. Besides, specifications of the particles are listed for the optical techniques.

Table 3.2: Measurements

Purpose	Measurement data	Measurement technique	Measurement location	Specifications particles
Insight in flow near the bottom	Particle trajectories	PTV	Near bottom, around inlet sill	diameter = 6 mm, density = 1050 kg/m^3 (rolling)
Representative data of depth-averaged flow	Point measurements (20 per condition)	ADV	At mid depth, upstream of and above inlet-sill crest	-
Insight in flow structures	Flow field	PIV	At water surface, around inlet sill	diameter = 3 mm, polypropylene (floating)
Data experimental condition: discharge distribution	Water depth	Point gauge	Above inlet-sill crest	-
Data experimental condition: average water depth above sill crest	Water level	Laser	Above downstream weirs and ca. 1 m upstream of the weirs	-

3.3. Parameters

Velocities have been measured in two or three directions depending on the measurement method. Point measurements performed with ADV (acoustic Doppler velocimetry) are in three dimensions and flow field measurements performed with PIV (particle image velocimetry) and PTV (particle tracking velocimetry) are in two dimensions. The velocity in longitudinal direction x, transverse direction y, vertical direction z are indicated with u, v, w, respectively. x is directed positive in streamwise direction, y is directed positive from the

side channel towards the main channel and z is directed positive downwards. The total velocity magnitude is indicated with U, where $U = \sqrt{u^2 + v^2}$ for 2D measurements and $U = \sqrt{u^2 + v^2 + w^2}$ for 3D measurements. The flow angle α is defined as: $\alpha = tan(\frac{u}{-v})$, see Figure 3.8. The presented velocities of the point measurements of 25 Hz are time-averaged over a duration of 4 minutes. The PIV measurements are averaged velocities over the non-interpolated instantaneous measurement data.

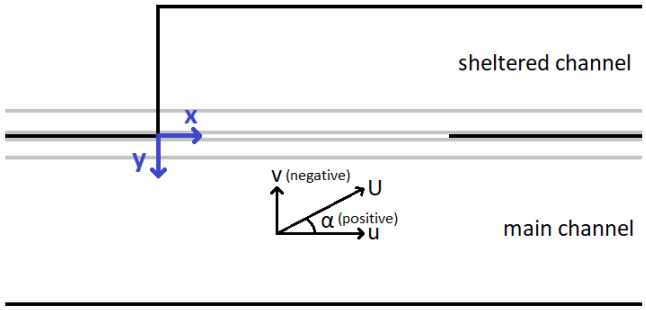

Figure 3.8: Definition of the velocity magnitude U for 2D measurements, longitudinal and lateral velocity components u and v and flow angle α, which is positive for a positive longitudinal and negative lateral velocity component.

4

Results

The results of the experiments and data analysis are presented in this chapter. Firstly, general observations of the flow are described. Secondly, the parameters are explained. Thirdly, the results of the data analysis are presented for the measurements at the water surface and at mid-depth level. Finally, the results of the bed measurements are shown.

4.1. General observations

Visual observations done with tracer particles and dye provide a general insight in the flow patterns. The horizontal flow patterns observed during the experiments have been drawn in Figure 4.1a. The lower channel in this figure is the main channel, the upper channel is the sheltered channel, the white structure is the sill and the brown plate at the right represents the longitudinal training wall. The brown plates at the left represent the river bank.

Figure 4.1a presents a large circulation zone at the upstream side of the sheltered channel. Another circulation zone occurs at the upstream end of the plate, which represents the longitudinal training wall, in the sheltered channel. In addition, the flow can separate from the wall of the main channel and create a circulation zone. The flow over the inlet is concentrated on the side next to the longitudinal training wall. Besides, the flow separates at the water surface. This effect is shown in Figure 4.1b, where streamlines diverge from less than 10 cm in the main channel to a width of around 50 cm above the sill for condition A2.

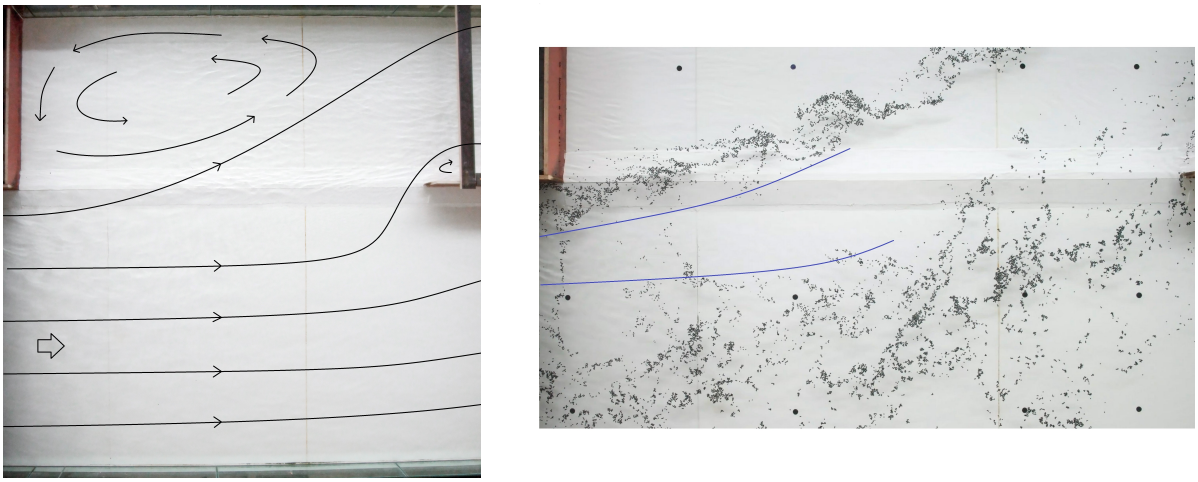

(a) (b)

Figure 4.1: Top views of the flume: (a) top view of the flume with hand-drawn flow lines and (b) top view of the flume during PIV measurements with floating particles in the experiment A2 with discharge $Q = 35$ m^3/s and downstream weir heights: $h_s = 60$ mm in the sheltered channel and $h_s = 80$ mm in the main channel. The blue curves indicate the area where the flow diverges in the upper layer.

Figure 4.2a shows flow separation just downstream side of the inlet from the longitudinal training wall in the sheltered channel. This results in secondary circulation which is visually observed with black tracer particles. The red tracer particles used to investigate the flow near the bottom float partly in the water column, see Figure 4.2b. This observation indicates upward flow near the bottom. Whether the upward motion of the particles was caused by upward flow from three-dimensional flow structures or the upward fluctuations in turbulent flow can be estimated with the ratio of the shear velocity u_* and the settling velocity w. Sediment is transported over the bed for u_*/w = 0.25 and particles come into suspension for u_*/w = 1 in the lower parts of the vertical. The density of the particles is 1005 kg/m^3 and the radius of the particles = 0.003 m and the viscosity depends on the temperature. The settling velocity according to Stokes is 0.098 m/s for 10°C and 0.075 m/s for 20°C. The average velocity for condition A1 is approximately 0.14 m/s. The water level slope is ca. 0.002-0.004 m/m. This results in a shear velocity of 0.04-0.6 m/s. So, u_*/w is larger than 0.25 and smaller than 1. Therefore, particles are in saltation, but not in suspension for condition A1. The saltating mode of the particles above the sill is probably enhanced by the rough surface of the glue layer that connects the sill to the bottom.
Figure 4.3 shows particles that travel along the sill (in x-direction), which indicates a recirculation zone behind the inlet sill in the vertical. Since the movement of particles along the downstream slope of the sill has been observed at the downstream side of the sill, this recirculation may not occur over the entire length of the sill.

(a) (b)

Figure 4.2: Photos of observations: (a) oblique view of flow separation behind the longitudinal training wall and (b) underwater shot with floating red tracer particle

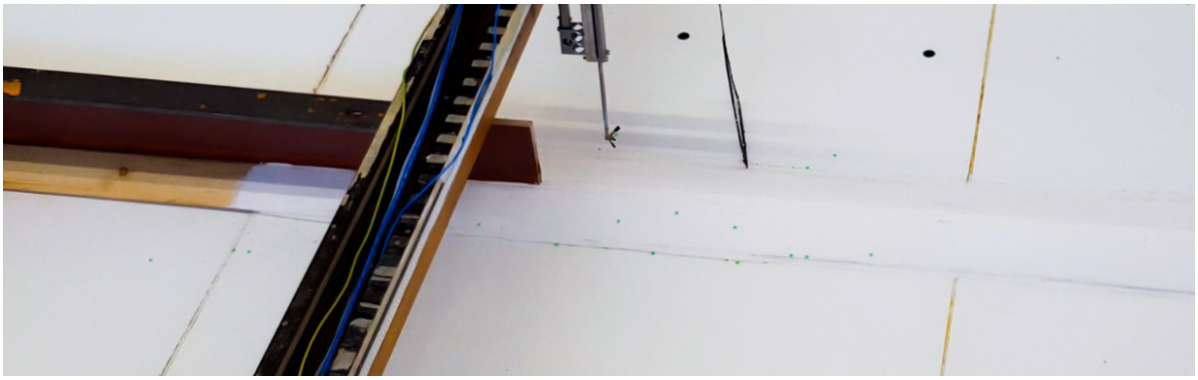

Figure 4.3: Particles on the downstream slope roll along the sill, which indicates flow separation behind the sill.

In conclusion, the following flow patterns have been observed:

- The flow towards the sheltered channel above the inlet is concentrated at the downstream side of the inlet.
- The flow divergence strongly at the water surface over the entrance sill.
- Three recirculation zones have been observed:

1. The largest zone is located at the upstream side of the sheltered channel. This secondary flow is induced by the flow separation from the edge of the bank at the upstream side of the inlet. Along the separation layer of this recirculation zone vortices have been observed.

2. Another recirculation zone is located behind the longitudinal training wall and it is the result of flow separation from the upstream edge of the bank at the longitudinal training wall.

3. The third recirculation zone is located in the main channel at the outer wall. This flow structure is the result of flow separation from the outer wall.

– A fourth recirculation zone may be located behind the sill. Then, the flow separates from the downstream or even upstream edge of the sill crest.

Besides, it has been observed that tracer particles with a density slightly larger than water were transported in the saltation mode. This indicates upward flow near the bottom above the sill.

4.2. Flow

The experimental data set consists of field measurements at the water surface, point measurements at mid-depth and trajectory measurements near the bottom. In addition, these measurements have been performed for three experimental conditions called A1, A2 and B1, see Table 3.1. The discharge was the same for the experiments. Condition A2 has a larger relative discharge towards the sheltered channel than condition A1 with approximately the same sill height to water depth ratio. Condition B1 has a larger sill height to water depth ratio and approximately the same discharge distribution compared to condition A1. The measurement data give insight into the flow structures and the effect of the discharge distribution and submergence on the three-dimensional flow over the inlet sill.

4.2.1. Mid-depth flow

Vectors of the flow velocity at mid-depth based on point measurements with ADV are shown in Figure 4.4. This section starts with a description of the mid-depth flow for condition A1. Then, the differences of condition A2 and B1 compared to condition A1 are described.

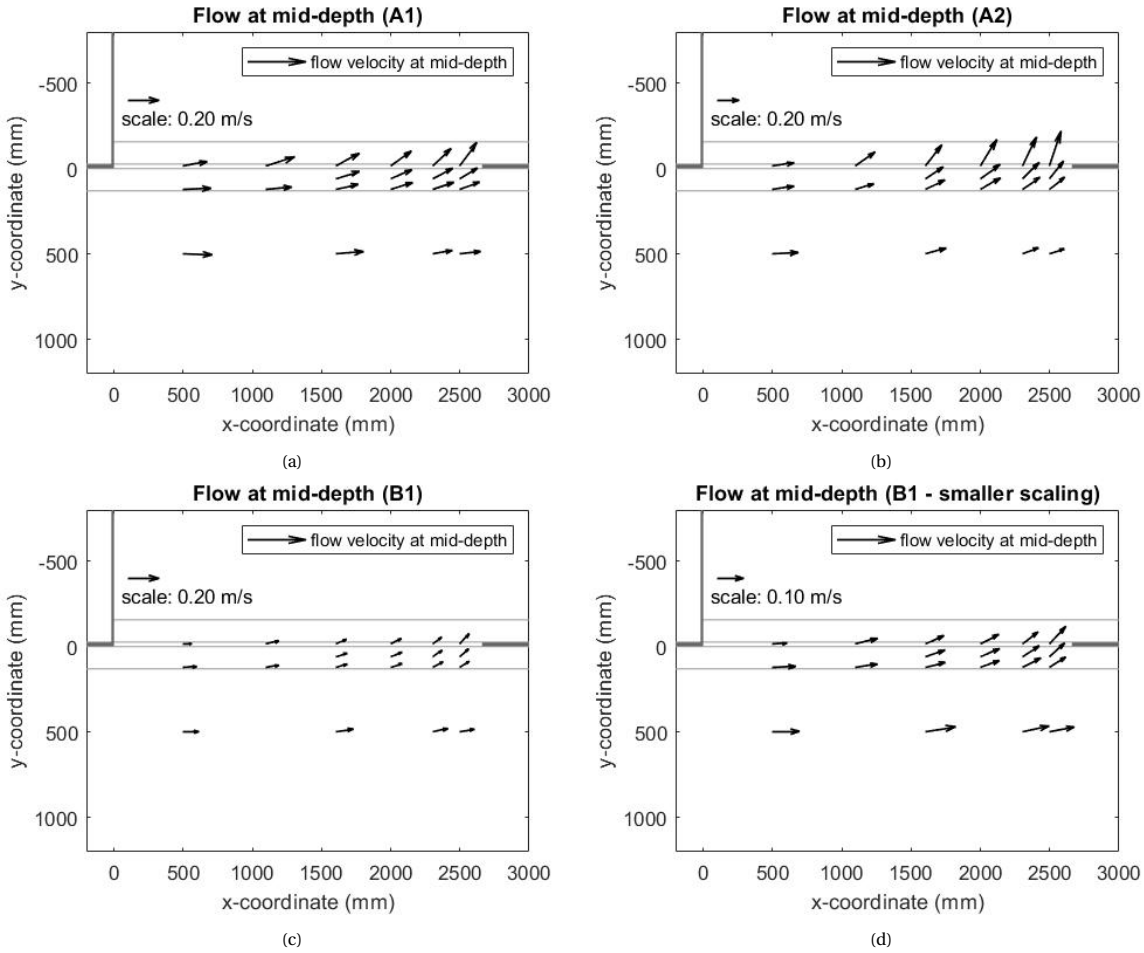

Figure 4.4: Top view with flow velocity vectors based on ADV measurements of the flow at mid-depth for different experimental conditions

The velocity magnitude in the main channel at y = 500 mm decreases in longitudinal direction for experimental condition A1. Besides, the flow angle in the main channel is slightly more directed towards the sheltered channel for larger longitudinal distances between x = 500-2300 mm, after which it slightly decreases towards x = 2500 mm. The flow at the upstream edge of the sill (y = 120 mm) has a smaller magnitude than in the main channel at y = 500 mm for longitudinal distances from x = 1500 mm. The flow at the upstream edge of the sill is more directed towards the sheltered channel than the flow in the main channel at y = 500 mm. Thus, in front of the sill, the velocity magnitude decreases and the angle increases in longitudinal direction next to the inlet, except between x = 2300-2500 mm in the main channel where the flow angle decreases in longitudinal direction.

The flow angle is even more increased at the middle of the upward slope (y = 60 mm) with a slightly larger flow magnitude. The flow angle is also increased at the top (y = -13 mm), both from the upstream edge of the sill (y = 120 mm) to the crest and, for x = 1600 - 2500 mm from the middle of the upward sill slope to the crest. Besides, the flow angle increases in longitudinal direction. So, the flow above the sill bends towards the sheltered channel and hence the flow angle increases on the upstream part of the sill in both longitudinal and opposite lateral direction (x and -y direction). The longitudinal velocity component decreases at the upstream edge of the sill (y = 120 mm) in longitudinal direction, as well as at the middle of the upstream slope (y = 60 mm). The longitudinal velocity component at the crest is smaller at x = 1000 mm than at x = 500, after which it decreases towards x = 2500 mm. This decrease goes along with an increase of the lateral velocity component. The longitudinal velocity component is smaller atop the sill than at the upstream edge of the sill for x = 500, 2300 and 2500 mm, approximately equal atop and at the upstream edge of the sill at 2000 mm and larger at the sill crest than at the upward edge of the sill for x = 1000 and 1600 mm. The absolute lateral velocity component at the crest increases in longitudinal direction, as well as the flow angle. The absolute

lateral velocity component is slightly larger at the middle of the upward slope than at the upstream edge and even larger atop the sill crest for the same longitudinal distance (i.e. x-value). So, the absolute lateral velocity increases in both x and y direction above the upstream side of the sill.

For condition A2, the velocity magnitude at mid-depth in the main channel at y = 500 mm decreases in longitudinal direction. The flow angle increases in lateral direction with the strongest increase from the middle of the upward slope to the crest, except for x = 500 mm where the flow angle decreases from the upstream edge of the sill (x = 120 mm) to the middle of the crest of the sill (x = 13 mm). These changes in velocity magnitude and flow angle are stronger for condition A2 than for condition A1.

The velocity of the flow at mid-depth is smaller for condition B1 compared to condition A1. The flow angles atop the sill crest of condition B1 are similar to condition A1, see also Figure 6.4. Besides, the flow in main channel has a relative larger velocity magnitude compared to the flow above the sill, which is in contrast with conditions A1 and A2.

4.2.2. Flow at the water surface

Field measurements with floating tracer particles, processed with the particle image velocimetry (PIV) technique, are presented in Figure 4.5. The measured flow field has been visualised with streamlines and velocity vectors at the point measurement locations. First the result of condition A1 is described and then the results of the conditions A2 and B1 are compared to condition A1.

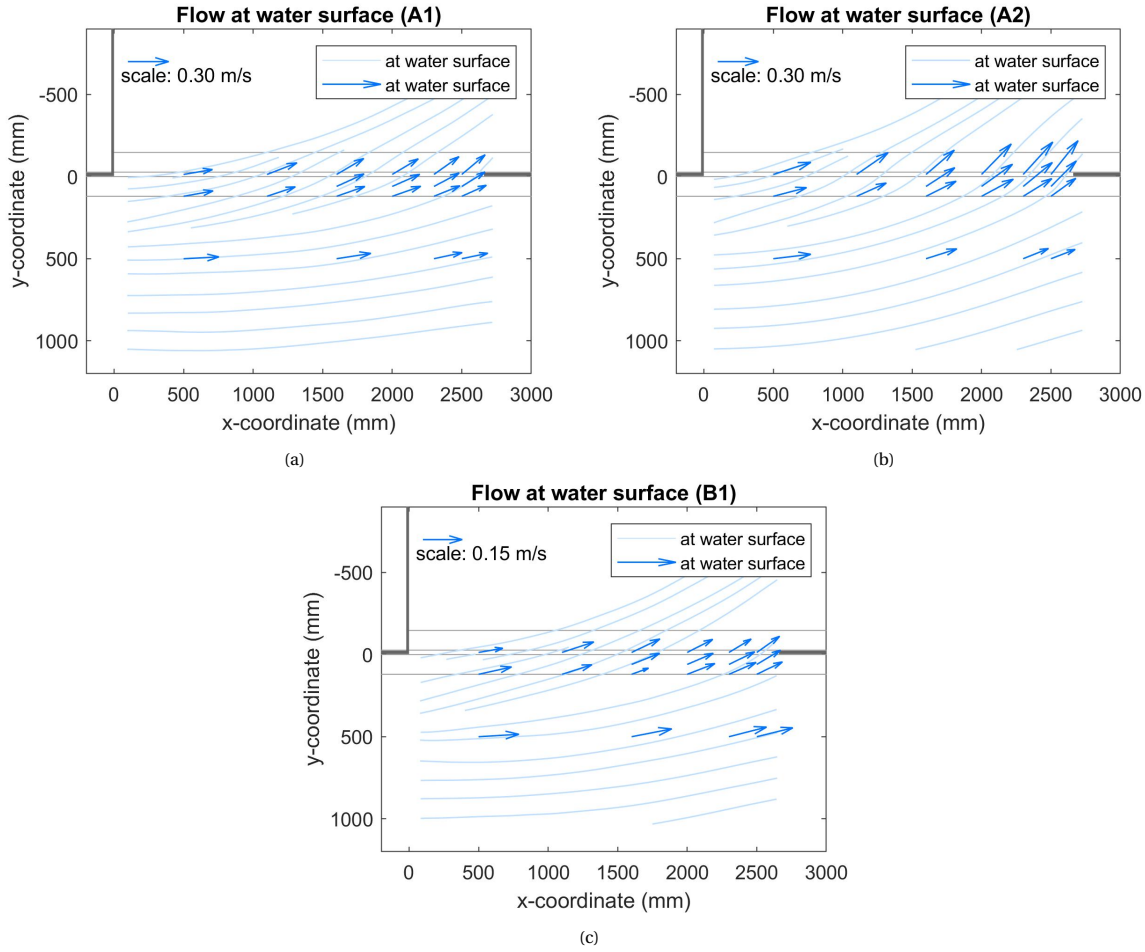

Figure 4.5: Top view of the flow at the water surface with streamlines and velocity magnitude based on PIV measurements for different experimental conditions

The flow in the main channel diverges in general for the three experiments due to the widening of the channel. The strongest divergent streamlines pass the inlet. The results show areas with convergence upstream of the sill crest between x = 0-1500 mm for condition A1, between x = 0-1000 mm for condition A2 and between 500-1300 mm for condition B1 and downstream of the sill crest for all conditions.

For condition A1, the streamlines starting at lateral distances y > 580 mm show hardly divergence, but are curved in the direction of the longitudinal training wall. The streamlines starting between y = 450 mm and 580 mm diverge. The two streamlines starting between y = 350 and 450 mm show a relatively large divergence until the sill crest and converge from the sill crest. The streamlines starting in the range y = 0 - 350 mm converge from approximately the sill crest. So, the streamlines in the sheltered channel converge. Moreover, the longitudinal velocity component decreases in opposite lateral direction towards the sheltered channel (-y direction) for the presented locations except at x = 1000 m. The longitudinal velocity component decreases in longitudinal direction (x direction) in the main channel at y = 500 mm, at the upstream edge of the sill (y = 120 mm), at the middle of the upward slope (y = 60 mm) and, from x = 1000-2500 mm, at the sill crest (y = -13 mm). The lateral velocity component shows a slight increase from y = 120 mm to y = 60 mm and a stronger increase for y = 60 mm to y = -13 mm. The lateral velocity component decreases in longitudinal direction (x direction) above the sill for all presented results, except between (x,y) = (1600,-13) and (2000,-13) mm where the lateral velocity components are approximately equal.

In addition to the mid-depth flow, the measured flow field at the water surface shows a larger part of the flow towards the sheltered channel for condition A2 compared to condition A1. In addition, the flow angles of the presented vectors are larger for condition A2 than for condition A1. For condition A2, the longitudinal velocity component decreases in opposite lateral direction to the sheltered channel (-y direction) for 1600 and 2000 mm, is approximately the same for x = 2300 mm and increases for x = 500, 1000 and 2500 mm. So, the flow increases over a larger part of the sill for condition A2 compared to condition A1, based on the measurements. The longitudinal velocity component increases at the edge of the sill from (x,y) = (1600,60) to (2000,60) mm after which it decreases towards (x,y) = (2500,60). This component decreases at the middle of the upward slope between x = 500-1000 mm, is approximately constant between x = 1000-1600 mm, increases between x = 1600-2000 mm and then decreases to x = 2500 mm. Besides, it decreases above the sill crest in longitudinal direction. This is different from condition A1, where the longitudinal velocity component decreases in longitudinal direction between all presented locations. The lateral velocity component is larger for condition A2 compared to condition A1 up to a factor 1.8. For condition A2, the lateral velocity component increases in both longitudinal and opposite lateral direction (x and -y direction) above the upstream side of the sill. This is the same as for condition A1, except between (x,y) = (1600,-13) and (2000,-13) mm where the velocity is approximately the same for condition A1 and increases for condition A2.

The measurements at the water surface show a smaller flow towards the sheltered channel for condition B1 compared to condition A1. The flow angles are in the same order of magnitude as for condition A1 and condition B1. However, the results show differences for the streamlines starting from y = 0-400, where the flow convergences for condition A1 and divergence for condition B1 and the flow angles at x = 100 mm are larger for condition B1 than condition A1. The results of condition B1 show a smaller longitudinal velocity component at the upstream edge of the sill (at y = 120 mm) than in the main channel at y = 500 mm. The velocity at (x,y) = (1600,120) mm is relatively small compared to the vectors around it and this outlier has been disregarded in the analysis. The longitudinal velocity component decreases for x = 500, 2000, 2300 and 2500 mm and increases for x = 1000 mm. At x = 1600, the longitudinal velocity component decreases from y = 60 to -13 mm. The qualitative differences of the longitudinal velocity component in lateral direction are the same as for condition A1. The longitudinal component decreases at the upstream edge of the sill, at the middle of the upward slope and above the crest in longitudinal direction between x = 1000-2500 mm. This is the same as for condition A1. The lateral velocity component increases for x > 1000 mm above the upstream side of the sill from x = 120 mm to x = -13 mm. This increase is smaller than for condition A1. The lateral velocity component increases above the sill in longitudinal direction, except between x = 1600-2000 mm at the crest and at the middle of the sill where the lateral velocity component is approximately equal. This is also the same as for condition A1.

4.2.3. Sediment transport

The near-bed measurements are presented in this section. The particles used for near-bottom measurements just sink. Therefore, the relative density is small compared to sediment particles. The behaviour of the particles is more like water than sediment particles. Assuming the particles behave similarly to water, knowledge on these particles is the basis of a qualitative analysis of sediment transport in the discussion chapter 7. The used particles have a diameter of 6 mm, so their centre of gravity is 3 mm above the bottom when they roll. The particles have been dropped into the water just before the inlet sill (around x ≈ -20 mm) and they have sunk 0.5 to 1 metre downstream. Therefore, this analysis focuses on the flow for x > 1000 mm. Moreover, the particle can lose contact with the bottom at the sill crest or at the downward slope of the sill, but these results have been partly filtered in the post-processing.

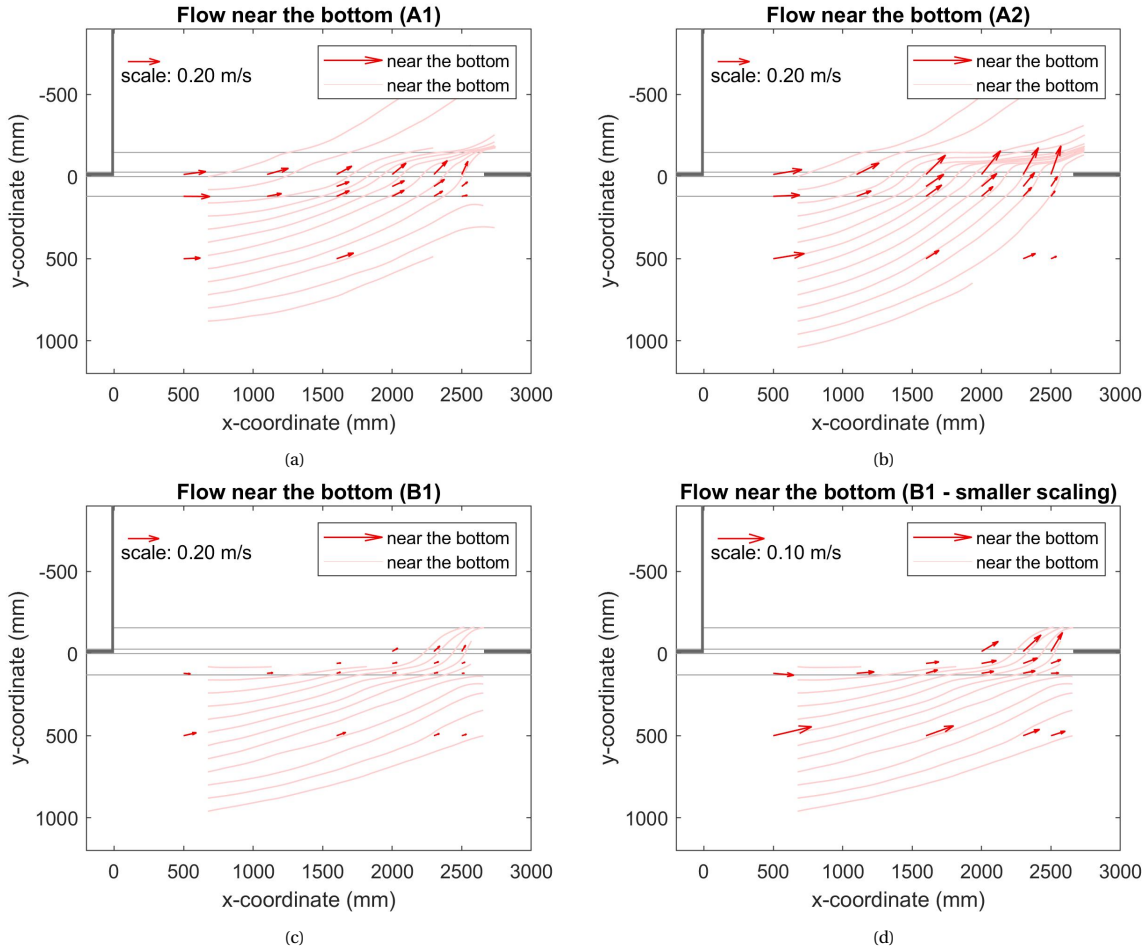

Figure 4.6: Top view of the flow near the bottom with streamlines and velocity magnitude based on PTV measurements for different experimental conditions

The streamlines near the bottom towards the sheltered channel show relatively gradual flow patterns for condition A1. In addition, the streamlines are less convergent and divergent until the sill crest compared to the flow at the water surface and at mid-depth. The result shows a different pattern near the bottom above the upward slope: the flow angle decreases and hence increases on the upward slope for streamlines that enter the slope at x = 1150-1800 mm. The measurements on the upward slope at y = 120 mm and y = 60 mm show small differences, except at x = 2500 mm where the flow diverges and the flow from y = 120 mm bends towards the main channel and the flow from y = 60 mm passes the inlet sill. The measurements show a larger increase from y = 60 mm to y = -13 mm in both longitudinal and lateral direction for x > 1000 mm. Moreover, a larger part of the flow near the bottom flows over the inlet sill compared to the flow near the water surface. In addition, the streamlines are strongly convergent at the downstream side of the sill, which goes along with an increasing flow angle atop the sill. The streamlines starting above the sill also converge above the downward

slope and these diverge after the sill. The other streamlines are converging and become more parallel at the downstream side.

Condition A2 shows similar results compared to condition A1. The main differences are: 1) more flow is directed towards the sheltered channel which goes along with larger flow angles and lateral velocity magnitudes, 2) the decrease in flow angle at the upstream side of the upward slope (between x = 120 mm and x = 60 mm) is relatively smaller and 3) the convergence at the downstream side of the slope is stronger.

The flow velocity for condition B1 is more than 2 times smaller than for condition A1. Since the flow pattern are considerably different from the patterns for condition A1, these are first described in detail, after which a comparison is given. The flow velocity in the main channel at y = 500 mm is about 2 times smaller than at the upstream edge of the sill at (y = 120 mm). In addition, the longitudinal velocity component in the main channel at y = 500 mm shows a decrease of more than a factor 2. This decrease is stronger than at the water surface and at mid-depth due to the stronger bending of the flow (i.e. the tangent of the streamlines) towards the sheltered channel. The flow shows a negative flow angle for (x,y) = (500,120) mm, thus the tracer particles were rolling downwards on the slope. The flow shows a positive flow angle for (x,y) = (1000,120) mm and thus particles can move uphill. The streamlines that cross the upstream edge of the sill at x = 1300, 1600 and 1750 mm show a decrease of the flow angle above the sill and after x = 2000 the flow angle start increasing, while an increase in the flow angle along the streamlines has only been observed above the sill in the flow layers at the water surface and at mid-depth. The tracer particles passed the inlet sill at the downstream side, hence accurate data are missing for a large part of the sill. The main differences and similarities of the near-bottom flow between condition B1 and condition A1 are: 1) the flow velocity is lower, 2) the flow angles are in the same order of magnitude, 3) the discharge over the sill is more concentrated at the downstream side for condition B1 compared to condition A1.

4.2.4. Differences over depth

The differences over depth are described and shown per experimental condition. This knowledge is essential for the identification of the three-dimensional flow structures in chapter 5. The focus of this description is on the flow above the sill.

Differences of the flow over depth for condition A1:

- The flow angle is larger at mid-depth than at the water surface atop the crest (y = -13 mm) for x = 2000, 2300 and 2500 mm near the longitudinal training wall.
- The flow angle is larger at the water surface than at mid-depth for the upstream edge of the sill (y = 120 mm), particularly at x = 500, 1000 and 1500 mm, as well as for (x,y) = (1000, -13) mm and (x,y) = (1500, 60) mm. These are locations at the upstream side and lower part of the upward slope.
- The flow angle is larger near the bottom than at mid-depth for the flow above the sill that passes the sill crest at x = 1600 - 2500 mm according to the streamlines near the bottom.
- The flow angle is larger at mid-depth than at the bottom for x = 500 at both y = -13 and 120 mm, for (x,y) = (1000,120) and (x,y) = (2500,120) mm. The first three locations are at the upstream side and the start of the inlet and the last location is at the end of the inlet from which the flow bends towards the main channel.
- The flow velocity magnitude and the longitudinal and lateral velocity components are smaller at mid-depth than at the water surface.
- The lateral component at mid-depth increases faster in longitudinal and opposite lateral direction (x and -y direction) than at the water surface. The difference of the longitudinal component varies less for $x \geq 1600$ mm.
- The velocity magnitudes are significant smaller near the bottom than at mid-depth. The longitudinal component and lateral component increase in upward direction near the bottom and at mid-depth, where the increases are stronger near the bottom.

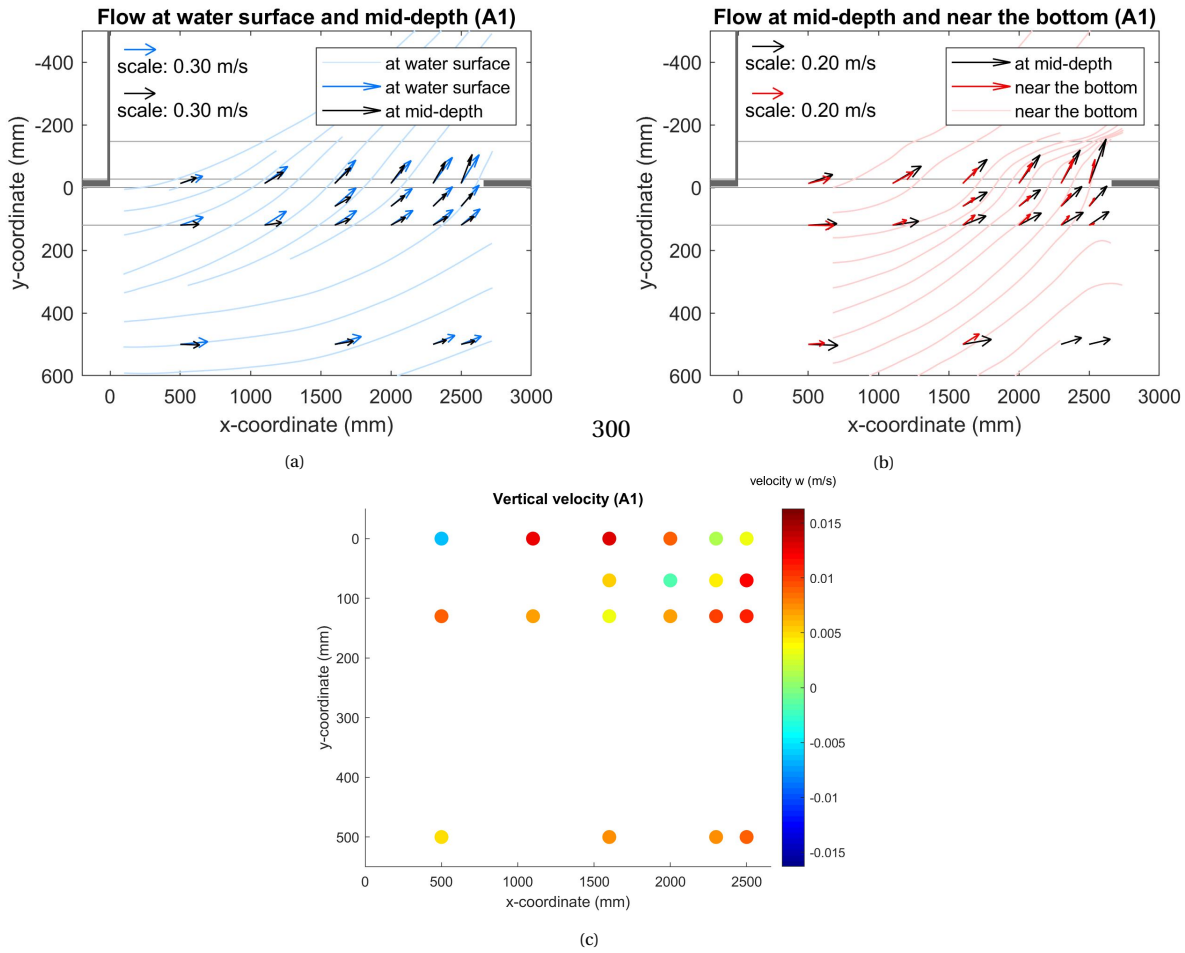

Figure 4.7: Top view of flow vectors at point locations above the inlet sill and vertical velocities for condition A1

- The lateral velocity component shows a larger increase at mid-depth than near the bottom, which results in a larger difference for larger longitudinal distances.
- The measured mid-depth flow is on average downwards ($w > 0$ m/s). Upward velocities are measured for (x,y) = (-13,500) mm and (x,y) = (60,2000) mm. Relatively small downward velocities ($w < 0.007$ m/s) are measured atop the sill for x = 2300 and 2500 mm, at the middle of upward slope for x = 1500 and 2300 mm and at the upstream edge of the sill for x = 1000-2000 mm. Large downward flow velocities are found upstream at (x,y) = (500,120) mm, atop the crest for x = 1000, 1600 and 2000 mm and at the end of the inlet at (x,y) = (2300,120), (2500,120) and (2500,60) mm.

Differences of the flow over depth for condition A2:

- Flow angles are larger at mid-depth than at the water surface atop the crest (y = -13 mm) for x > 1000 mm, at the middle of the upward slope (y = 60 mm) at x = 2300 and 2500 mm, which are locations near the downstream end of the opening near the longitudinal training wall.
- Flow angles are larger at the water surface than at mid-depth for (x,y) = (500,-13) mm, (500, 120) mm, (1000,120) mm and (1600,120) mm above the sill, which are locations at the begin of the inlet.
- Flow angles are larger near the bottom than at mid-depth for x ≥ 1000 mm at y = 60 and 120 mm. These are all measurement locations above the upward slope, except (x,y) = (500,120) mm.
- Flow angles are larger at mid-depth than near the bottom atop the sill for x ≥ 1000 mm and at (x,y)= (500,120) mm.

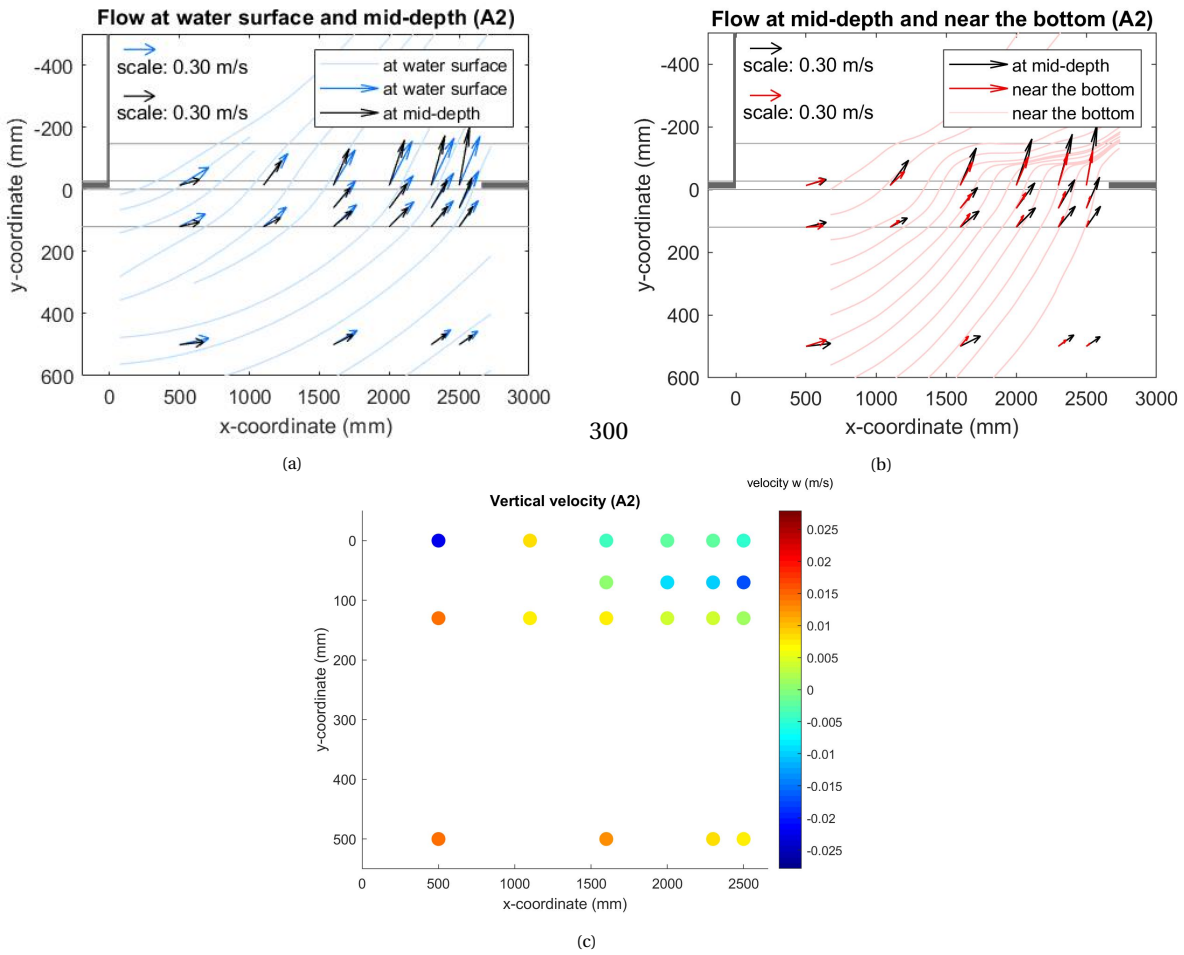

300

Figure 4.8: Top view of flow vectors at point locations above the inlet sill and vertical velocities for condition A2

- The flow velocity is smaller at mid-depth than at the water surface. The lateral component at mid-depth increases faster in longitudinal and opposite lateral direction (x and -y direction) than at the water surface. Note the velocity at (x,y) = (1600,120) mm at the water surface is an outlier.

- The velocity magnitudes are considerably smaller near the bottom than at mid-depth. The longitudinal component and lateral component increase in upward direction near the bottom and at mid-depth, where the increase is stronger near the bottom.

- The curvature and difference in flow angle are smaller at the middle of the upwards slope (y = 60 mm) than in front of the upward slope (y = 120 mm). The curvature decreases even further towards the crest after which it changes direction and, at the same locations, the difference in flow angle decreases or even changes in sign for $1000 \leq x \geq 2500$ mm.

- Large upward flow velocities ($w < -0.15$ m/s) can be found at (x,y) = (500,-13) and (2500,60) mm. The measured velocities around (x,y) = (500,-13) are directed upward: the upward velocity is even 0.015 m/s at (x,y) = (500,120) mm and around 0.008 m/s at (x,y) = (1000,-13) and (1000,120) mm. The results show a gradual decrease of a downward velocity in longitudinal direction at the upward edge of the sill (x = 500-2500 mm). At the middle of the upward slope (x = 1600-2500 mm, y = 60 mm), the velocity is slightly downward at x = 1600 mm, upward at x = 2000 mm with w = -0.007 m/s after which the velocity increases to w = -0.016 m/s at x = 2500 mm. So, the vertical velocities at the middle of the sill are smaller, in other words the flow more upward directed. The velocities at x = 2000-2500 mm atop the crest are smaller than at the middle of the upward slope.

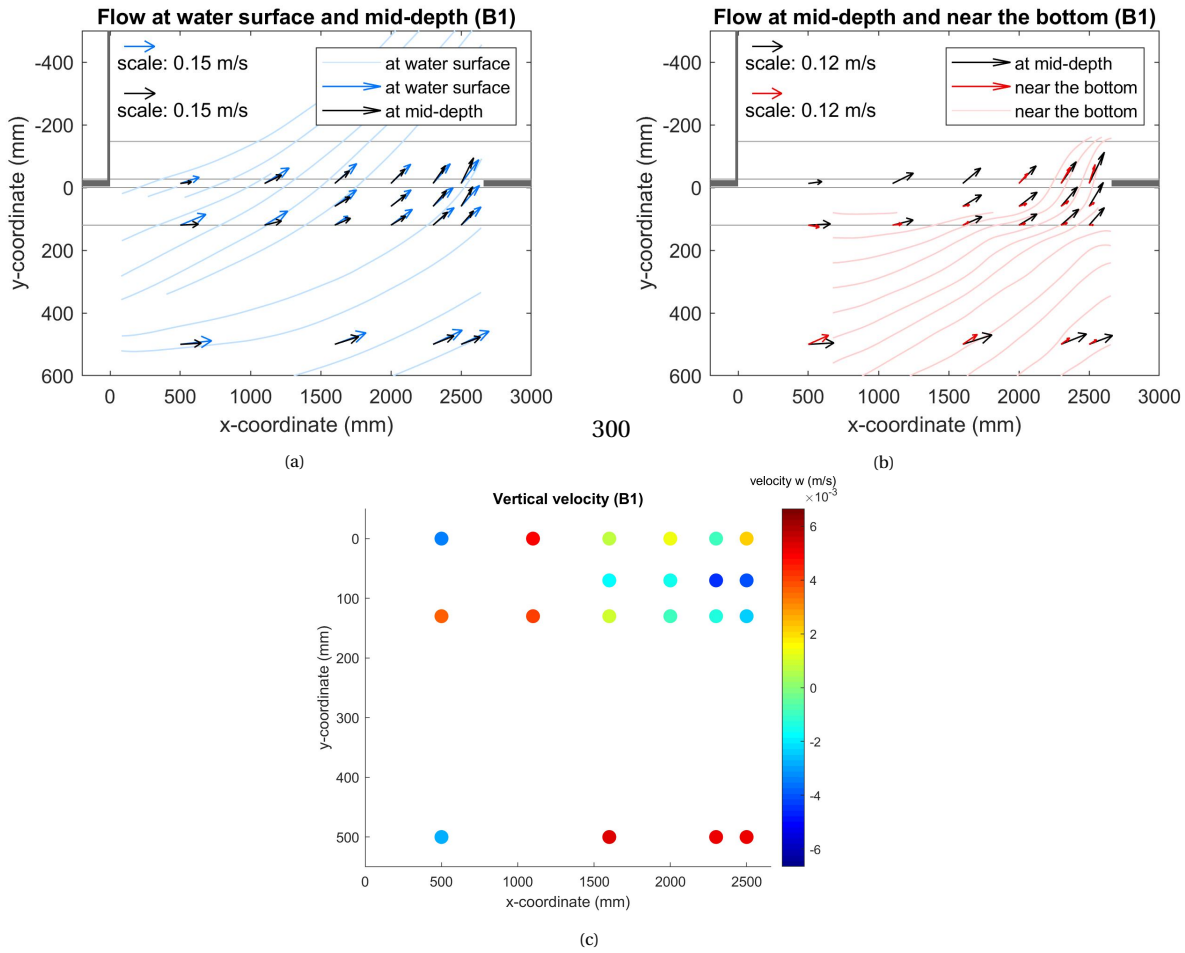

Figure 4.9: Top view of flow vectors at point locations above the inlet sill and vertical velocities for condition B1

Differences of the flow over depth for condition B1:

- Flow angles are larger at mid-depth than at the water surface for x = 2500 mm at y = -13, 60 and 120 mm and for x = 2300 at y = -13 and 60 mm, which are locations at the end of the opening near the longitudinal training wall.
- Flow angles are larger at the water surface than at mid-depth for x ≤ 1000 mm and for x = 1600 at y = 60 mm and 120 mm and for x = 2000 mm at y = 120 mm, which are located near the middle of the inlet at the upstream side.
- Flow angles are larger near the bottom than at mid-depth for x ≥ 1000 mm at y = 60 and 120 mm, which are all measurement locations above the upward slope, except (x,y) = (500,120) mm. Also the flow angle at (x,y) = (1600,120) mm is larger near the bottom than at mid-depth.
- Flow angles are larger at mid-depth than near the bottom at the upstream edge (y = 120 mm) at x = 500, 1000, 2000 and 2300 mm and at the middle of the upward slope.
- The velocity magnitudes are considerably smaller near the bottom than at mid-depth. The lateral component increases above the upward slope towards the sheltered channel near the bottom and at mid-depth, where the increase is largest near the bottom. The longitudinal velocity component increases also in opposite lateral direction (-y direction).
- The flow at condition B1 shows a strong curvature at the downstream end of the inlet near the longitudinal training wall. Above the sill, negative curvature goes along with a larger flow angle at mid-depth

than near the bottom and positive curvature goes along with larger flow angle than near the bottom than near the water surface. However this is not the case for (x,y) = (1600,500) mm in the main channel.

- The net vertical velocity at mid-depth above the sill is not considerably upward or downward. The strongest downward vertical velocity components (w > 0.004 m/s) are (x,y) = (500,120) mm, (x,y) = (1000,120) mm and (x,y) = (1000,-13) mm. A moderate downward velocity component (w ≈ 0.002 m/s) has been measured atop the crest near the longitudinal training wall at (x,y) = (2500,-13) mm. The mid-depth velocities at x = 1600 and 2000 mm at the sill crest and at x = 1600 mm at the upstream edge of the sill are downward directed.
- The relative large upward velocity components (w < -2 m/s) has been measured at x = 2300 and 2500 mm above the middle of the upward slope (y = 60 mm) and at (x,y) = (500,-13) mm. Also the velocities at locations x = 2000, 2300, 2500 mm at the upstream edge of the sill, x = 1600 and 2000 mm at the middle of the sill and at x = 2300 mm at the top of the sill are upward directed.

4.3. Conclusion

The main results are been summarized in this section.

For condition A1, the flow angle increases in both longitudinal and lateral direction. The longitudinal velocity component increases and the lateral velocity component decreases in longitudinal direction. The flow at the water surface diverges strongly for larger longitudinal distances above the sill. The vertical velocity at mid-depth is downward in general.

For condition A2 compared to condition A1, the flow angle is larger and the velocity magnitude of the flow to the sheltered channel is larger. The flow at the water surface has a larger curvature at the downstream side of the inlet. The flow has strong divergence around the middle of the inlet.

For condition B1 compared to condition A1, the flow angle at the upstream toe of the sill is larger at mid-depth and the same at the water surface. The flow angle atop the crest is smaller. The flow curvature is smaller at the downstream side of the inlet. The velocity magnitude of the flow to the sheltered channel compared to the flow to the main channel is smaller. The flow at the water surface also has a strong divergence at the downstream side of the inlet. The flow angle near the bottom is smaller and the same goes for the velocity magnitude.

The flow angle is smaller in general for lower depths at the upstream side of the inlet and larger for lower depths at the downstream side of the inlet. The vertical velocity is upward in general at the upstream side of the inlet, except at (x,y) = (500,-13) mm, and downward at the downstream side of the inlet. The vertical velocity is downwards in general for condition A1, slightly downwards for condition A2 and slightly upwards for condition B1.

5

Analysis - flow structures

This first chapter with analyses is about the flow structures (section 5.1-5.3).This analysis starts with an overview of possible flow structures deduced from literature. Then, the flow structures in the results will be identified. These flow structures are summarized in an overview, consisting of figures with a brief explanation.

5.1. Possible flow structures

Flow processes and flow structures around inlet sills of longitudinal training wall and similar structures are discussed in the literature review. This knowledge has been used to create an overview of possible flow structures around the inlet sill in this section.

Flow separation, mixing and recirculation

Velocity gradients in longitudinal direction result in lateral transport creating turbulent mixing layers, for example separation layers (section 2.2.1). Possible separation layers at the inlet are shown in Figure 5.1. The 2D depth-averaged model results from Van Linge [2017] show the recirculation zone at the upstream side of the sheltered channel (Figure 2.10). The flow from the upchannel separates from the wall at the edge of the river bank at upstream side of the inlet opening. The upstream part of the sheltered channel is smaller than the flow from the main channel towards the channel. This velocity difference creates a turbulent mixing layer. Similarly, the flow can separate from the edge of the longitudinal training wall downstream of the inlet. Since the velocity of the flow from the upchannel towards the sheltered channel has a larger velocity than in the zone behind the separation layer, a stagnation zone or recirculation zone is expected at this location. The results from Van Linge [2017] show a stagnation zone along the longitudinal training wall in the sheltered channel (Figure 2.10). The flow from the upchannel is divided over the downchannel and sheltered channel. The channel widens and hence the flow decelerates. For a strong deceleration, the flow can separate from the wall of the downchannel and create a stagnation or recirculation zone. This separation layer in the main channel is not present in the depth-averaged results from Van Linge [2017]. Furthermore, velocity gradients between the flow towards the main and sheltered channel can also create additional turbulence.

In addition to horizontal velocity gradients, the flow can separate due to vertical gradients behind the inlet sill and so create a stagnation or recirculation zone. In case of recirculation, the flow becomes helical due to the velocity component along the sill crest, similar to oblique weirs (section 2.2.2, Figure 2.6).

Bend effect at the inlet

Velocity gradients in lateral direction can occur due to secondary bend flow (section 2.2.1), see Figure 2.4. The bend effect has hardly any effect on the discharge distribution according to the 1D flow analysis from Van Linge [2017], since the secondary flow in lateral direction is two orders of magnitude smaller than the longitudinal flow. The channels in the experiment are not curved and so this effect is not present in the results. Moreover, curved flow towards the sheltered channel results in larger water level in the outer bend than

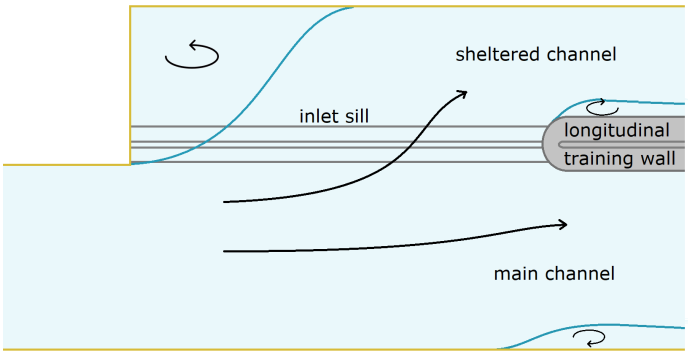

Figure 5.1: Sketch of the inlet area of longitudinal training walls with possible separation layers delineated by blue lines and the recirculating flow inside the separation zones indicated by arrows

in the inner bend and hence a secondary circular flow, which forms a helical flow together with the primary curved flow. This helical flow gives in a larger flow angle (to the sill crest) at larger depths and a smaller flow angle at smaller depths. See Figure 2.15 for the velocity profiles of the horizontal velocity components of a helical flow.

The flow angle increases in longitudinal direction over the crest (Figure 2.10). The decrease of the radius of the curvature results in an increase of the strength of the helical flow over the crest. The net flow in the direction of the crest (x-direction in the experimental setup) is upstream at the water surface and downstream near the bottom.

Sill effect for oblique flow
The conceptual model from Wols et al. [2006] about oblique weirs can be applied for the inlet sill by considering the upstream flow angle for the case without sill as baseline situation. According to this theory, the curvature of the flow is enhanced due to the increase in velocity at the upstream slope. This effect is not significant for high water depths relative to the sill height or a very long sill. So, this sill effect does not induce new flow structures, but it results in a deviation of the curvature without sill.

Although, upstream of the sill energy is assumed to be conserved. Then the flow direction changes towards the crest-normal direction due to the increase in velocity at the upstream slope. For larger water levels, the relative increase of the velocity above the weir is smaller, resulting in a larger angle with respect to the weir crest.

This approach is based on the energy balance at the upstream side of the sill. Because of possible energy losses, the validity of this approach for inlet sills can be discussed. In the experiments, the discharge distribution towards the sheltered channel was 35% for condition A1, 43% for condition A2 and 33% for condition B1 and the width of the main channel was 1733 mm. So, the discharge towards the sheltered channel takes place in the main channel over respectively 615, 743 and 570 mm (the discharge distribution multiplied by the width of the main channel). The length of the inlet is 2660 mm. The horizontal widening of the flow towards the sheltered channel in the experiments is a factor 3.6 to 4.7. This widening is considerably and can lead to energy losses. However, the flow towards the sheltered channel is gradual with curved streamlines upstream and hence smoothing the effect of the widening and therefore this reduces the energy losses due to the widening. Moreover, the inlet sill is built of stones and the bed friction of these stones gives reason to expect energy losses. Another cause of energy loss is the flow separation that starts from the upstream edge of the river bank. However, this effect is not present in the experiments because the edge is located at the sill crest instead of the upstream toe of the sill.

Blocking effect
An obstacle can block flow, for example submerged bottom vanes with a large angle to the flow (section 2.2.2). To obtain more insight in the corresponding flow structures, the physics behind the blocking effect has been discussed in this section and visualised in Figure 5.2.

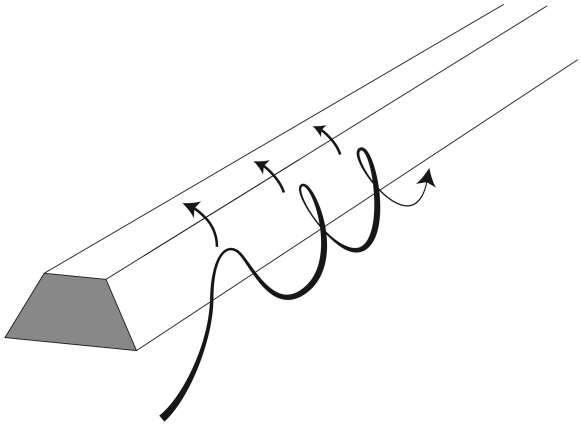

Figure 5.2: Possible flow structures along the inlet sill of a longitudinal training wall

Possible flow structures around the entrance sill of a longitudinal training wall are shown in Figure 5.2. The helical flow in the main channel as a result of blocking is comparable to the lower helical flow structures along bottom vanes due to the diving flow component and horizontal curvature of the flow around the bottom vane, see Figure 2.9c. The flow over the sill is pulled by a pressure difference. Since the flow over the sill is curved in yz-plane (cross section over the width of the sill), this results in another helical flow, for curved streamlines in the xy-plane (top view).

Marelius and Sinha [1998] found that the dominant flow structures consist of two suction side vortices and a horseshoe vortex, see their experimental results in Figure 2.8. The suction side vortices are the vortices described in the paragraph above. The horseshoe vortex is present at the back side of the vane and not relevant for inlet sill.

5.2. Identified flow structures

To identify the flow structures in experimental results, the flow around the inlet is analysed in this paragraph. First, the horizontal flow is discussed: divergent and convergent flow, flow separation and circulation zones. Then, the three-dimensional structures are analysed 1) flow structures with smaller flow angles for larger depths and 2) flow structures with larger flow angles for larger depths. Finally, the development of lateral flow component on the upward slope is discussed to give more insight into the deformation of the vertical velocity profile.

5.2.1. Horizontal flow patterns

The streamlines in the main channel diverge or are nearly aligned for the three experiments, because the channel widens. The results show divergent streamlines for the flow towards the sheltered channel. The streamlines in the main channel show less divergence for the flow that remains in the main channel, see Figure 4.5. Hence, the flow in the main channel below the figures should diverge, because 1) the measured flow angles in the main channel are directed inward both at the water surfaces and the bottom, 2) the geometry of the main channel is uniform and 3) the inflow of the flume is also nearly uniform. The flow circulation pattern was visually observed with floating particles, but it was not captured with a camera.

The flow towards the sheltered channel above the inlet is concentrated at the downstream side of the inlet. The curvature of the flow explains this pattern, since the flow is stronger in the outer bend due the centrifugal force. The results show strong divergent streamlines at the water surface over the entrance sill. In the area with strong divergence at the surface, the flow is upward or less downward compared to the mean vertical velocity for condition A1, see Figure 4.7. The three-dimensional flow structure is further discussed in section 5.2.4.
Moreover, the streamlines converge in the sheltered channel from approximately the sill crest. This convergence can be explained by the reduction of the channel width. The effective width of the inlet, defined as

$B_{opening,eff} = B_{opening} \cdot sin(\alpha)$, is smaller than the width of the sheltered channel. Hence, the flow has to diverge from the main channel towards the sheltered channel. However, the depth increases on the downstream slope which reduces the acceleration corresponding to the convergent flow.

A special type of flow divergence is flow separation from the wall. As mentioned in chapter 4, three recirculation zones have been observed:

1. The largest is located at the upstream side of the sheltered channel. This secondary flow is induced by the flow separation from the edge of the bank at the upstream side of the inlet. Along the separation layer of this recirculation zone vortices have been observed.

2. Another recirculation zone is located behind the longitudinal training wall and it is the result of flow separation from the upstream edge of the bank at the longitudinal training wall.

3. The third recirculation zone is located in the main channel at the outer wall. This flow structure is the result of flow separation from the outer wall due to the widening of the channel and corresponding deceleration of the flow.

5.2.2. Vertical flow at mid-depth

To gain understanding of the vertical velocity, first the average vertical flow above the slope is discussed. The average of the velocity measurements at mid-depth is downward for condition A1, upward for condition A2 and slightly downwards for condition B1, see Figure 4.7c, 4.8c and 4.9c.
The relative differences between the conditions can be explained as follows. Since the upward slope is an order of magnitude smaller than the water level depression, the average flow is upward above the upstream slope. Therefore, the upward flux is larger for a larger discharge towards the sheltered channel and a larger sill height to water depth ratio. Hence the vertical velocities are smaller (in other words the flow is directed relatively upward) for condition A2 and B1 compared to condition A1 due to the larger discharge to the sheltered channel and the larger sill height to water depth ratio respectively.
Upward flow is expected at mid-depth above the upstream slope of the sill, because the water level depression is an order of magnitude smaller than the sill height. For a deformation of the vertical velocity profile due to quick acceleration, the streamlines in the vertical plane have a smaller upward gradient than the mid-depth level, see Figure 5.3. So, this process has a reducing effect on the upward flow above the slope, but it does not explain downward flow. The explanation of the downward flow has to be found in the three-dimensional flow structures. Helical flow due to curvature is downward directed in the inner bend. In addition, blocking can result in a helical flow with downward velocities above the sill slope.

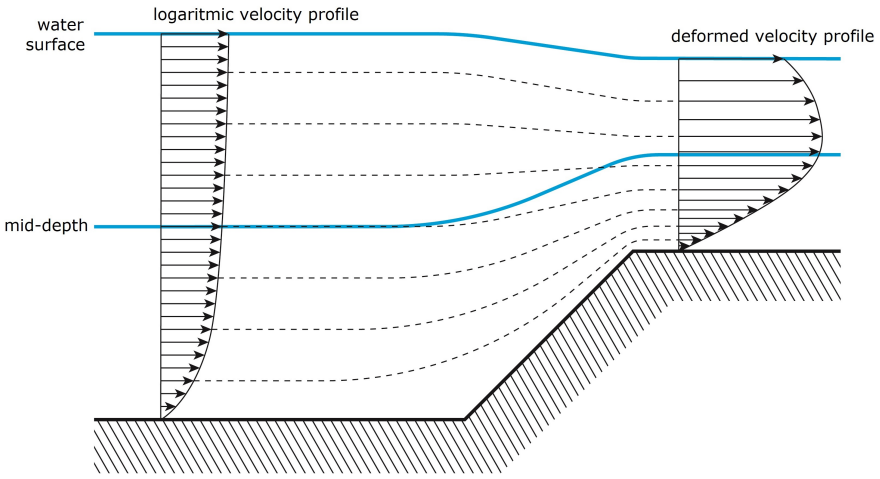

Figure 5.3: Sketch of flow above the upward slope for deformation of the vertical profile due to quick acceleration resulting in a downward flow relative to the mid-depth level

So far, the general vertical flow at mid-depth has been discussed. Now the details of the flow atop the crest will be analysed.

5.2.3. Flow structures with smaller flow angles for larger depths

This paragraphs describes the analyses about the details of the flow atop the crest. Measurements show net results which can be used to identify dominant flow structures. Note that there may be flow structures which are not dominant and cannot be identified. The analysis has been split in two parts: i) flow with smaller flow angles for larger depths has been analysed in this subsection and ii) flow with larger flow angles for larger depths has been analysed in the following subsection.

Smaller angles at larger depths are measured above the inlet sill near the bank and at the upstream toe of the sill. Figure 2.8 shows the flow structure due to the blocking effect with a downward diving flow in front of the obstacle that results in a secondary circular flow above the upward sill slope with smaller flow angles at larger depths. Besides, another flow is pulled along the upward sill slope over the sill crest. Moreover, a flow curvature with its centre downstream in x-direction and upstream in y-direction can induce a helical flow with smaller angles at larger depths.

The flow velocities at (x,y) = (500,-13) mm is smaller than the measurement velocities around. Depth-averaged results from Van Linge [2017], Figure 2.13 show a quick development of the longitudinal velocity profile. The equivalent distance of x = 500 mm is 38 m (longitudinal distance in experiment / length inlet in experiment · total length in model = 500 mm /2660 mm· 200 m = 38 m). The magnitude of the total velocity and its longitudinal and lateral components are considerably smaller at the equivalent longitudinal distance of 38 m. So, this observation is in line with the depth-averaged model results and part of the primary flow patterns.

The velocity is upward at (x,y) = (500,-13) mm in contrast to the measurement locations around. For the blocking effect with a circular flow in front of the sill, the pressure difference over the sill is larger. This larger pressure difference results in a larger flow velocity, which can make the difference whether the flow will separate. In this case, the flow is more upward (thus the vertical velocity is smaller) than for flow without this effect.

The circular flow as part of the blocking effect can explain the smaller flow angles for larger depths. This is measured, among others, at (x,y) = (500,120) and (1000,120) mm between the water surface and mid-depth 4.7a, 4.8a and 4.9a and at (x,y) = (500,120) mm between mid-depth and near-bottom level 4.7b, 4.8b and 4.9b. The difference in flow angle atop the sill crest at (x,y) = (500,-13) mm is very small, except for condition A2. For this condition, the flow angle is smaller at the water surface than at mid-depth, which cannot be explained here by flow curvature, blocking or quick acceleration.

Processes that produce downward flow are less present at the side of the river bank. Firstly, the flow angle is small and the difference in flow angle is also small for condition A1 (see Figure 4.7a and 4.7b). A possible explanation is that the slope is effective longer for a smaller flow angle, hence the acceleration is milder and the deformation of the flow is smaller. So, the downward flow relative to the mid-depth level corresponding to the quick acceleration with deformation is smaller or absent. Secondly, the small curvature at these location results in less strong helical flow compared to other locations.

A pressure difference in front of a bottom vane induces a downward diving flow that induces other secondary flow structures: circulation and upward flow in front of the obstacle that is pulled over it. The pressure gradient upstream of the bottom vane is most abrupt for an orientation perpendicular towards the flow. The pressure gradient is more gradual for a slope. The blocking effect is not present for a horizontal bottom (with a slope of 0 degrees). So, this blocking depends on the slope. The experimental data are not detailed enough to show the flow structure. Therefore, a conceptual, literature or modelling study would be needed to gain more insight in how the pressure gradient affects the flow structure.

Summarized, the blocking effect as drawn in 2.8 can explain parts of the flow, where the effects of helical flow induced by curved flow and deformation due to flow acceleration are smaller. However, some features remain not understood using these concepts. Besides, the data lack detail to show the precise flow structure.

5.2.4. Flow structures with larger flow angles for larger depths

This second part of the analysis of the flow structures is about flow with larger angles at larger depths. The aim is to identify dominant three-dimensional flow structures.

Differences in flow angle, where the flow angles are larger for larger depths, has been observed atop the sill near the longitudinal training wall, for example at (x,y) = (2300,-13) and (2500,-13) mm for all conditions, see Figures 4.7a, 4.7b, 4.8a, 4.9a and 4.9b. The nearly identical flow angles at mid-depth and near the bottom at these locations for condition A2 form an exception, see Figure 4.8b. Helical flow induced by curved flow and deformation of the velocity profile due to flow acceleration can cause larger flow angles at larger depths. A secondary helical flow induced by curved flow has an inward directed flow at the water surface and an outward directed flow at the bottom. Hence, the flow angle is relatively larger at lower depths. The velocity profile can deform because of strong accelerations. Then, the lateral flow is maximum at a level below the water surface and the lateral flow is relatively larger at lower depths and so the flow angle is larger at lower depths.

Helical flow is initiated by curved streamlines and hence these should be present. Besides, the helical flow is downward in the outer bend and upward in the inner bend. The results show larger differences between the flow angle for stronger curvature of the streamlines at (x,y) = (2300,-13) mm and (2500,-13) mm (Figure 4.7a, 4.7b, 4.8a, 4.8b, 4.9a and 4.9b). This relationship is also present in the results of condition A2 in which the difference in flow angle between mid-depth and the bottom is small at the locations (x,y) = (2300,-13) mm and (2500,-13) mm that are in the vicinity of the tipping point of the streamlines (Figure 4.8b). In conclusion, the flow is curved and flow angles correspond qualitatively with curvature and so helical flow structures are present. The helical flow gives a gross downward flow in the outward bend and a gross upward flow in the inner bend.

The deformation of the velocity profile has been discussed in section 5.2.5. The conclusion is that both helical flow and flow acceleration can explain the observed deformation of the velocity profile.

The smaller vertical flow at (x,y) = (2300,-13) mm is compared to (x,y) = (2500,-13) mm for condition A1 and B1 (see Figures 4.7c and 4.9c). Here, the divergent flow at the water surface (see Figures 4.7a and 4.7a) results in an upward secondary flow in the zone with divergent flow around (x,y) = (2300,-13) mm. The corresponding flow structure is a separatrix, see Figure 5.4a. This separatrix cannot be identified directly in the results, since the separatrix is a gross flow structure where results show the net flow structures. The separatrix can be recognized as a deviation in the curvature of the flow, see Figure 5.4b. Hence, the results do not show all characteristics of a separatrix. For example, the helical flow in the inner bend rotates in the same direction and with a smaller magnitude compared to the helical flow in the outer bend of the separation zone. Hence, the net effect is an inward flow from the outer bend (in -x direction) near the bottom, an upward flow and an outward flow (in +x direction) at the surface. This explains the results consisting of upward peaks in the vertical velocity and the relative gradual change of the difference in flow angle. Moreover, the downward velocity at (x,y) = (2500,-13) mm for condition A1 and B1 (see Figure 4.8c) can be explained by helical flow or the upward slope above which the flow curvature and hence helical flow can partly be related to the separatrix.

For condition A2, the results show a larger upward velocity at (x,y) = (2500,-13) mm than for smaller longitudinal distances as for example at (x,y) = (2300,-13) mm, see Figure 4.8c. The vertical flow is more upward compared to the mid-depth level due to the larger lateral velocity that has to accelerate above the upward slope. (Note, deformation of the velocity profile is a secondary effect of the accelerating flow. Deformation would result in a reduction of the upward flow at mid-depth atop the sill crest, see Figure 5.3.) The effect of the separatrix is hardly visible in the results of the vertical flow velocities for condition A2 (see Figure 4.8c). The vertical velocity at (x,y) = (1600,-13) mm is a small local trough in longitudinal direction, which can be explained by the smaller divergence of the flow compared to other conditions.

The blocking effect results in larger flow angles for smaller depths (i.e. higher in the water column) for smaller longitudinal distances above the sill. The curvature results in helical flow with smaller flow angles for smaller depths for larger longitudinal distances above the sill. This results in the divergence of the flow at the water surface and hence a secondary flow structure: a separatrix.
The location of the separatrix seems depends on the dominance of the effects of blocking and curvature in

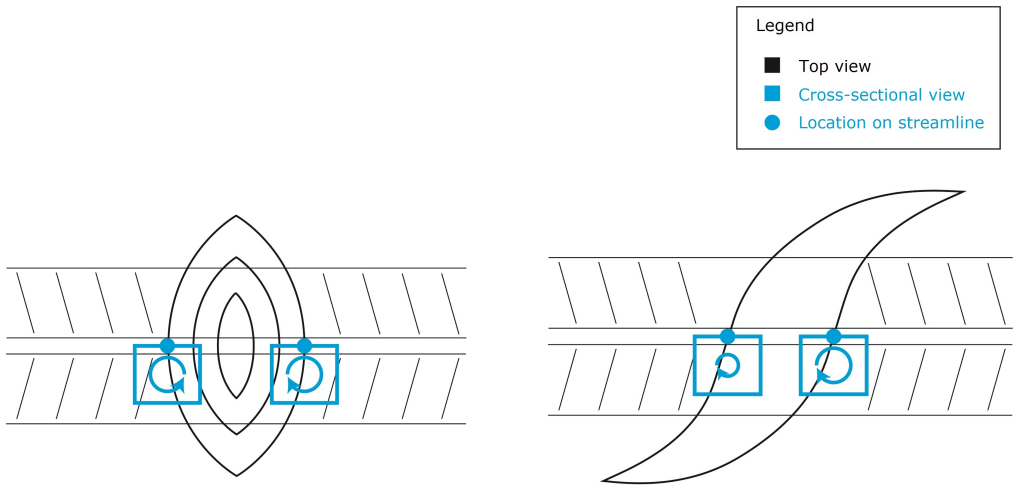

(a) separatrix with opposite circular flows at the sides

(b) flow structure of a separatrix in curved flow in which the circular flows at the sides have the same direction and different strengths

Figure 5.4: Drawings of the separatrix at the inlet consisting of a top view of the horizontal streamlines at the water surface in black and two cross sections in red connected at the red dot

the upper part of the water column. For condition A1 and A2, the water level and total discharge are approximately the same and the discharge distribution is varied. Considered simplistically, the additional discharge towards the sheltered channel in condition A2 compared to condition A1 has been pulled through the inlet at the downstream side of the inlet and compresses the other flow towards the upstream side of the inlet. Since more discharge has to be pulled through the inlet, the flow is curved stronger, hence the helical flow due to curvature is dominant over other flow structures, over a larger part of the sill. This explains the location of the separatrix for condition A2 at a smaller longitudinal distance compared to condition A1. This simple concept is not realistic, because the water is a continuum that does not consists of two separate flow parts with their own structures. However, the curvature is larger for a larger discharge through the same inlet area (water depth x length inlet) and curved flows are strongest in the outer bend, thus the flow is more concentrated in the outer bend for larger discharges through the same inlet area. This will be illustrated with a cross-comparison of conditions A1 and B1.
For condition A1 and B1, the total discharge and discharge distribution were approximately the same and the water depth was varied. So, the inlet area where the discharge towards the sheltered channel has been pulled through was larger for condition B1 compared to condition A1. In addition, the dimensionless sill height is smaller. Therefore, the flow was less curved for condition B1 compared to condition A1, the helical flow due to curvature was smaller and hence the blocking effect was relatively stronger. In conclusion, the averaged flow velocity atop the sill has a positive correlation with the effect of the helical flow due to curvature compared to the blocking effect in the experiments.

Summarized, the flow curvature above the inlet at the side of the longitudinal training wall is identified as a primary-flow structure with helical flow as secondary-flow structure. Besides, the secondary flow cell as a result of a difference in curvature shows similarities with a separatrix. The helical flow is present above the entire sill for flow curvature, but it is dominant and hence identifiable at this side of the longitudinal training wall. The secondary flow cell is a resulting flow structure of the blocking effect at the upstream side and helical flow due to curvature at the downstream side in the upper part of the water column. Hence, the location depends on the dominance of the three-dimensional flow structures. The averaged flow velocity atop the sill has a positive correlation with the effect of the helical flow due to curvature compared to the blocking effect in the experiments. This analysis does not give evidence for deformation of the velocity profile due to acceleration.

5.2.5. Development of lateral flow component above the upward slope

The flow at the upstream side of the sill crest has a larger velocity component at mid-depth than at the water surface. The flow develops along a streamline. However, this is too complicated to plot in an oblique view, because the streamlines are different over depth. Hence, the flow over a cross section is presented instead, see Figure 5.5. This figure shows the lateral flow component at mid-depth and at the water surface connected with a curve is drawn through these measurements and the origin based on the assumed no-slip condition at the bottom. Atop the sill crest at y = -13 mm, the lateral velocity component is larger at mid-depth than at the water surface. Different flow processes may underlie this observation: 1. quick flow acceleration resulting in the deformation of the velocity profile and 2. helical flow due to flow curvature.

The flow in a depth-averaged river model is assumed to be characterized by a logarithmic velocity profile to calculate the bed shear stress. A logarithmic vertical velocity profile means that i) the flow velocity is zero at the bed, ii) the flow higher in the water column is always larger compared to flow lower in the water column and iii) the flow angle is the same over depth. Flow acceleration can result in deformation of the velocity profile, see Figure 2.5. The difference between the maximum velocity and the velocity at the water surface is smaller than 10% of the averaged velocity in these figures as well as for condition A1 and B1. Since the flow does not accelerate in longitudinal direction, the profile does not deform in that direction due to this process. Therefore, deformation of the velocity profile due to acceleration occurs only for the lateral component. This results in a different distribution of the longitudinal and lateral velocity components and thus the flow angle over depths changes.
Helical flow due to curvature is outward directed at the water surface and inward directed near the bottom, see section 2.3, Figure 5.1. This creates a larger lateral velocity component in lower layers. So, both helical flow and flow acceleration can explain the observed deformation of the velocity profile.

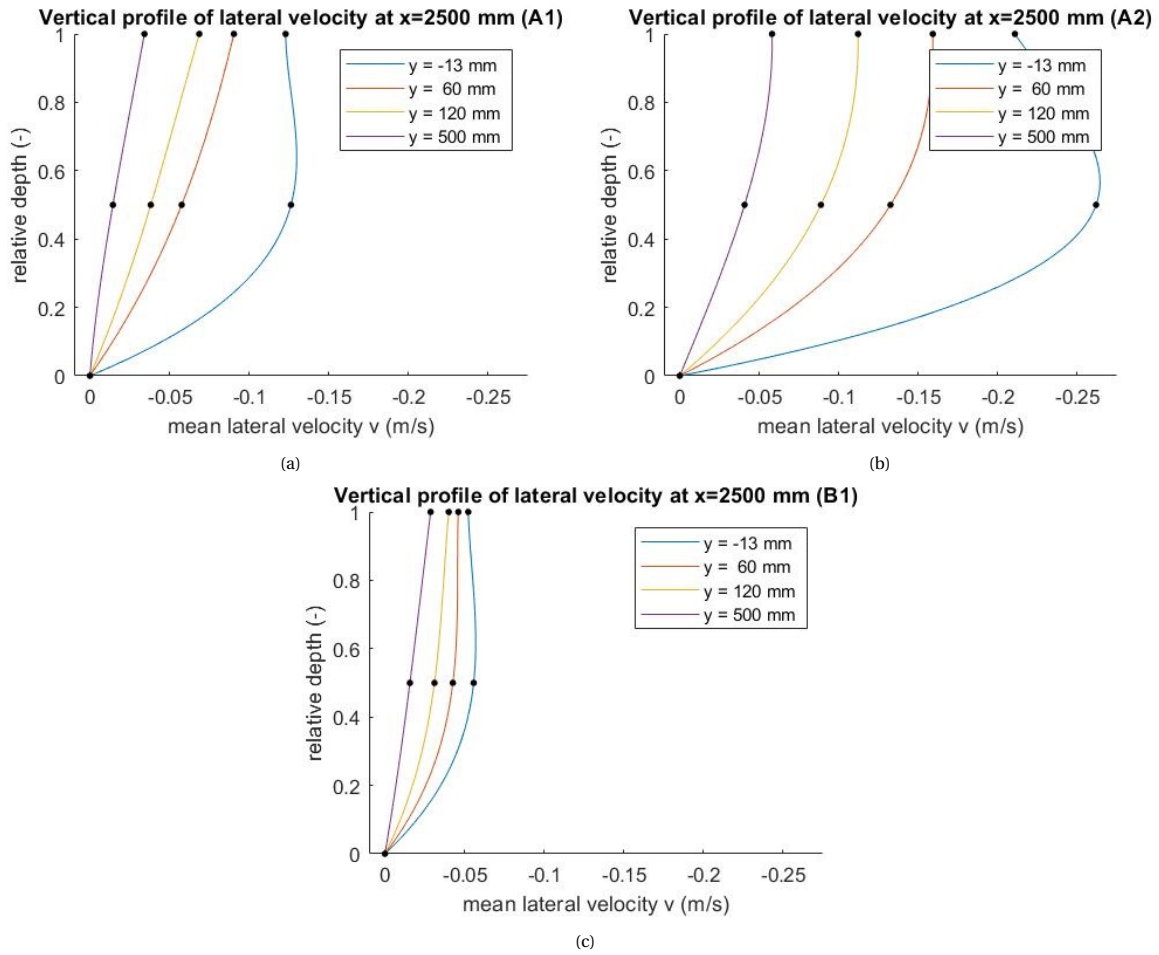

Figure 5.5: Impression of vertical profiles of lateral flow velocities for locations in a lateral section at the downstream side of the sill (x = 2500 mm) and for different experimental conditions

5.3. Conclusion

This paragraph summarized the flow structures identified from the measurements. The flow structures have been summarized in Figure 5.6. This is a top view with black streamlines representing the primary flow patterns and blue lines showing the secondary flow patterns which are induced by the primary flow.

The flow patterns in this overview figure are:

1. divergent streamlines in the main channel
2. convergent streamlines in the sheltered channel
3. a recirculation zone at the upstream edge of the sheltered channel
4. a recirculation zone at the upstream side of the longitudinal training wall in the sheltered channel
5. a recirculation zone at the downstream side of the sill
6. a helical flow in front of the sill and flow over the sill show the blocking effect (see Figure 2.9)
7. a helical flow due to curved flow* (see Figure 2.15)
8. a separatrix located between the upstream area where the blocking dominates and the downstream area where helical flow due to curvature dominates (see Figure 5.4)

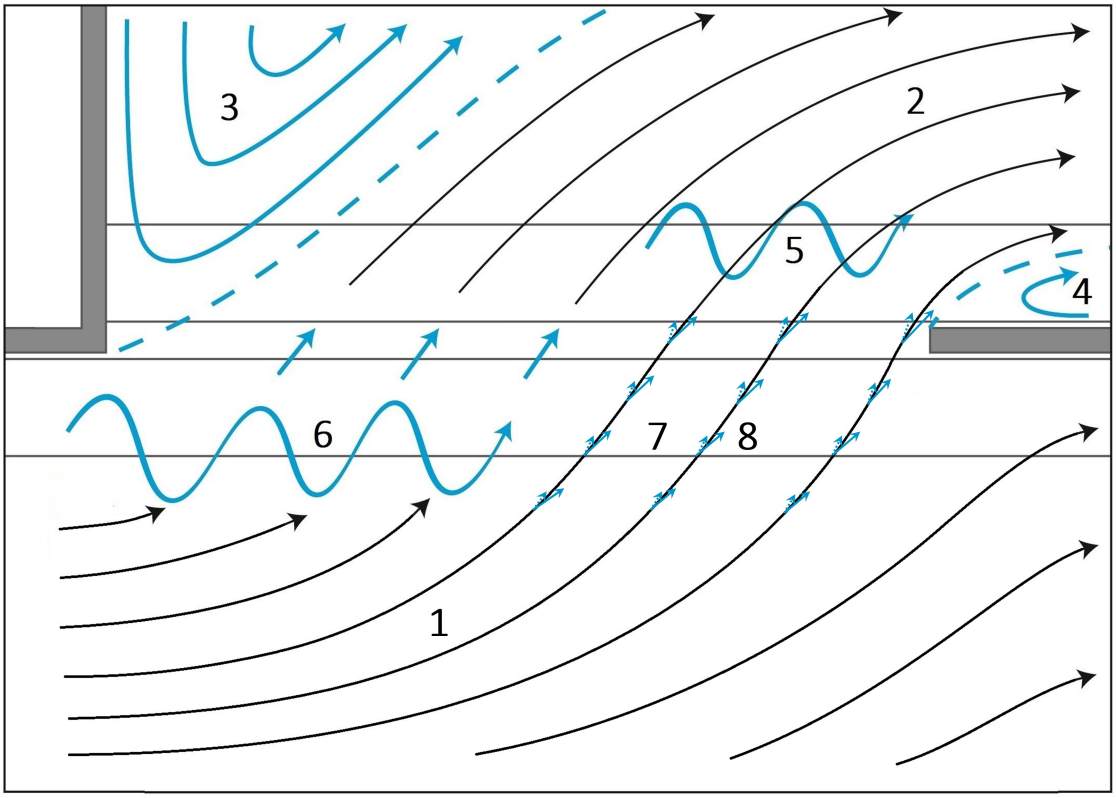

Figure 5.6: Top view of the inlet area of longitudinal training walls with primary in black and secondary flow patterns in blue.

* The small dotted arrows in Figure 5.6 indicate the flow near the bottom and the small solid arrows indicate the flow near the water surface as result of the helical flow. Helical flow due to the curved flow is also present in the area behind the sill. It is not known how this flow develops, since the flow has not been measured at mid-depth at the downstream side of the sill. Therefore, the helical flow at the downstream side has not been visualised.

6

Analysis - comparisons

This second chapter with analyses consists of comparisons. First, the results have been compared for the different conditions. Then, the measurements have been compared to the results of the depth-averaged models from Van Linge [2017]. This forms the basis of the deduction of the effect of the variation in flow on the sediment transport in chapter 7.

6.1. Comparison experiments

The flow has been varied in horizontal direction by the discharge distribution and in vertical direction by the sill height to water depth ratio. The effect of these variables of the flow structures has been analysed in this chapter. A discussion of the effects of the variables on flow and a deduction of the effects of the variables on sediment transport can be found in section 7.2 and 7.3.

6.1.1. Effect of discharge distribution on flow

The effect of variation in the discharge distribution on the flow structures is analysed in this section. The discharge over the inlet sill is the integral of the lateral velocity component over the crest length. A larger discharge distribution Q_s/Q_m results in a larger discharge towards the sheltered channel with larger lateral flow velocities. Figure 6.1 shows the velocity components at mid-depth and near the bottom for the condition A1 and A2, where condition A2 has a larger discharge ratio Q_s/Q_m than condition A1. The spreading of the velocity components provide knowledge on the effect of the discharge distribution on three-dimensional flow structures. Since the lateral velocity integrated over depth is the specific discharge, the lateral velocity provides insight in the distribution of the specific discharge over the sill.

The relative difference of the lateral velocity component increases with a factor of 1-1.5 and the relative difference of the longitudinal velocity component increases with factor 1-4 with an average around 2-2.5. So, the relative difference for the lateral component is less strong and has less variation than the longitudinal component. In conclusion, the lateral velocity, which determines the discharge, increases less than the longitudinal component for a larger discharge distribution towards the sheltered channel.

The relative increase of the total velocity is larger for the flow at mid-depth than the flow at the water surface. This is also the case for the lateral and longitudinal velocity components, except between x = 500-100 mm for the longitudinal component. This can be explained as follows: the curvature has a smaller radius and a larger velocity above the upward slope of the sill for condition A2 compared to condition A1 and the depth is approximately the same. Hence the helical flow relative to the mean flow velocity is stronger (see Equation 2.2).

The relative difference in the longitudinal velocity increases between x = 1100-1600 mm and decreases between x = 1600-2000 mm for the near-bed velocity. This pattern is reversed for the velocity at the water surface. This corresponds with the secondary flow for a separatrix for condition A2, which is not present for condition A1 (see also streamlines in Figure 4.7a and 4.8a).

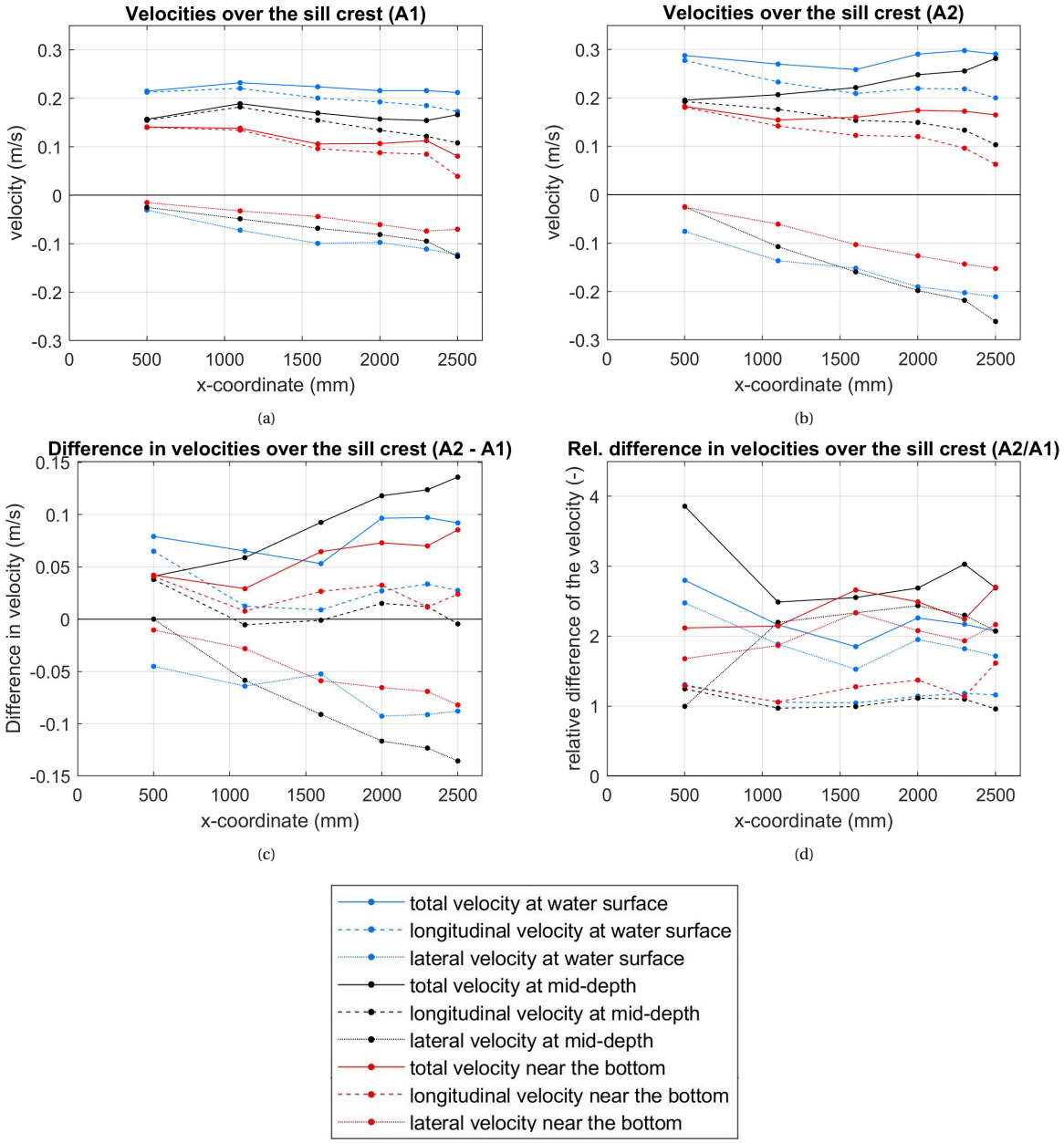

Figure 6.1: Total velocity and velocity components along the crest for the flow at mid-depth and near the bottom for two experimental conditions with variation in the discharge distribution: $(Q_s/Q_m)_{A1} = 0.55$ and $(Q_s/Q_m)_{B1} = 0.75$

Besides, there is a reversed effect for the longitudinal velocity between x = 2000-2500 mm. The relative difference in longitudinal direction decreases between x = 2000-2300 mm and increases from x = 2300-2500 mm for the near-bed velocity. The longitudinal velocity at mid-depth and at the water surface decrease between x = 200-2500 mm. These patterns are also present at the lateral velocities. It corresponds to the secondary flow for the separatrix in condition A1, which does not exist in condition A2. Thus, the relative difference for condition A2 relative to condition A1 can be interpreted as the disappearance of the separatrix. The pattern in the relative velocity difference is not reversed compared to the pattern near the bottom, which can be explained by a stronger helical flow due to the curvature between x = 2300-2500 mm than between x = 2000-2300 mm for condition A2. This corresponds with the larger lateral velocity and difference between the flow angle at the water surface and at mid-depth, see Figure 4.7a and 4.8a.

Moreover, the relative difference for the velocity at the water surface between x = 500-1000 mm is larger at

mid-depth than near the bottom. This can be explained by a stronger blocking of the flow due to the sill as obstacle for condition A2 than for condition A1. In addition, the relative difference is decreasing for the velocity at the water surface and at mid-depth and increasing near the bottom. This shows that the blocking effect decreases between x = 500-1000 mm.

In conclusion the key points are:

- The effect of a larger discharge distribution is smoother and smaller on the lateral velocity component than the effect on the longitudinal velocity component.
- The helical flow due to curvature is stronger for condition A2 at the side of the longitudinal training wall.
- The divergence in curved streamlines with helical flow, a separatrix, is located around x = 2300 mm for condition A1 and around x = 1600 mm for condition A2.
- The blocking effect is stronger for condition A2 compared to condition A1. This difference in blocking reduces between x = 500-1000 mm.

6.1.2. Effect of sill height to water depth ratio on flow

The sill height to water depth ratio is a dimensionless ratio for vertical variation. Figure 6.2 shows the velocity components at the water surface, at mid-depth and near the bottom for the condition A1 and B1, where condition B1 has a larger water depth than condition A1. The variation in the velocity components over the sill crest provides knowledge of vertical variation of the flow on three-dimensional flow structures.

Since the total discharge is kept equal during the experiments and the water depth is larger for condition B1 compared to condition A1, the discharge towards the sheltered channel and lateral velocities above the crest are smaller for the larger water depth in condition B1 compared to condition A1, see Figure 6.2a and 6.2b. At the water surface, at mid-depth and near the bottom, the lateral velocity component for condition A1 and B1 and the difference of the lateral velocity component over the sill crest have a similarly shaped curve, see 6.1c. So, the flow structures persist, based on these data (in which near-bottom data lacks over a large part of the sill crest).

At the side of the river bank (x = 500), the relative decrease of the lateral velocity at mid-depth is much larger (ca. factor 5) than at the water surface, see Figure 6.2d. Besides, no accurate measurements are available for (x < 2000 mm) due to the small passage frequency at this part of the crest. So, for condition B1 compared to condition A1, the decrease in the lateral velocity at the side of the river bank is larger for lower depths. In other words, the flow near the bottom over the sill compared to the flow at the water surface is more concentrated towards the side of the longitudinal training wall for condition B1, with a smaller sill height to water depth ratio, compared to condition A1. This is caused by an enhanced blocking effect relative to other three-dimensional flow structures. Although, this is hardly visible in the difference in flow angles over depth in the upper half of the water column, the streamlines and passage of particles show a blocking for the flow in lower water depths compared to higher water depths.

Comparing the longitudinal velocity for condition B1 compared to condition A1, the result shows a smaller relative reduction (u_{B1}/u_{A1}) at the water surface compared to mid-depth until x <≈ 1950 mm and a larger reduction for x ≈ 1950 mm. The smaller reduction is due to larger effect of blocking compared to other effects between x = 500-2000 mm for condition B1 compared to condition A1, since blocking results in smaller flow angles at lower depths and hence larger longitudinal velocities at lower depths. The larger reduction is due to the larger influence of the blocking compared to other mechanisms. The curvature is more gradual for condition B1 compared to condition A1, see the streamlines at the water surface in Figure 4.5. This can be explained by a smaller sill effect due to the larger water depth relative to the sill height [Wols et al. 2006]. Since the sill effect gives a larger curvature, it results in a smaller effect in a smaller curvature. For a smaller curvature, the intensity of the helical flow due to curvature is lower. In conclusion, the flow is more gradual for condition B1 compared to condition A1 due to a smaller sill effect. In addition, the reduction of the longitudinal velocity component at mid-depth is smaller than near the bottom for x = 2000-2300 mm and larger for x = 2300-2500 mm. This indicates a less strong separatrix for condition B1 than condition A1. This result

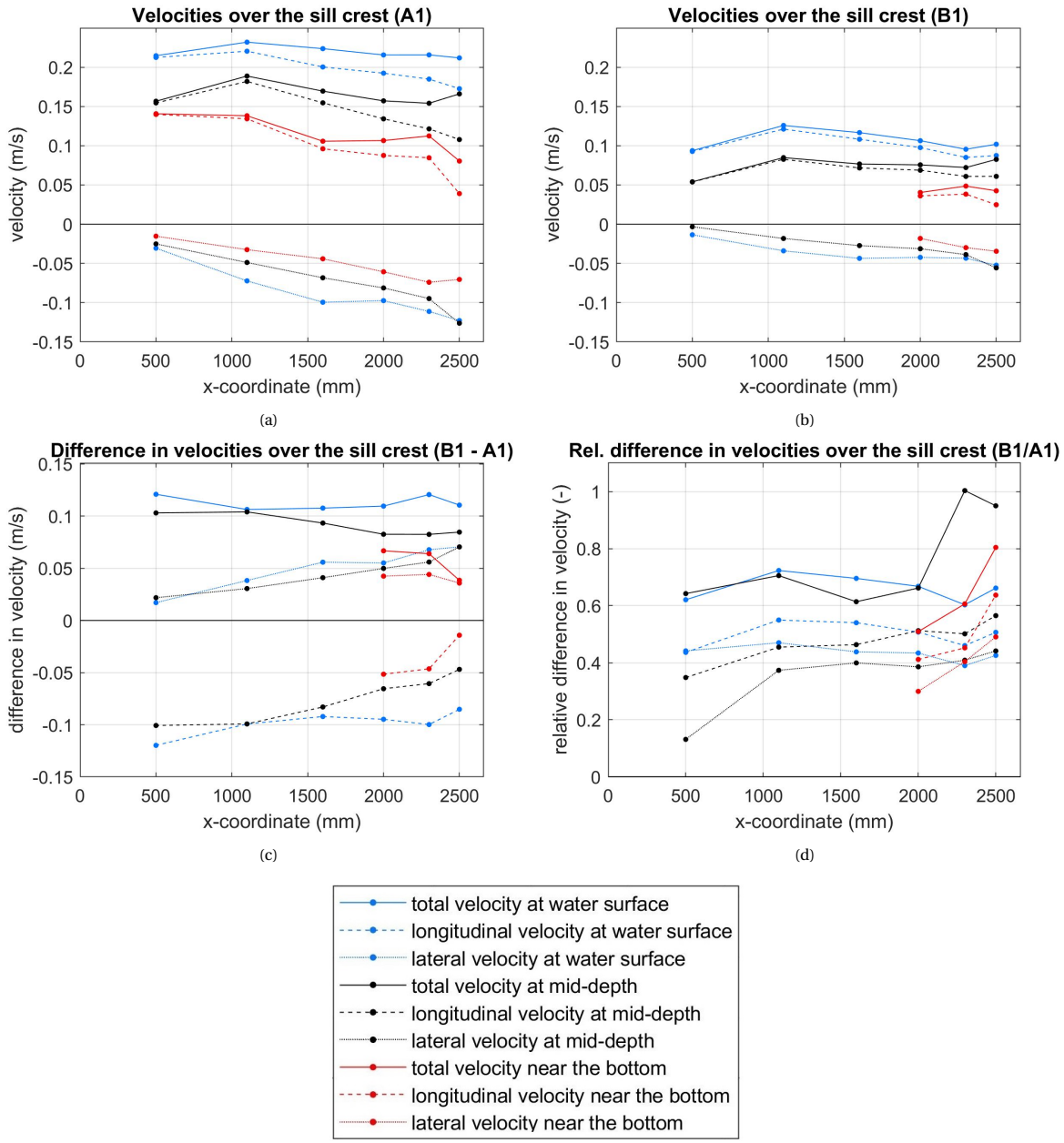

Figure 6.2: Total velocity and velocity components along the crest for the flow at mid-depth and near the bottom for two experimental conditions with variation in the sill height to water depth: $(W/d)_{A1} = 1.10$ and $(W/d)_{B1} = 0.43$

can also be explained by the reduced sill effect that results in more gradual flow.

The longitudinal velocity at x = 2300 mm is locally larger for the flow near the bottom compared to the curves at the water surface and at mid-depth for condition A1. A similar pattern is visible for condition B1. Besides, the flow is divergent at the water surface and the flow is upward at x = 2300 mm for both conditions. Hence, a separatrix flow structure, with inward flow near the bottom and outward flow near the water surface in longitudinal direction, explains the measurements. So, the sill height to water depth does hardly affect the location of the separatrix flow structure atop the crest.

The lower velocity results in a smaller acceleration over the sill and hence less deformation of the velocity profile. The absolute deformation is approximately the same and the deformation relative to the depth-averaged velocity magnitude is larger for condition B1 than for condition A1, see Figure 5.5. This cannot be explained

by acceleration, because the velocity for condition B1 is actually lower. The explanation can also not be found in the stronger curvature and hence larger helical flow, because the effect is opposite. This is further discussed in section 7.3.

In conclusion the key points are:

- The flow over the sill is more concentrated at the side of the longitudinal training wall for lower depths for a smaller sill height to water depth ratio.
- The curvature is milder at the upstream side (x = 0 - 1500 mm) and hence the helical flow due to the curvature is weaker for a smaller sill height to water depth. Hence, the effect of blocking is relatively larger over the effect of helical flow due to curvature for a smaller sill height to water depth ratio.
- The blocking effect is stronger for a smaller sill height to water depth ratio.
- At the side of the longitudinal training wall, the helical flow is stronger for a smaller sill height to water depth ratio due to a stronger curvature in the lower part of the water column.
- The secondary flow cell, the separatrix, is less strong for a smaller sill height to water depth ratio.
- The location of the deviation in curvature and the corresponding secondary flow cell, the separatrix, has not changed for variation in the sill height to water depth.

6.2. Comparison experimental model and depth-averaged model

To investigate differences between real flow and depth-averaged calculations, the experimental results are compared to depth-averaged model results from Van Linge [2017]. The mid-depth measurements are assumed to be representative for the depth-averaged flow and the measured velocities near the bottom are assumed to be representative for the flow that drives the bed-load transport.

6.2.1. Horizontal velocity patterns

The horizontal flow angles and magnitudes are briefly discussed in this section. Figure 2.10 shows results from Van Linge [2017]. This is repeated with similar figures of the experimental results with streamlines and velocity magnitudes at the water surface. The flow angle and lateral velocity component increase gradually over the crest length for the depth-averaged calculations. The experimental results also show an increase in lateral velocity over the crest, but the streamlines show an area with stronger divergence interpreted as a separatrix.

The recirculation zone at the upstream side of the sheltered channel is present in both the experimental and depth-averaged modelling results. The size of the recirculation zone in the depth-averaged calculation is similar to condition A1 and larger than condition A2, see the flow angles. (Note the width of the sheltered channel is larger than the part shown in the results. The size seems slightly larger for condition B1, but this cannot be concluded based on these data.) For condition A2, the discharge (distribution) towards the sheltered channel is larger than for condition A1. Therefore, a larger flow has to be pressed through the same inlet and hence the lateral velocities are larger resulting in compression of the recirculation cell. For condition B1, the discharge and the flow velocity are smaller than for condition A1, which results in a smoother flow patterns with less convergence and divergence.

The stagnation point at the downstream side of the sill in the main channel is not present in the experimental results, because it is a location with a higher water level which the floating particles do not pass. This stagnation point exists due to the separation of the flow towards the sheltered and main channel. Visual observations showed that floating particles dropped in this zone stay there for some time (ca. 5-30 seconds), which indicates the presence of the stagnation zone. Then the particles are pulled with the flow after some time, which can be explained by turbulence.
The depth-averaged results show a zone with larger velocities in front of the sill at the upstream side. This can be explained by the widening of the channel at the inlet. The experimental results also show a similar zone. However, for condition A2, the velocities at the side of the longitudinal training wall are larger. This is due to the strong divergence at the water surface in combination with stronger flow in outer bends due to the

centrifugal force. Again, condition A2 is an exception because of the larger flow velocities.

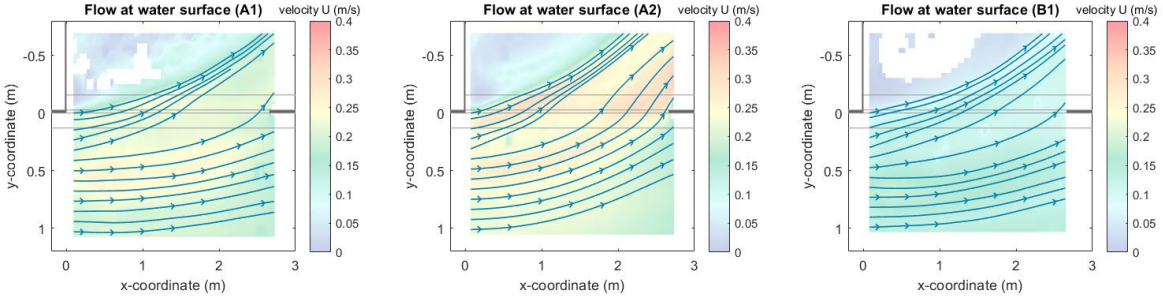

(a) experimental condition A1

(b) experimental condition A2

(c) experimental condition B1

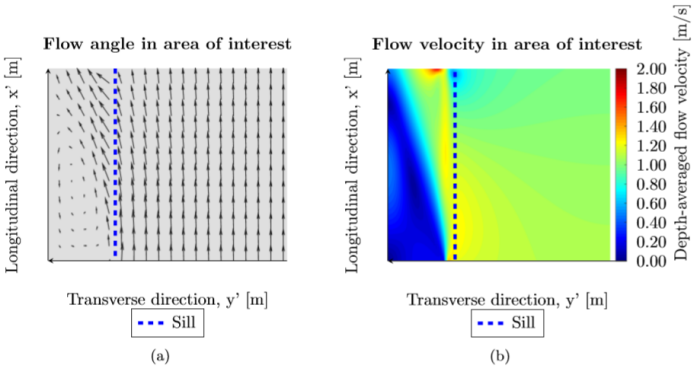

(d) depth-averaged calculation

Figure 6.3: Top view with streamlines and velocity magnitude at the water surface for the experiments and flow angles and velocity magnitudes for the depth-averaged calculation [Van Linge 2017]

6.2.2. Velocity components atop the sill crest

To gain more insight into the three-dimensional flow structures, the velocity components atop the sill crest from the experiments have been compared to the depth-averaged flow calculations. Therefore, the mid-depth and near-bottom measurements have been used, because the mid-depth flow is assumed to be related to the depth-averaged calculations and the near-bottom flow drives the sediment transport. Figure 6.4 shows mid-depth velocity measurements atop the inlet for the 3 experimental conditions A1, A2 and B1, as well as the velocities atop the inlet based on depth-averaged modelling by Van Linge [2017]. The sign of the lateral component is negative for the experimental results, because the vertical coordinate is oriented oppositely the system in the study of Van Linge.

The velocity magnitude increases in longitudinal direction. The increase is strongest until 700-1000 mm, depending on the experimental condition, and until 70 m for the calculations, so this is similar for experiments and calculations. The increase is reached in a shorter distance for a larger velocity (average velocity above the sill), where the order from a condition with high to low velocities is A2-A1-B1. From the top around 700-1000 mm or 70 m, the increase of the flow angle has a larger effect on the longitudinal velocity than the increase of the total magnitude and hence the longitudinal velocity decreases.
The local top around x = 2200 mm for condition A1 and B1, which is absent in the depth-averaged calculations is due to the deviation in the helical flow (separatrix), as discussed in section 6.1. A similar local top or increase for the longitudinal velocity near the bottom compared to the curve at mid-depth is not present for condition A2 at the separatrix around x = 1600 mm. The flow upstream in x-direction from the separatrix is less curved, hence the curve shows a larger decrease in the near-bottom flow before x = 2000 mm for condition A1 and B1 and before x = 1100 mm for condition A2 compared to the curve of the mid-depth flow.

Besides, the ratio of the lateral component to the longitudinal component is smaller for condition A1 and B1 compared to the depth-averaged calculation and condition A2. Besides, condition A1 and B1 have a smaller

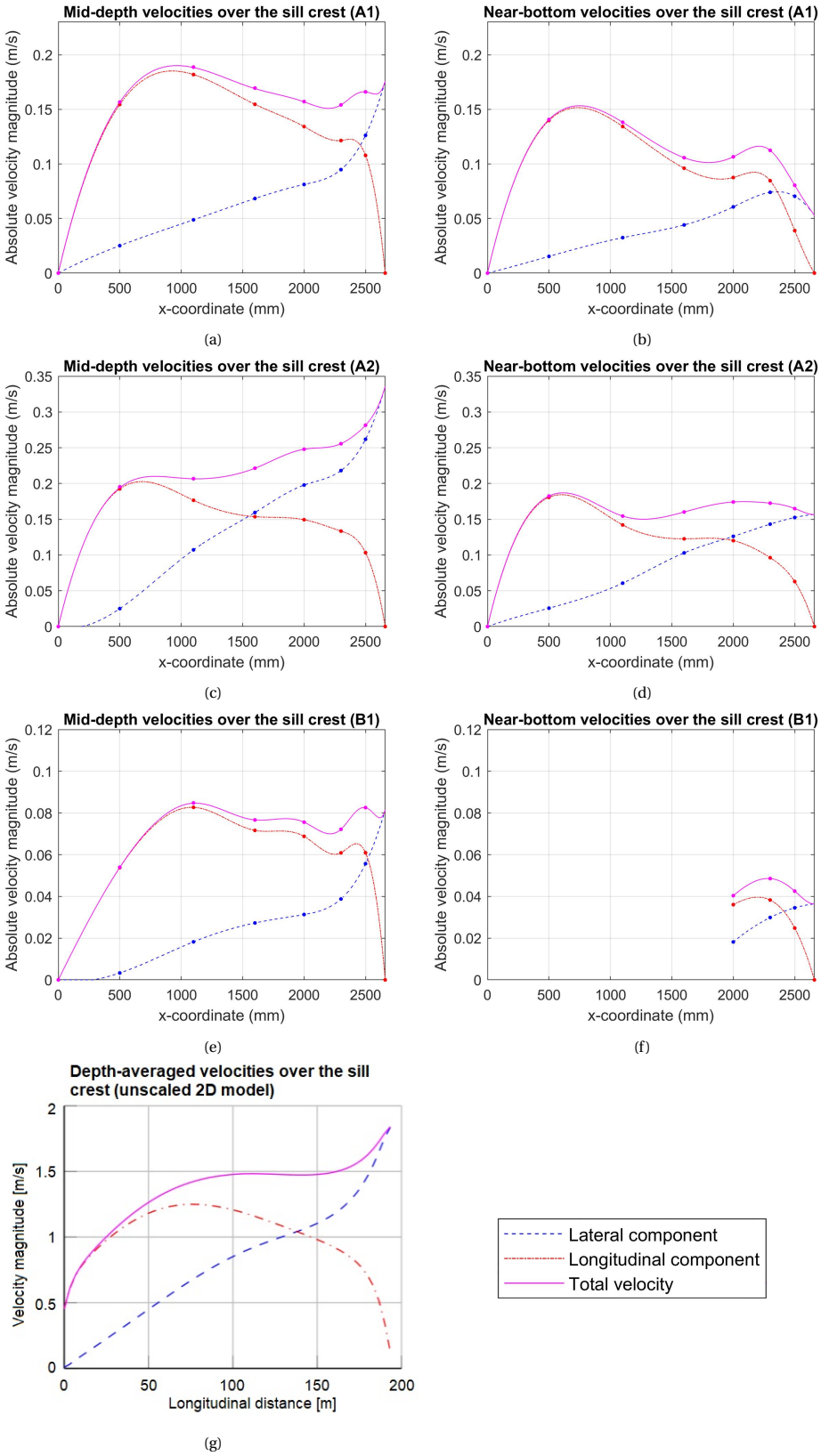

Figure 6.4: Total velocity and velocity components along the crest (a-c) for the flow at mid-depth for different experimental conditions and (d) for the depth-averaged flow in a numerical model with the geometry in 1:1 scale

specific discharge distribution q_s/q_m (0.9 and 0.8) compared to condition A2 (1.2) and the depth-averaged calculations (1.3). So, the discharge distribution is related to the ratio of the velocity components atop the sill crest.

The lateral velocity component shows an increase along the sill crest in downstream direction for both the experimental results at mid-depth and the depth-averaged model results. The curve is nearly linear between longitudinal distance = 0-100 m in the model results. This is also the case for the flow at mid-depth and near the bottom for condition A1 between x = 0-1600 mm. For the flow at mid depth for condition A2 and B1, a linear relation can be drawn between the origin and the data points at x = 1100 and 1600 mm, but the measurement at x = 500 mm is lower than this trend. The local decrease between x = 0-1000 mm can be explained by blocking. The blocking effect is spread over x = 0 - 1800 mm for condition A1, where the blocking effect is concentrated between x = 0-1200 for condition A2, see also the difference in flow angle in Figure 4.7a, 4.7b, 4.8a and 4.8b. The location of the separatrix is already discussed. The blocking effect is much stronger for condition B1 compared to other conditions.
The gradient of the lateral velocity at mid-depth decreases between x = 1100-2000 mm. Similarly, the depth-averaged calculations show a descending gradient between x = 100-130 m. The gradient of the lateral velocity at mid-depth increases from x = 2000 mm in the experiments, as well as from longitudinal distance = 150 m in the model results. So, the trend of the depth-averaged flow calculations is consistent with the mid-depth experimental results, except the local reduction of the lateral component at the upstream side of the crest for condition A2 and B1 due to blocking.

The lateral component of the near-bottom velocity for condition A1 is, similar to the mid-depth flow, nearly linear between x = 0-1100 mm, after which the velocity gradient slightly decreases from x = 500-1100 mm to x = 1100-1600 mm and increases from x = 1100-1600 mm to x = 1600-2000 mm. For condition A2, the gradient of the lateral velocity component increases from x = 0-500 mm to x = 500-1100 mm and from there to x = 1100-1600 mm, after which the gradient slightly decreases from x = 1100-1600 mm to x = 1600-2000 mm. This shape can be interpreted as a reduction of the near-bed flow due to dominance of the blocking effect between x = 0-1600 mm. This corresponds with the smaller near-bed flow angle than the mid-depth flow angle at (x,y) = (1100,-13) mm. Besides, the consecutive increasing and decreasing gradient around x = 1600 mm corresponds with the separatrix. The local top around x = 2300 mm for condition A1 can also be related to the separatrix, as well as the decreasing gradient from x = 2000-2300 mm to x = 2300-2500 mm for condition B1.

The lateral component increases over the sill length at mid-depth and near the bottom, except between x = 2300-2500 mm near the bottom for condition A1. In addition, the gradient increases less between x = 2300-2500 mm for condition A2 and B1. Possible explanations are 1) the helical flow is restricted due to the longitudinal training wall and blocking dominates and 2) the wall shear stress plays a role. Restriction of the helical flow is possible, but development of a circular flow in front of the sill due to blocking a few meters next to the strong flow over the sill is not realistic. Another explanation is the shear stress with the bottom and wall. The effect of the shear stress on the flow is larger for a higher velocity. This relation is checked by dividing the lateral velocity at x = 2500 mm at mid-depth by this value near the bottom. The ratio is larger for condition A2 than for condition A1 and larger for condition A1 than for condition B1. The relation is less than quadratic ($\tau_b \propto U^2$), which can be explained by the helical flow due to curvature.

In conclusion the key points are:

- The location of the top of the longitudinal velocity atop the crest is negatively related to the average velocity of the flow towards and hence in the sheltered channel.
- The effects of the separatrices are present in the experimental results by a decrease and increase in the longitudinal velocity, which is absent in the depth-averaged results.
- The ratio of the lateral and longitudinal component is related to the specific discharge distribution.
- The trend of the depth-averaged flow calculations is similar to the experimental results for the flow at mid-depth, except the local reduction of the lateral component at the upstream side of the crest for condition A2 and B1 due to blocking.
- The lateral velocity component of the mid-depth and near-bed velocity is reduced at the upstream side of the crest for condition A2 and B1 due to blocking.

- The effects of the separatrices are present in the experimental results by an increase and decrease in the lateral velocity, which is not in the depth-averaged results.
- The lateral velocity component atop the sill between x = 2300-2500 mm has a smaller gradient near the bottom than at mid-depth. Possible explanations are restriction of helical flow due to the longitudinal training wall and the wall shear stress.

6.2.3. Effect of the dimensionless sill height on the flow

The (dimensionless) specific discharge atop the crest increases over longitudinal distance for both the depth-averaged with W ≤ 0.62 and the experiments, see Figure 2.11, 6.1 and 6.2. The specific discharge is made dimensionless with the specific discharge averaged over the inlet width (i.e. sill length). Figure 2.11 shows that the increase of the dimensionless specific discharge over longitudinal distance is smaller for a larger dimensionless sill height. In other words, the discharge is distributed more equally for a larger dimensionless sill height. The dimensionless sill height is the sill height to the energy head (W = w/H). Figure 6.2 shows a larger increasing trend of the relative mid-depth lateral velocity between x = 500-1000 m, a nearly constant trend between x = 1000-2000 mm and an increase between x = 2000-2500 mm with a smaller gradient than between x = 500-1000 m. The decrease of the relative difference of mid-depth lateral velocity component for condition B1 compared to condition A1 decreases over longitudinal distance. So, the specific discharge relative to the average specific discharge over the longitudinal distance is steeper for condition B1 than for condition A1.

The energy head is $H = v^2/2g + h + p/(\rho g)$. Since the atmospheric pressure head is 10.33 m, differences in the flow (in order of 0.1 m/s) and water depth (in order of 0.05 m) in the experiment are negligible. The dynamic pressure head is insignificant compared to the water level relative to the reference level. Hence, when keeping the atmospheric pressure out of consideration and taking the bottom as reference level, the sill height to water depth ratio remains. The ratio (w/d) is 0.48 m for condition A1 and 0.30 m for condition B1. So, condition B1 has a smaller dimensionless sill height and the discharge distribution is steeper. This is in accordance to the depth-averaged results. In conclusion, the dimensionless specific discharge over the longitudinal distance has a larger gradient for smaller sill height to water depth levels.

Moreover, the lateral velocity at the water level over the longitudinal distance is smoother for condition B1 compared to condition A1. Hence, the three-dimensional flow patterns are less strong. It was already observed in Figure 4.5 that the flow patterns at the water surface are more gradual for condition B1 compared to condition A1 and now it has been confirmed by this more quantitative analysis of the flow atop the sill.

The depth-averaged results show a more gradual increase of the flow angle over the crest in downstream direction for a larger dimensionless sill height, see Figure 2.12. However, the trend of the flow angle over the longitudinal direction atop the crest between condition A1 and B1 does not change considerably, based on comparison of the relative difference of the longitudinal and lateral velocity components for the water level and mid-depth level in Figure 6.2d.

6.3. Conclusion

The effect of a larger discharge distribution towards the sheltered channel is smoother and smaller for the lateral velocity component than for the longitudinal velocity component. At the side of the longitudinal training wall, the helical flow due to curvature is stronger for a larger discharge distribution. The divergence in curved streamlines with helical flow, a separatrix, is located more upstream for a larger discharge distribution towards the sheltered channel. The blocking effect is stronger for a larger discharge distribution. This difference in blocking is smaller at the downstream side between the distances at the upstream side of the inlet until 3/8 of the inlet width.

For a smaller sill height to water depth ratio, the flow over the sill is more concentrated at the side of the longitudinal training wall for lower depths. In addition, the curvature is milder at the upstream half of the inlet and hence the helical flow due to the curvature is weaker. So, the effect of helical flow due to curvature is smaller for a smaller sill height to water depth ratio at the upstream half of the inlet. Less particles pass the sill which

indicates a larger blocking effect relative to other three-dimensional flow structures. At the downstream side of the inlet, the helical flow is stronger for a smaller sill height to water depth ratio due to a stronger curvature in the lower part of the water column. The secondary flow cell (separatrix) is less strong and has the same location for a smaller sill height to water depth ratio.

The flow angle increases gradually over the cress length for the depth-averaged calculations, but the experiments show a strong divergence of the streamlines in the flow towards the sheltered channel. The lateral velocity component increases gradually over the crest for both the depth-averaged calculations as the experimental results. A larger absolute and relative discharge towards the sheltered channel results in larger lateral velocities and a smaller circulation cell. A smaller discharge towards the sheltered channel results with a larger water level result in smoother flow patterns with less convergence.
The stagnation point at the downstream side of the sill has been observed visually. The velocities in the main channel in front of the sill at the upstream side of the inlet are larger compared to other locations, except the flow in the outer bend towards the sheltered channel for the condition with a larger absolute and relative discharge towards the sheltered channel.

The trend of the depth-averaged flow calculations atop the sill crest is similar to the experimental results for the flow at mid-depth with the following exceptions: 1) the experimental results show a local reduction of the lateral component of the mid-depth and near-bed velocity at the upstream side of the crest (for condition A2 and B1), which is caused by blocking. and 2) the effects of the separatrices are present in the experimental results by consecutively a decrease and an increase in the longitudinal velocity and at the same location consecutively an increase and a decrease in the lateral velocity, which is absent in the depth-averaged results.
The ratio of the lateral and longitudinal component is correlated with the specific discharge distribution atop the sill crest. The location of the top of the longitudinal velocity atop the sill crest is negatively correlated with the average velocity of the flow towards and hence in the sheltered channel. The lateral velocity component atop the sill between x = 2300-2500 mm has a considerably smaller gradient near the bottom than at mid-depth. Possible causes are a restriction of helical flow due to the longitudinal training wall and a larger wall shear stress.

The distribution of the discharge over the inlet width is distributed more equally for a larger dimensionless sill height in both the depth-averaged calculations and the experiments. The depth-averaged results show a more gradual increase of the flow angles in downstream direction on the crest for a larger dimensionless sill height, but trend of the flow angles over the crest length does not change considerably in the experimental results.

7

Discussion

7.1. Experimental design

The first part of this research deals with the question of how the experiment can be designed to reach the research goal. The experimental design is discussed in this section.

Geometry

The geometry that is needed to represent the flow patterns at the inlet consists of a main channel and a side channel. An inlet connects the side channel to the main channel. A sill is located at the inlet and is aligned with the channel axes. inlet sill and longitudinal training wall 1) a main channel with 2) an inlet with a sill aligned with the channel axis that connects the main channel to 3) a parallel side channel that starts from the inlet and, downstream of the inlet, 4) a structure that separates both channels. The side channel is called sheltered channel in this study.

The setup of the 2D model has been used as starting point in the experimental design, because later this has been used to identify the three-dimensional flow structures by analysis of the difference between the experimental results and depth-averaged modelling results. The dimensions affect the discharge distribution and thus the flow structures around the inlet. Therefore, the scale of the dimensions in the experimental design compared to the 2D model is the same for the width of channels and size of inlet sill (1:75).
The scale of the width of the main channel (1:125) is smaller compared to the other dimensions. This makes a larger sill height to water depth ratio possible, given a required depth for point measurements with ADV which are needed at mid-depth. This is interesting, because the effect of submergence on the discharge distribution - and hence the flow around the inlet - is larger for larger dimensionless sill heights (w/H) and so variation of the water depth of the flow structures can better be investigated. Besides, the bed level is the same for both channels and horizontal for practical reasons. These choices could be made, because the aim was to obtain qualitative knowledge on the three-dimensional flow.
Moreover, to prevent seepage under the sill, a thick glue layer has been applied, which changed the dimensions of the sill. The error is in order of 10%. The effect on the flow is expected to be smaller, because the dimensions of the sill are approximately the same. In addition, the width of the sill has been increased at both sides, hence the ratio of the channel widths remains approximately equal. The dimensions in the 2D model, the original design dimensions and the real design dimensions are presented in Figure 7.1.

In addition to the reproduction of the flow structures at the inlet, additional secondary flow effects have been reduced by choices in the geometry. The placement of the bank of the upchannel at the sill crest instead of at the upstream sill toe is important to prevent secondary flow effects above the sill as result of the sharp edge at the upstream side of the inlet. In addition, the geometry of the sill is extended over the entire length of the experimental setup to reduce secondary flow effects as result of a break in this geometry. So, these choices reduce additional flow effect which disturb the main flow structures.

Parameter	Units	Values		Relative error (-)*
		Experiment	2D model	
B sheltered	m	1.12	90	0.93
B main	m	1.86	230	0.61
B crest	m	0.027	2	1.01
B slope	m	0.12	7.5	1.2
h sill	m	0.052	3	1.29
L inlet	m	2.66	200	1.00
discharge	m3/s	0.035	2000	0.00
h side	m + bed level		6.39	0
h main	m + bed level		6.47	0
slope bed	-	0	0.0001	0
slope sill	-	0.429	0.4	1.07
B main / L inlet	-	0.699	1.15	0.61
L inlet / B sheltered	-	2.375	2.222	1.07
B main / B sheltered	-	1.661	2.556	0.65

* relative error for scale 1:75

Figure 7.1: Dimensions of the experiment and the 2D model and the error compared to a scaling of 1:75 of the experiment compared to the 2D model

Summarized, the additional simplifications to the 2D model are:

- the location of the bank of the upchannel at the sill crest instead of at the upstream toe of the sill;
- the bed level of both channels is the same in the experiment instead of a lower bed level in the sheltered channel compared to the bed level in the main channel;
- a horizontal bed in the experiments instead of a slope of 10^{-4} m/m.

For the same discharge distribution and the same water level at the inlet, a smaller main channel results in a larger ratio of the lateral component over the longitudinal component. Besides the curvature is stronger, because a larger part of the flow - with a larger width - has to flow through the same inlet. The larger lateral component relative to the longitudinal component increases the blocking effect and the stronger curvature increases the helical flow. However, the net effect of the smaller main channel on the flow is not known.
The effect of a smaller main channel shows similarities with the effect of a larger discharge distribution Q_s/Q_m. For given boundary conditions (upstream discharge and downstream water levels), the width ratio affects the discharge distribution. The differences in width from B_s/B_m = 1/2.56 in the 2D model to B_s/B_m = 1/1.67 in the experimental results gives an increase of the discharge towards the sheltered channel Q_s/Q_{up} of 25 *à* 30%, see Figure 2.14. This confirms the hypothetical relation between the width ratio and discharge ratio.

The same bed level in the channels instead of a lower bed level in the sheltered channel results reduced stagnation of the flow behind the sill in case of flow separation. This can make the difference whether recirculation happens or not. The horizontal bed slope is valid, since the difference in bed slope (10^{-4}) is small compared to the created water level differences by the downstream weirs.

Experimental conditions
For experiments with variation in the discharge distribution, the total discharge and the water depth above the sill were kept approximately equal. This results in a larger discharge through the same inlet area (water depth x inlet length), where the discharge is more concentrated in the outer bend, i.e. downstream side of the inlet. This results in less blocking of the flow at lower depths due to the sill as an obstacle, more deformation of the vertical velocity profile due to acceleration above the sill and more helical flow due to curvature.
Another option could be the same absolute discharge towards the sheltered channel and water depth above

the sill and variation in the discharge distribution. A smaller discharge in the upchannel and the same discharge towards the sheltered channel, results in a stronger curvature of the flow and hence three-dimensional flow structures: less blocking of the flow at lower depths due to the sill as an obstacle and more helical flow due to curvature.
The latter option with the same discharge in the sheltered channel is preferable, because it does not mix the effects of a larger flow velocity atop the sill and a larger discharge distribution Q_s/Q_m. Although the discharge has been varied with the same total discharge, it was possible to draw conclusions about the effect of the discharge distribution on sediment transport over the inlet sill, see the discussion in section 7.2.

For experiments with variation in the sill height to water depth, the total discharge and the discharge distribution were kept approximately equal. This resulted in a larger flow velocity for a larger sill height to water depth. Therefore, the tracer particles near the bed behaved differently, because the gravitational force on a tracer particle was relatively larger compared to the lift and drag forces. This resulted in a lower flow angle and velocity magnitude of the tracer particles and, hence, the differences in flow angle and velocity magnitude over depth between near-bottom and mid-depth were larger compared to the difference in flow angle between mid-depth and the water surface. To prevent these side effects, the ideal experimental conditions with variation in the sill height to water depth have the same cross-section-averaged velocity in the sheltered channel. Conclusions about the effects of the sill height to water depth due to three-dimensional flow structures could not be drawn, because the side effects are dominate over and opposite to the effect of a different sill height to water depth for the same total discharge, see section 7.3.

The velocity in the sheltered channel does affect the flow structures, see the comparison of the velocity components in section 6.2. An alternative is to keep the velocity in the sheltered channel constant during the experiments instead of the total discharge. Note that this variation in the conditions with the same downstream weirs results in a different water depth and thus other side effects will arise. Since this is labour intensive to realise, the approach should be optimized. A method for this is to choose a set of downstream weirs with a certain height, adapt the discharge, measure the velocity in the sheltered channel on certain locations in depth and width and repeat the last two steps until the same velocity has been reached. This time of this procedure can be reduced to circa 20-30 hours by preventing redundant measurements as follows:

1. Measure the velocity spread over the sheltered channel at e.g. 9 locations for 3 extreme conditions and determine
   - the most representative location (M) for the cross-sectional-averaged velocity.
   - the required number of measurements (N) that is needed to obtain accurate values of the cross-sectional-averaged velocity.
2. Adapt the discharge and measure the velocity in the sheltered channel on representative location M. Repeat the procedure step 2 until the aimed velocity has been obtained
3. Measure the velocity at N locations in the sheltered channel. If needed, adapt the discharge and repeat the measurements at N locations until the chosen velocity is reached with sufficient accuracy.

Finally, it should be noted that the discharge ratio and the sill height over water depth ratio are not independent. Figure 2.14 shows that the dimensionless discharge towards the sheltered channel Q_s/Q_{up} decreases for a smaller dimensionless sill height W = w/H [-], where w [m] is the sill height and H [m] is the energy head. Since the curve decreases toward zero, the sill height to water depth ratio should also be negatively related to the discharge distribution towards the sheltered channel.

Measurements
The identification of the three-dimensional structures with measurement data are discussed in this section.

The flow field at the water surface and near the bottom give insight in the horizontal flow patterns and the differences in flow over depth. Data of the vertical velocity at mid-depth obtained with point measurements support interpretations about flow structures. These types of measurements form a solid base for an analysis of the three-dimensional flow structures. The measurements at mid-depth also give the opportunity to analyse the differences in flow over depth in the upper and lower half of the water column. The latter is important

to gain insight in the difference of the depth-averaged velocity and the near-bottom velocity that drives sediment transport. Besides, the differences between mid-depth measurements and depth-averaged calculation the difference between mid-depth and near-bottom can be distinguished, which is important to distinguish side effects in the horizontal flow due to the experimental conditions and the three-dimensional effects.

The tracer particles can be dispensed equally over the width of the main channel with a particle dispenser or by hand. The concentration at the area of interest, which is the sill, has to be large enough for accurate results (6-10 particles per interrogation area) and small enough to prevent that particles clump together. Therefore, additional tracer particles should be added during the flow field measurements in areas with strong divergence. These particles should be added close enough to enter the area with strong divergence instead of spreading at both side and particles that are intended to roll has to be released at sufficient distance from the sill, ca. 1 m in this case, to ensure these particles have reach the bottom before they enter the sill.

The point measurements at mid-depth in the main channel provide quantitative knowledge on the effect due to variation in experimental conditions. Therefore, these measurements provide insight in the order of magnitude of the effect in the main channel compared to other flow effects. This effect could also be deducted qualitatively from the flow conditions or interpolation of the flow field measurements.
The flow angle and curvature are smaller at the upstream side in the depth-averaged results and hence less strong flow structures due to respectively blocking and helical flow was expected. Therefore, the concentration of the locations of the point measurements was increased in downstream direction. However, the blocking effect is more dominant at the upstream side of the sill and the helical flow at the downstream side of the inlet. The shape of the flow structures due to blocking could not be identified due to the limited concentration of point-measurement locations. So, the point measurements should have been more detailed for identification of the blocking effect. This requires 3-4 measurements over the width of the slope, also measurement just before the inlet can be useful. Besides a distance of 25 cm would provide more insight, for example this could have helped to explain the outlier at (x,y) = (500,-13) mm.

Upward flow above the sill due to turbulence lift rolling particles from the bed. These upward motions reduce the accuracy at which the movement of the particles represent the flow near to the bottom. The saltating mode of the particles on the upward slope can be induced by the irregularities in the sill shape at the transition between the bottom and the glue and between the glue and the sill. This saltation could have been prevented by smaller flow velocities or particles with a higher density, but these solutions would give side effects due to the submerged weight and momentum of the tracer particles.

7.2. Effect of the discharge distribution on sediment transport

The second question is about the effect of a horizontal change in the flow, variation in the discharge distribution, on the sediment transport over the inlet sill of longitudinal training walls.
For a larger absolute and relative discharge towards the sheltered channel, the flow angle and velocity magnitude above the sill increase in general. Besides, the area in which blocking dominates in the upper part of the water column decreases in downstream direction above the upward slope and crest and hence the area in which curvature dominates in the upper part of the water column increases in downstream direction above the upward slope and crest. This results in a shift of the separatrix in downstream direction. In addition, the area in which blocking dominates in the lower part of the water column increases in downstream direction above the crest and hence the area in which curvature dominates in the lower part of the water column reduces in downstream direction above the crest.

The larger flow magnitude at the sill is caused by the larger absolute discharge towards the sheltered channel in the experimental condition. The larger flow angle is due to both the larger absolute and relative discharge. The same absolute discharge towards the sheltered channel means the same the lateral velocity component averaged over the inlet area (sill length x water depth). For a smaller initial velocity with only a longitudinal component, a larger change in flow angle is needed to reach the same lateral velocity.
A larger relative discharge and the same absolute discharge towards the sheltered channel means that the initial velocity with only a longitudinal component has to be smaller. So, for a larger relative discharge and the same absolute discharge towards the sheltered channel, a larger change in flow angle is needed to reach the same lateral velocity. For a larger absolute discharge, more flow has to be pulled through the same area,

hence the effective inlet width should be larger and thus the flow angle larger.
So, both the absolute and relative discharge distribution are positively related to the flow angle. To draw conclusions about sediment transport, it has been assumed that the three-dimensional effects are qualitatively similar for a larger relative discharge towards the sheltered channel with the same absolute discharge towards the sheltered than that both are larger. The additional curvature for a larger relative discharge and the same absolute discharge towards the sheltered channel is a horizontal flow effect and it is not regarded in the analysis of the sediment transport, firstly, because this flow effect is included in depth-averaged flow models and, secondly, because it is unknown whether the effect of the difference in flow angle over depth related to three-dimensional flow patterns is larger or smaller than the additional curvature.

The effect in the lower part of the water column is important for sediment transport: the flow angle near the bottom compared to the depth-averaged flow decreases atop the crest for a larger discharge distribution. This is the result of a stronger blocking effect compared to spiral flow due to curvature. Compared to theoretical sediment transport based on the near-bottom flow velocity magnitude and the depth-averaged flow angles, the three-dimensional flow effects reduce the lateral transport velocity component and the transport angle atop the crest, in accordance with the force balance of Van Rijn 1993 and hence it reduces the transport capacity over the sill. For saltation, the particles have an additional downward tendency due to rebounds [Sekine and Parker 1992].

For a smaller flow angle, the momentum in lateral direction is smaller, which increases the lateral distance in which particles travel from the upstream toe to the crest. This can be explained as follows:
We consider the particles A and B with the same initial velocity at x = 0, where particle A has a larger distance from the sill at x = 0 than particle B. The flow angle above the sill is larger for particle A than for particle B and thus the momentum in lateral direction is smaller for particle B. Assuming the curvature is approximately the same for particle A and B, the longitudinal distance in which particles travel from the upstream toe of the sill towards the crest is larger for particle B compared to particle A. This is due to the flow angle and momentum. If the trajectories of particle A and B cross, at this location, particle B has a relative larger longitudinal momentum compared to lateral momentum and the flow is the same. Hence, particle B will continue with a smaller flow angle than particle A. See the blue line compared to the black and red line in Figure 2.20 for a sill slope angle of 15 degrees.
Now, we add the effect of a larger discharge distribution to this case. The flow angles near the bottom compared to the flow angles at mid-depth are relatively smaller for a larger discharge distribution. Hence, the three-dimensional flow patterns result in a decrease of the transport angle and therefore a decrease of the sediment transport over the inlet sill. In conclusion, the three-dimensional effects due to a larger discharge distribution towards the sheltered channel reduce the sediment transport over the inlet sill compared to a theoretical sediment transport based on the near-bottom flow velocity magnitude and the depth-averaged flow angles.

7.3. Effect of the sill height to water depth on sediment transport

The third research question is about the effect of a vertical change in the flow, variation in the sill height to water depth, on the sediment transport over the inlet sill of longitudinal training walls.

The effect of the sill height to water depth ratio on the three-dimensional flow structures has been analysed in section 6.1.2. From the results follows that, for the condition with a smaller sill height to water depth ratio, the lateral velocity component decreases at the water surface and at mid-depth. The relative decrease of the lateral velocity component is larger at mid-depth until 3/4 of the longitudinal distance. This can indicate larger blocking, a smaller helical flow or a smaller deformation of the velocity profile due to acceleration.
A smaller blocking is expected for a smaller sill height to water depth ratio. The side effect of the experimental conditions is a considerably smaller flow velocity above the sill. This results in more gradual flow patterns for conditions with a smaller sill height to water depth, similar to oblique weirs [Wols et al. 2006].
So, the larger relative decrease of the lateral velocity component at mid-depth than at the water surface can be explained by both a smaller helical flow due to curvature and the reduced deflection of the flow angle due to the lower sill. Besides, since the flow velocity results in a smaller acceleration, the deformation of the velocity profile due to acceleration is also smaller.

The smaller flow velocity results in a smaller component of the drag force in upward direction and hence a smaller transport angle of the tracer particles for the near-bottom measurements. This explains the observation that particles for near-bed measurements pass the sill only at the downstream half of the sill and less particles pass the sill in total.
The dimensionless specific discharge over the longitudinal distance atop the sill crest has a larger gradient for a smaller sill height to water depth ratio, based on the velocity data at mid-depth. This horizontal flow effect is also present in depth-averaged models. However, the effect of the sill height to water depth ratio on flow cannot be derived from the experimental results due to the large side effects.

In conclusion, the side effects of the chosen experimental conditions result in smaller flow angles and less passage of tracer particles near the bottom for conditions with a smaller sill height to water depth ratio. Therefore, the effect of the sill height to water depth ratio on the flow and hence sediment transport cannot be deduced.

8

Conclusions and recommendations

The objective of this research was to obtain a better insight in the flow processes and structures and the resulting sediment transport at the inlet sill of longitudinal training walls. The research questions have been answered in the first section of this chapter. In addition, recommendations for further research have been given in the second section of this chapter.

8.1. Conclusions

How can an experiment be designed to make relevant observations on bed-load transport over an inlet sill of longitudinal training walls?

The geometry of the experiment has to induce flow patterns that are representative for the flow at the inlet sill of the longitudinal training walls in the Waal. Besides, the geometry has to be comparable to the 2D model from Van Linge [2017] for identification of three-dimensional effects. In an ideal design, the dimensions are equal, except the width of the main channel. The width of the main channel can be adapted to make larger levels of submergence possible for investigation of the effect of the sill height to water depth on bed-load transport over inlet sills of longitudinal training walls. In addition, the attachment of the setup to the flume should be considered in the design, for example attachment of wood by a glue layer. Additional secondary flows, induced by the edge of the bank at the upstream side of the sill or the ends of the sill, should be prevented, because these disturb the flow at the upstream side of the sill. This can be done by respectively relocation of the upstream bank from the upstream toe to the crest of the sill and extension of the sill over the length of the flume.

Variation of parameters to affect the flow in horizontal and vertical direction is important to obtain insight into the flow structures. An example is the variation of the discharge distribution and sill height to water depth. This is sufficient and relatively simple to realise in comparison with variation in geometrical dimensions. For variation of the parameters, the flow velocity in the sheltered channel should be kept constant. This is important, since the velocity affects the flow structures.

Locations of the point measurements at mid-depth should be spread in horizontal direction over the upstream side of the sill. Although the flow is concentrated at the downstream side, detailed measurements are also needed at the upstream side, because different flow structures are dominant over the length of the sill. Hence, having sufficient point measurements at the upstream side of the inlet is essential to identify the blocking effect that is relative to other flow structures dominant at the upstream side of the sill.

How does the discharge distribution affect the bed-load transport at an inlet sill of longitudinal training walls?

The experiments contain conditions with a difference in the relative and absolute discharge towards the sheltered channel. Both a larger relative discharge and a larger absolute discharge towards the sheltered channel result in a larger flow angle above the sill. The qualitative effect on the three-dimensional flow structures is

assumed to be the same for a larger relative and absolute discharge. The effect of the discharge distribution on bed-load transport over the inlet sill of longitudinal training walls has been determined for the three-dimensional flow effects.

For a larger discharge distribution towards the sheltered channel, the area in which blocking dominates in the lower part of the water column decreases in downstream direction above the crest and hence the area in which helical flow due to flow curvature dominates increases in downstream direction above the crest. The blocking effect has been enhanced relative to the effect of curvature atop the crest.
The sediment transport both at the upstream side of the inlet and the downstream side of the inlet is smaller for the flow near the bottom compared to the flow at larger depths.
So, the effect on the three-dimensional flow structures consists of: 1) the blocking effect at the downstream side is larger at the crest and 2) the helical flow due to curvature is smaller on the crest. Hence, the flow angle atop the crest is smaller for the flow near the bottom compared to flow at larger depths and thus the depth-averaged flow. This reduces the transport angle atop the crest near the bottom, in accordance with the force balance of Van Rijn [1993], and hence it reduces transport capacity over the sill. For saltation, the particles have an additional downward tendency due to rebounds [Sekine and Parker 1992]. For a smaller flow angle, the momentum in lateral direction is smaller. This increases the lateral distance in which particles travel from the upstream toe to the crest. This reduces the sediment transport due to the limited length of the sill. In conclusion, the three-dimensional effects due to a larger discharge distribution towards the sheltered channel reduce the sediment transport over the inlet sill compared to a theoretical sediment transport based on the near-bottom flow velocity magnitude and the depth-averaged flow angles.

How does the sill height to water depth ratio affect the sediment transport at an inlet sill of longitudinal training walls?

Both the sill height to water depth ratio and the flow velocity have been varied in the experiments. For a smaller sill height to water depth ratio and a smaller flow angle, this results in considerably smaller measured angles and velocity magnitudes near the bottom and hence the measurements suggest a strong blocking effect in the lower part of the water column. However, the blocking effect is expected to be smaller for a smaller sill height to water depth ratio. Besides, extrapolation of the effects in the upper part in the water column to the lower part of the water column is not possible, since qualitative differences over depth in the upper part of the water column differ considerably from differences over depth in the lower part of the water column. Therefore, no conclusions can be drawn about the effect of the sill height to water depth ratio on the sediment transport at an inlet sill of longitudinal training walls based on the experimental results. Therefore, further research on the blocking effect and the variation in the sill height to water depth ratio is recommended.

8.2. Recommendations

What recommendations can be made to develop a parameterisation of bed-load transport over an inlet sill of longitudinal training walls for two-dimensional river models based on the findings of this research?

Firstly, it is recommended to develop a parameterisation with local flow data as input, because of variation of the flow over the sill crest and the different flow structures. A parameterisation will not give an accurate representation, when it describes sediment transport as a function of the discharge towards the sheltered channel and the geometrical dimensions.

Secondly, as a next step in the development of the parameterisation, the flow structures due to blocking have to be investigated to identify the shape and to understand the process. The reason for this recommendation consists of the lack of knowledge on the blocking effect and the importance for the parameterisation.
The blocking effect is present for a vertical wall, for example for bottom vanes. The blocking effect is absent for a horizontal bed. Blocking is not understood for slopes, for example, for which conditions blocking occurs and the shape of the resulting flow structure. Data at the upstream side of the inlet are not detailed enough to identify the shape of the structure. Further research is needed for the following reasons:

- The measurements show that the differences in flow angle over depth can be opposite for the upper and lower part of the water column. A clear example is (x,y) = (1100, 120) mm and (x,y) = (1600, 120)

mm for condition A1, where the flow angle is larger at both the water surface and near the bottom than at mid-depth. This does not correspond to a helical flow upstream of the sill along the sill. So, the shape of the flow structure is not known.

- The blocking effect induces probably the divergence at the downstream side in longitudinal direction of the area with blocking and hence the secondary circulation cell in the shape of a separatrix.
- If the blocking effect consists of a helical flow in longitudinal direction in front of the sill (see Figure 5.2d), the flow patterns are separated. In other words, the flow patterns due to blocking are not present together with other three-dimensional flow patterns at the same location. In this case, the parameterisation should consists of two parts for the individual processes. For example in the following format: description of blocking effect if condition = 1 and no correction if condition = 0. If blocking due to the inlet sill of longitudinal training walls has a moderate form, without helical flow in front of the sill that breaches the curved streamlines towards the sheltered channel, a formula can be developed that represents the blocking effect without condition.

So, further research about the blocking effect is needed for understanding the blocking process and the effect of blocking on divergence of streamlines. In addition, insight in the blocking effect is important to determine the approach of the development of the parameterisation. Moreover, the accuracy of representation of the three-dimensional flow patterns by the secondary flow option in Delft3D given depth-averaged streamlines should be assessed for the separatrix.

The blocking effect has to be investigated in an experimental study. Experiments with variation of the sill height to water depth ratio and the sill slope can contribute to insight in the blocking processes. It is highly recommended to keep the discharge towards the sheltered channel equal to investigate the effect of variations in flow or dimensions. In addition, the effect of the total discharge for the same discharge distribution is recommended to investigate. Finally, the following principles can be considered for the geometrical design.
Firstly, assuming the curvature is larger for a larger ratio of the discharge towards the sheltered channel over the cross-sectional area atop the crest (in accordance with the experiments), a smaller inlet is expected to result in a stronger curvature and relatively less blocking.
The flow patterns become less strong for a longer inlet, in accordance with the theory about oblique weirs.
Secondly, a higher sill results in more blocking, in accordance with the theory about oblique weirs. However, it results in a smaller water depth above the sill and hence larger flow velocities, which can result in a stronger curvature and hence relatively less blocking. So, the maximum blocking might not occur for the largest sill height. Thirdly, assuming the blocking effect is maximum for a vertical wall with overflow and absent for a horizontal bottom, a steeper sill results in larger blocking that affects the flow structure.
Summarized, it is recommended to use local flow parameters as input parameters for a to-be-developed parameterisation of sediment transport over the inlet sill of longitudinal training walls, because of the three-dimensional flow structures at the inlet. As following step in the development, the blocking effect needs be investigated in more detail by an experimental study. The velocity averaged over the cross-sectional area in the sheltered channel has to be kept constant for experimental conditions with variation of other parameters.

References

[1] O. Aichel. Abfusszahlen für schiefe wehre (discharge ratios for oblique weirs). *Z. VDI.*, 95(1):26–27, 1953.

[2] S. Ali. *Flow over Weir-like Obstacles*. Doctoral thesis, 2013.

[3] P. Antoine. Ptvlab (particle tracking velocimetry - lab), 2020. URL https://www.mathworks.com/matlabcentral/fileexchange/41235-ptvlab-particle-tracking-velocimetry-lab.

[4] A.W. Baar. *Impact of small-scale transverse bed slope effects on large-scale morphology: Experimental and modelling studies*. Doctoral thesis, 2019.

[5] R.A. Bagnold. Bedload transport by natural rivers. *Water Resources Research*, 13:303–312, 1977.

[6] J.A. Battjes. Vloeistofmechanica b70 collegehandleiding. Report, Technische Universiteit Delft, 1989.

[7] P. Blom. *Turbulent free-surface flow over a sill*. Doctoral thesis, 1993.

[8] M.G. Bos. *Discharge measurement structures*, volume 20 of *ILRI Publication*. International Institute for Land Reclamation and Improvement (ILRI), Wageningen, 1976. ISBN 90 70754 15 O.

[9] J. Bridge and S. Bennett. A model for the entrainment and transport of sediment grains of mixed sizes, shapes and densities. *Water Resources Research*, 28:337–363, 1992.

[10] D.W. Clutter and A.M.O. Smith. Flow visualization by electrolsis of water. *Aerospace Engineering*, 20(1): 24–27, 1961.

[11] F.P.L. Collas, N. Van Kessel, L. Van den Heuvel, A.D. Buijse, and R.S.E.W. Leuven. Langsdammen waal: resultaten vismonitoring 2016. Report, Radboud University, Deltares, and Bureau Waardenburg, 2016. URL https://repository.ubn.ru.nl/handle/2066/160635.

[12] M.J. Czapiga. Discharge distribution longitudinal training walls for moderate discharge conditions, February 2020.

[13] G. De Marchi. Saggio di teoria del funzionamento degli stramazzi laterali. *L'Energia Elettr.*, page 849–860, 1926.

[14] T.V. De Ruijsscher, S. Naqshband, and T. Hoitink. Flow bifurcation at a longitudinal training dam: Effects on local morphology. *9th International Conference on Fluvial Hydraulics, River Flow 2018*, 40:379–380, 2018.

[15] T.V. De Ruijsscher, A.J.F. Hoitink, S. Naqshband, and A.J. Paarlberg. Bed morphodynamics at the intake of a side channel controlled by sill geometry. *Advances in Water Resources*, 134, 2019. doi: 10.1016/j.advwatres.2019.103452. URL https://www.scopus.com/inward/record.uri?eid=2-s2.0-85074465604&doi=10.1016%2fj.advwatres.2019.103452&partnerID=40&md5=c16df1f0076cb930e8d7fd0d6fc66418.

[16] Deltares. *Delft3D-FLOW, User Manual*, 2020.

[17] S. Dey. *Fluvial Hydrodynamics*. Springer-Verlag, Berlin Heidelberg, 1 edition, 2014. ISBN 978-3-642-19061-2. doi: 10.1007/978-3-642-19062-9.

[18] J. Doornekamp, Verkeer en Leefomgeving Rijkswaterstaat Water, Rijkswaterstaat Oost-Nederland, Rijkswaterstaat Zuid-Nederland, and Rijkswaterstaat West-Nederland Zuid. Rivierkundig beoordelingskader voor ingrepen in de grote rivieren. Report, Rijkswaterstaat Water, Verkeer en Leefomgeving, 2019.

[19] W.H. Hager. Lateral outflow over side weirs. *Journal of Hydraulic Engineering*, 113(4):491–504, 1987.

[20] S.M.M. Jammers. *Sediment transport over sills of longitudinal training dams*. Master thesis, 2017. URL http://resolver.tudelft.nl/uuid:4570fe94-c2f2-4d4c-96a0-fb53d7e7dc3f.

[21] E.H. Ka-Leung Lee. Physical modeling for side-channel weirs. Report, Center for Research in Water Resources., 2002.

[22] T.B. Le. *Training rivers with longitudinal walls*. Doctoral thesis, 2019. URL https://doi.org/10.4233/uuid:cf588b41-0bcc-490f-9cf0-ea0d95a92678.

[23] F. Marelius and S. Sinha. Experimental investigation of flow past submerged vanes. *Journal of Hydraulic Engineering*, 124(5):542–545, 1998.

[24] E. Mosselman. Transport van sediment over steilranden en overlaten. Report, Deltares (WL), 1998.

[25] E. Mosselman. *Basic equations for sediment transport in CFD for fluvial morphodynamics*. Computational Fluid Dynamics: Applications in Environmental Hydraulics. John Wiley & Sons Ltd, The Atrium, Southern Gate, Chichester, West Sussex, England, 2005.

[26] NCR. Theme a) optimizing the longitudinal training dams, 2019. URL https://kbase.ncr-web.org/rivercare/project-groups/a-longitudinal-dams/.

[27] B.T. Nguyen. *Flow over oblique weirs*. Thesis, 2006.

[28] A.J. Odgaard and Y. Wang. Sediment management with submerged vanes. i: Theory. *Journal of Hydraulic Engineering*, 117(3):267–283, 1991.

[29] B.C. Phillips and A.J. Shutherland. Spatial lag effects in bed load sediment transport. *Journal of Hydraulic Research*, 27(1):115–133, 1989.

[30] B.C. Phillips and A.J. Shutherland. Temporal lag effects in bed load transport. *Journal of Hydraulic Research*, 28(1):5–23, 1990.

[31] I.L. Rozovskii. *Flow of water in bends of open channels*. Academy of Science of the Ukrainian SSR, Kiev, 1957.

[32] M. Sekine and G. Parker. Bed-load transport on transverse slope.i. *Journal of Hydraulic Engineering*, 118 (4):513–535, 1992. ISSN 07339429 (ISSN). doi: 10.1061/(ASCE)0733-9429(1992)118:4(513).

[33] W. Thielicke. Pivlab - particle image velocimetry (piv) tool. Report, 2020. URL https://www.mathworks.com/matlabcentral/fileexchange/27659-pivlab-particle-image-velocimetry-piv-tool.

[34] W. Thielicke and E.J. Stamhuis. Pivlab – towards user-friendly, affordable and accurate digital particle image velocimetry in matlab. *Journal of Open Research Software*, 2, 2014. doi: 10.5334/jors.bl.

[35] N.B. Tuyen. *Experiments on flow over oblique weirs*. Master thesis, 2005.

[36] B.W. Van Linge. *Hydraulic evaluation of longitudinal training dams*. Master thesis, 2017. URL http://resolver.tudelft.nl/uuid:63160c45-f3ed-4ad2-84c8-9a1db1e04f0a.

[37] W.J. van Os. Cfd modelling of flow over a sill. Report, Delft University of Technology, 2019.

[38] L.C. Van Rijn. Mathematical modelling of suspended sediment in non-uniform flows. Report, Delft Hydraulics, 1984.

[39] L.C. Van Rijn. *Principles of sediment transport in rivers, estuaries, and coastal seas*. Aqua Publications, Amsterdam, the Netherlands, 1993. ISBN 9080035629.

[40] J.R. Villemonte. *Effect of submergence on discharge of sharp-crested weirs*. Doctoral thesis, 1949.

[41] B.A. Wols, W.S.J. Uijttewaal, R.J. Labeur, and G.S. Stelling. Rapidly varying flow over oblique weirs. *International Conference on Hydroscience and Engineering*, 2006.

A

Appendix - Literature review

A.1. Flow

A.1.1. Correction for energy losses in depth-averaged models

Side weirs

The discharge distribution at side weirs has been investigated in many studies. The developed descriptions are based on the general side weir formula, Equation A.1:

$$q_w = C_s C_d 2/3\sqrt{2q}(H_0 - a)^{3/2} \tag{A.1}$$

where H_0 is the energy level upstream in the main channel, a is the weir crest height above the bed level, C_d is the discharge coefficient and C_s is the submergence coefficient. The basic formula without coefficients is derived for a case with critical flow atop the weir and without energy losses, see Figure A.1a. The discharge coefficient is added for correction of energy losses due to variation in weir types and flow conditions. The submergence coefficient makes the formula also applicable for transitional and submerged conditions, see Figure A.1b for submerged flow investigated in this study.

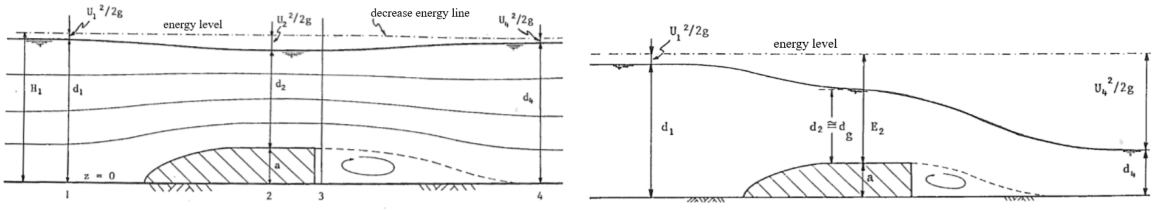

(a) (b)

Figure A.1: Broad-crested weir with respectively sub-critical and critical flow [Battjes1989]

A complete analytical solution for the discharge coefficient comparable to the method of De Marchi [1926] is not possible and empirical discharge coefficients do not apply for the longitudinal training walls. Therefore, the discharge coefficient that corrects for lateral flow conditions [Hager 1987] remains as a solution [Van Linge 2017]. The side weir submergence coefficient from Ka-Leung Lee [2002] gives the best fit with depth-averaged-model results of the flow around longitudinal training walls, according to Van Linge [2017]. Before application, the discharge formulation of Hager and the side weir submergence coefficient from Ka-Leung Lee need to be validated with data of the flow above the inlet sill of longitudinal training walls. Hager [1987] used the general weir formula for plain weirs as starting point and added corrections for the effect of the approach velocity, weir shape, lateral outflow angle and flow depth on the discharge over side weirs, see Figure A.2. The Hager formula is given in Equations A.2 with correction factors A.3-A.6.

$$\omega = \omega_h \cdot \omega_u \cdot \omega_\phi \cdot \omega_\Theta \tag{A.2}$$

$$\omega_h = (y - W)^{\frac{2}{3}} \tag{A.3}$$

$$\omega_u = \frac{u_2}{u_1} = \left(\frac{H - w}{h - w}\right)^{\frac{1}{2}} \tag{A.4}$$

$$\omega_\phi = sin(\phi) = [\frac{y - W}{3 - 2y - W}]^{\frac{1}{2}} \tag{A.5}$$

$$\omega_\Theta = (1 - (tan(\Theta) + i_b)[\frac{3(1-y)}{y - W}]^{\frac{1}{2}}) \tag{A.6}$$

where ω_h is the correction factor for the flow depth, ω_u is the correction factor for the approach velocity, ω_ϕ is the correction factor for the lateral outflow angle ϕ and ω_Θ is the correction factor for the channel shape, where Θ represents the width contraction angle. In these formulas, the dimensionless parameters y = h/H and W = w/H are used.

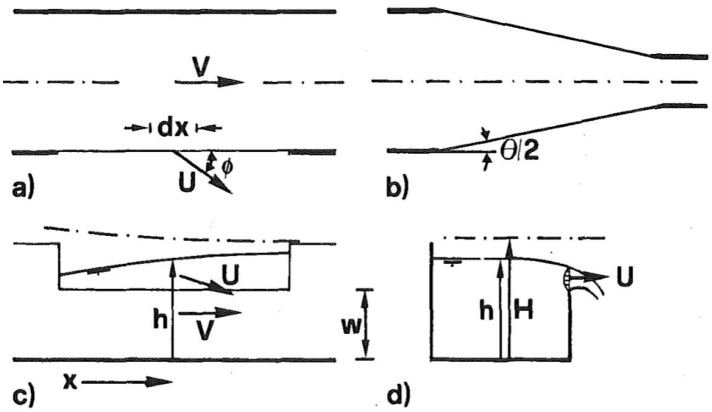

Figure A.2: Lateral outflow geometry and plan view with (a) the outflow angle ϕ, (b) the channel angle Θ, (c) a longitudinal section and (d) a transverse cross section [Hager 1987]

Ka-Leung Lee [2002] developed a submergence factor C_s for side weirs with a rectangular channel shape, see Equation A.7.

$$C_s = \begin{cases} 1 & \text{if } 0.0 < S < 0.5 \\ 1 - 28.84(S - 0.5)^{4.85} & \text{if } 0.5 < S < 1.0 \end{cases} \tag{A.7}$$

where S is the submergence $(H_2 - a)/(H_1 - a)$ and the subscripts 1 and 2 are cross sections indicated in Figure A.1a. In summary, the approach with the Hager formula and submergence factor of Ka-Leung Lee accounts for the effects of the flow depth, approach velocity, lateral flow angle, channel shape and submergence on the discharge. The correction factor for the channel shape does not apply for the longitudinal training walls near Wamel, because there is no reduction of the main channel width.

Inlet sill of longitudinal training walls

Van Linge [2017] found that the plain weir formula with discharge coefficient of Hager [1987] and the submergence coefficient of Ka-Leung Lee [2002] are the most suitable, from the available formulas, for modelling the discharge over the inlet sill of longitudinal training walls in depth-averaged models. Therefore, the results of different available descriptions have been compared to the results of a model with an implemented sill geometry on a small grid. These coefficients have been validated for side weirs but not for inlet sills of longitudinal training walls. Moreover, Van Linge [2017] proposes new submergence coefficients in the same format as Villemonte [1949] and Ka-Leung Lee [2002] improved by curve-fitting, Equation A.8 and A.9.

$$C_s = \sqrt{1 - S^a} \tag{A.8}$$

$$C_s = 1 - \frac{1}{2^b}(S - 0.5)^b \tag{A.9}$$

where $a = 9.14 * (\frac{L_w}{B_{main}})^{-0.84}$ and $b = 10.29 * (\frac{L_w}{B_{main}})^{-0.72}$. These coefficients result in high R-squared values of respectively 0.98 and 0.97 by comparing the results of the model with implemented geometry [Van Linge 2017]. Before these coefficients can be implemented, the coefficients need to be validated with experimental or physical measurement data.

A.1.2. Experimental flow measurements just upstream of the inlet sill

De Ruijsscher et al. [2019] performed an experimental study to investigate the morphology around longitudinal training walls. Flow measurements of this study are shown in Figure A.3. The streamwise location x of the maximum specific discharge into the sheltered channel depends on the sill height during low flow. The angle hardly varied with depth during high flow. The variation of the flow angle with depth indicates the presence of three-dimensional flow structures.

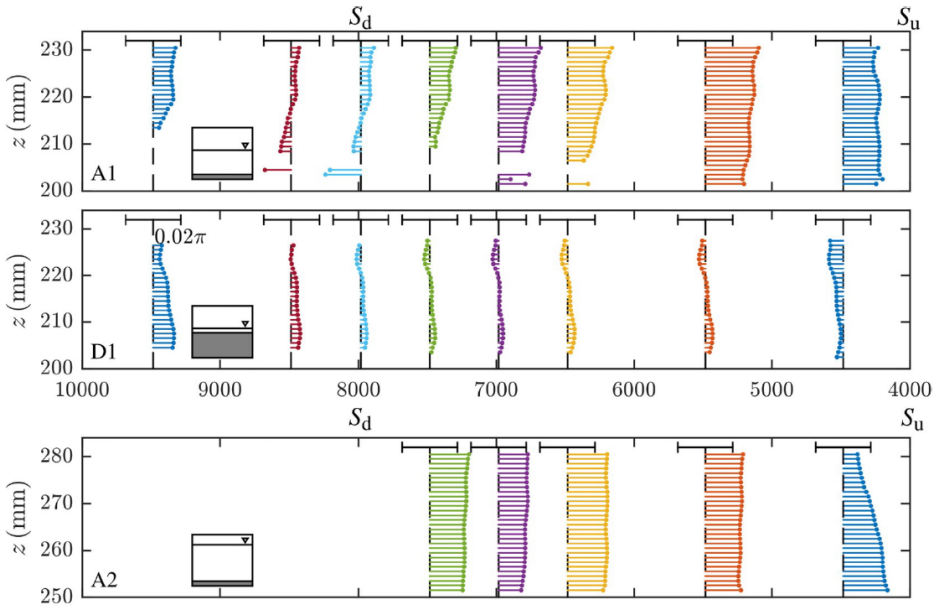

Figure A.3: Flow angle ϕ with respect to the main flow direction in (x,z)-space, with the scale indicated by the horizontal bars with length 0.02π (A1 and D1) and 0.06π (A2), were experiment A2 has a larger discharge and experiment B1 has a larger sill compared to experiment A1. [De Ruijsscher et al. 2019]